The African School of Physics

Lecture : Object Identification and Data Analysis

Version 2012

Slides from ASP2010 (Ketevi Assamagan, Daniel Froidevaux, Simon Connell)

The LHC Project

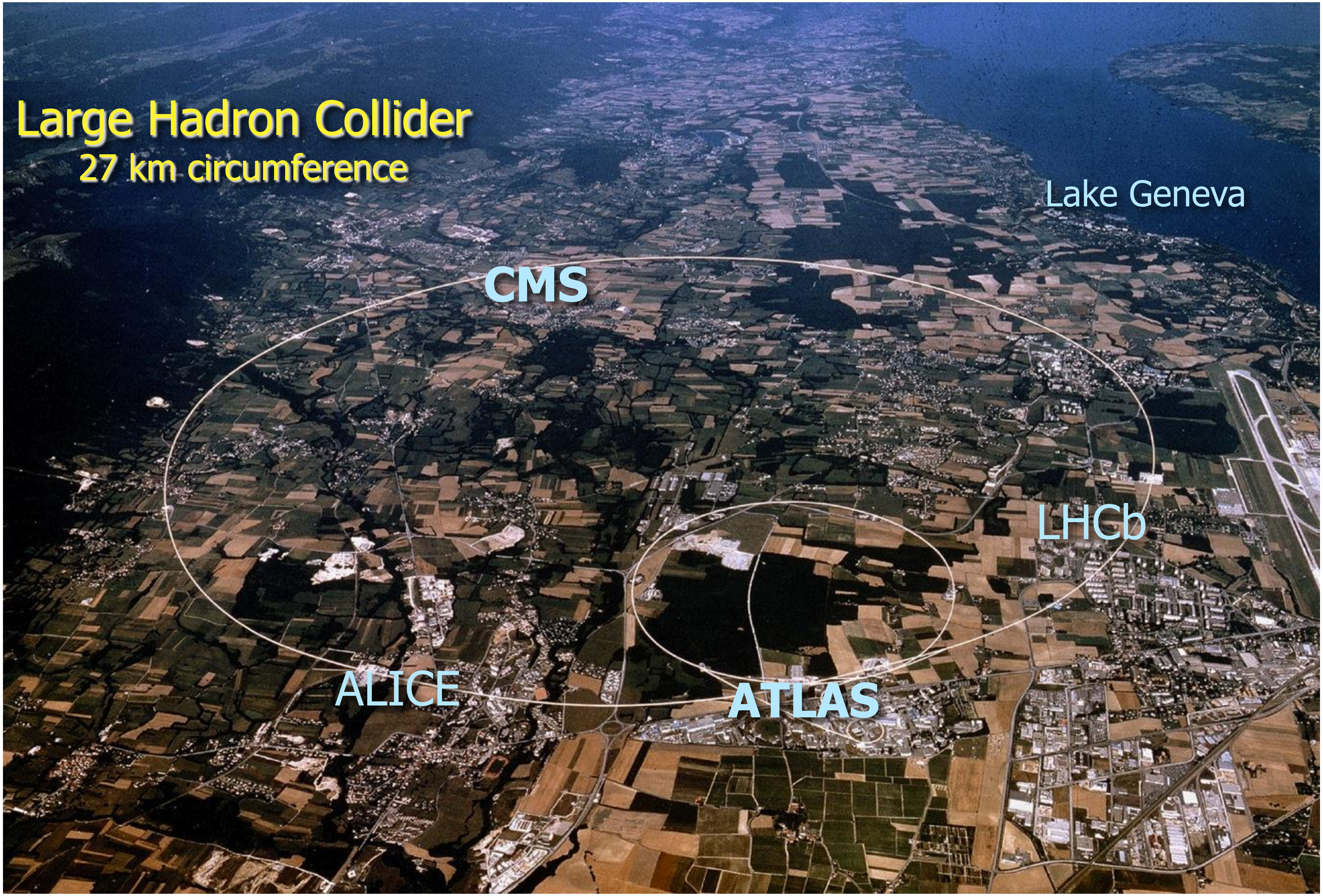

On July 4th, CERN announced the discovery of a Higgs-like boson. What are its properties … ? What else is out there … ?

pp $\sqrt{s}$ = 14 TeV $L_{design} = 10^{34}$ cm^{-2} s^{-1} (after 2013)

7 TeV $L_{initial}$ < few x 10^{33} cm^{-2} s^{-1} (2011)

8 TeV $L_{initial}$ < 6 x 10^{33} cm^{-2} s^{-1} (2012)

Heavy ions (e.g. Pb-Pb at ~ 1150 TeV)

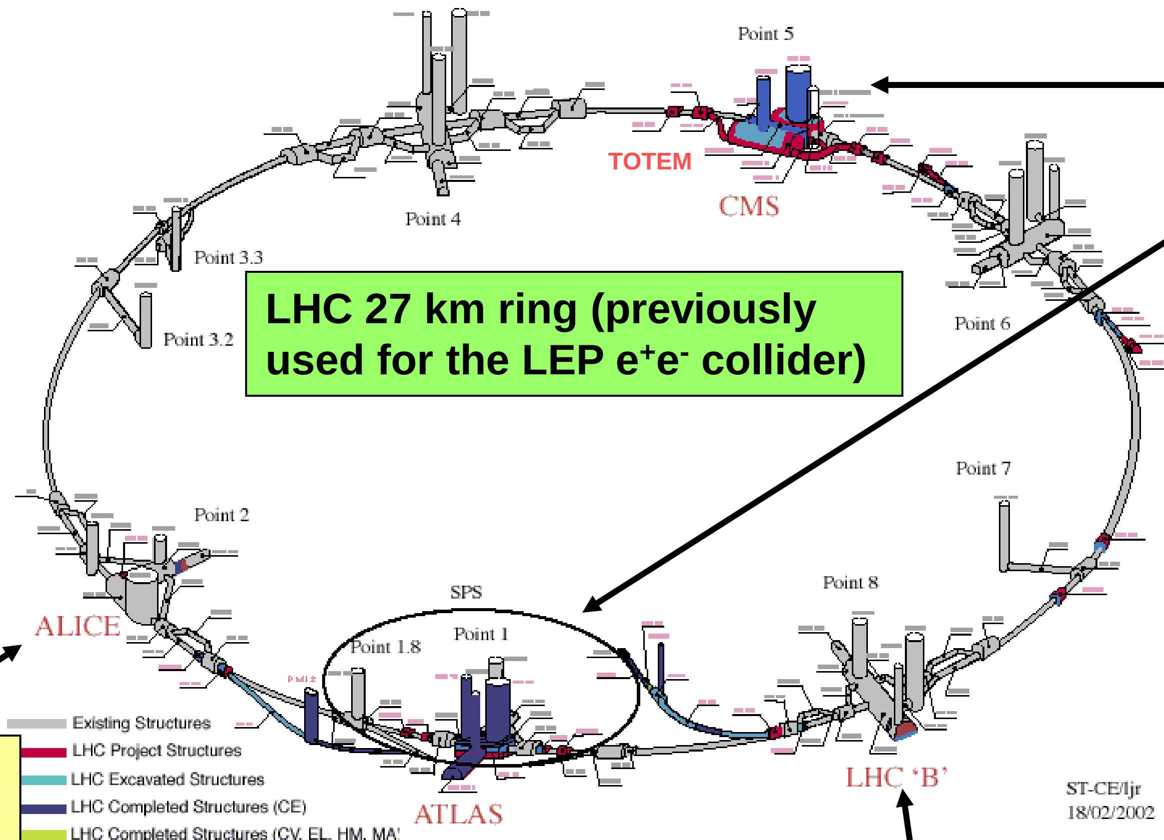

LHC 27 km ring (previously used for the LEP e^+e^- collider)

ATLAS and CMS: general purpose

ALICE: Heavy Ions

LHCb: B-physics, CP-violation

Plus 3 much smaller experiments with very forward detectors at
Point-1: LHCf
Point-5: Totem
…

ALICE: study of quark-gluon plasma

- L3 solenoid
- Large TPC
- Si microstrip, drift and pixels detectors
- Particle identification: RICH, TRD, TOF
- $PbWO_4$ crystals + Pb/scintillator ecal
- Single arm forward muon system

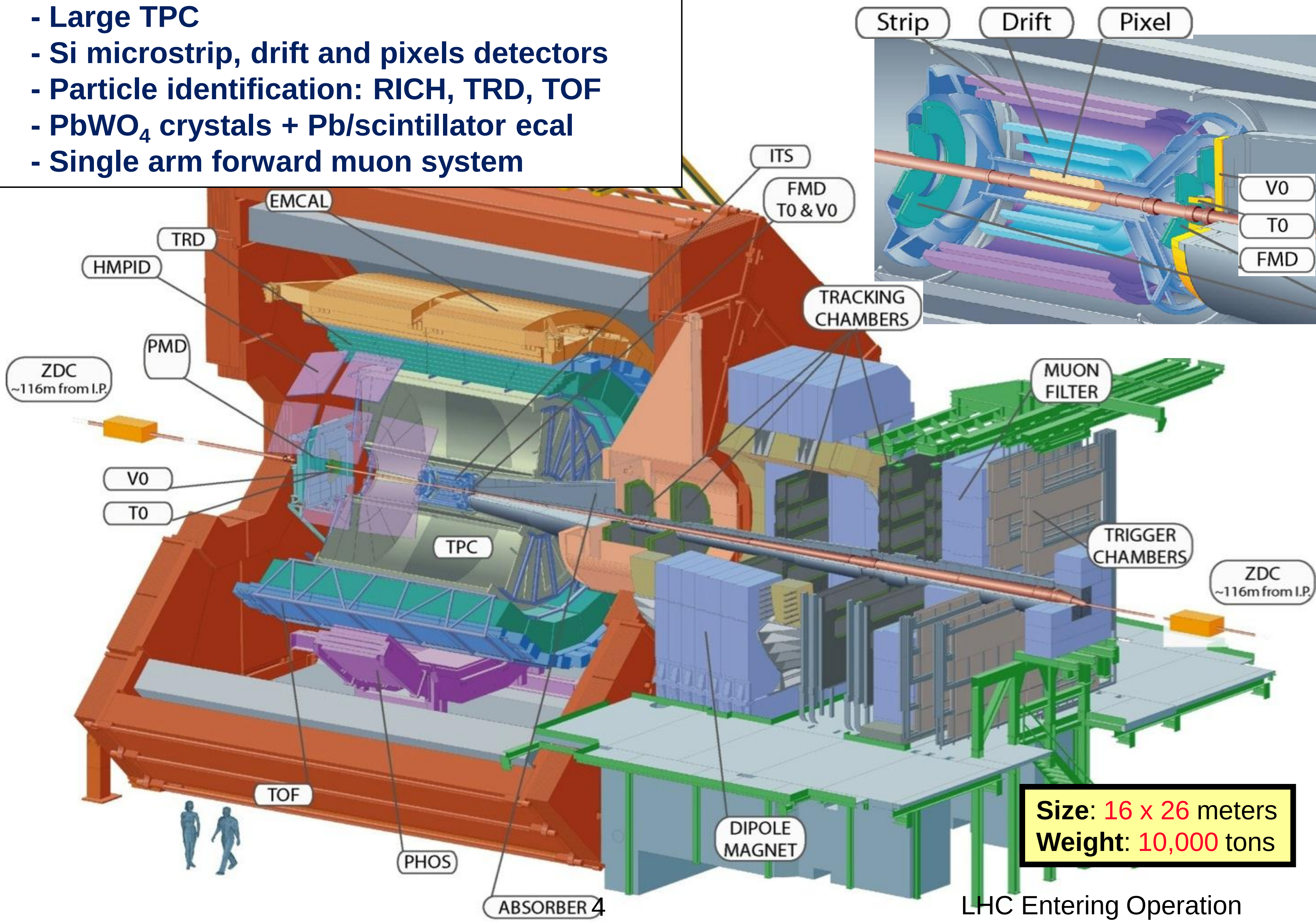

Size: 16 x 26 meters
Weight: 10,000 tons

ATLAS Detector

ATLAS superimposed to the 5 floors of building 40

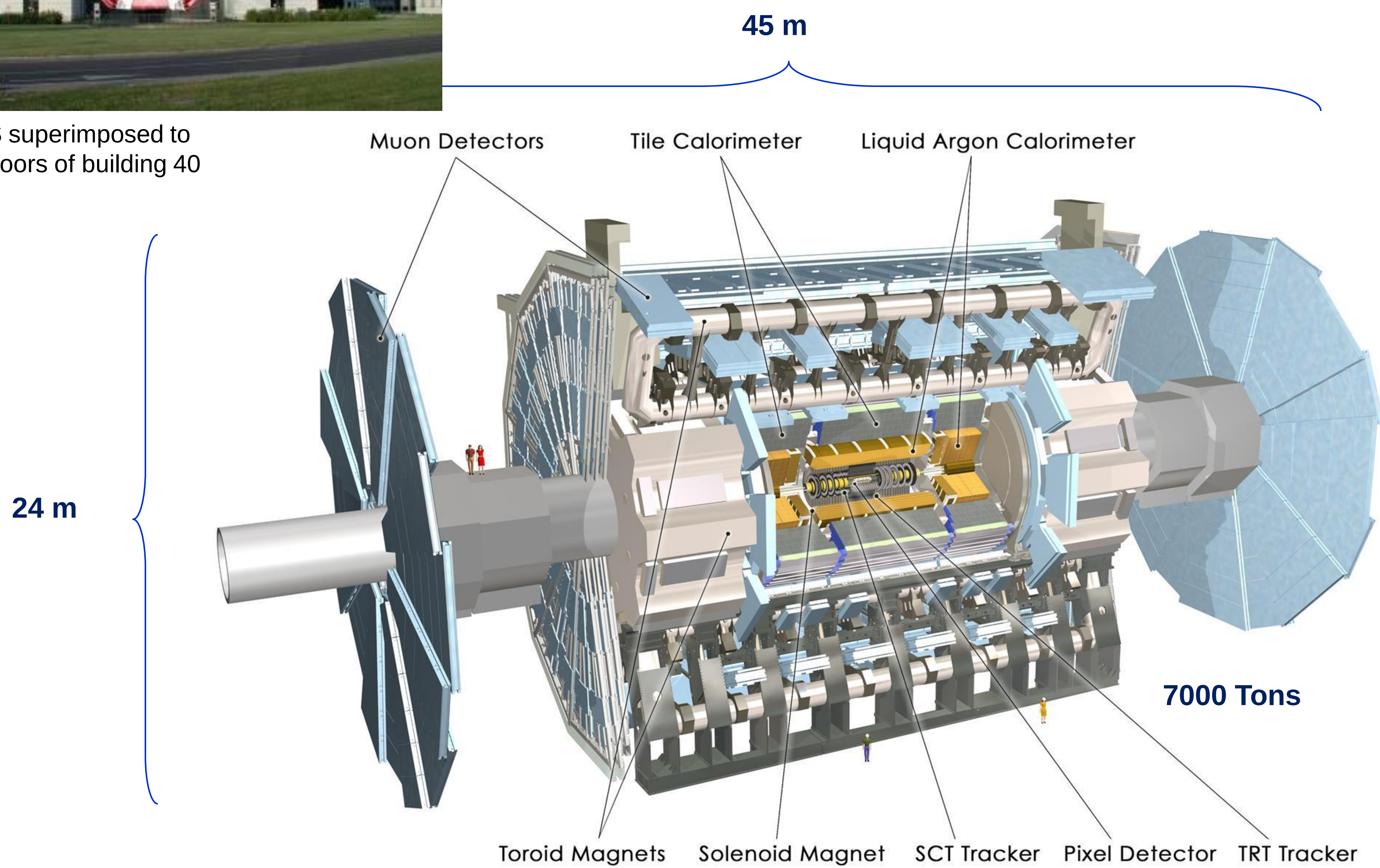

7000 Tons

CMS Detector

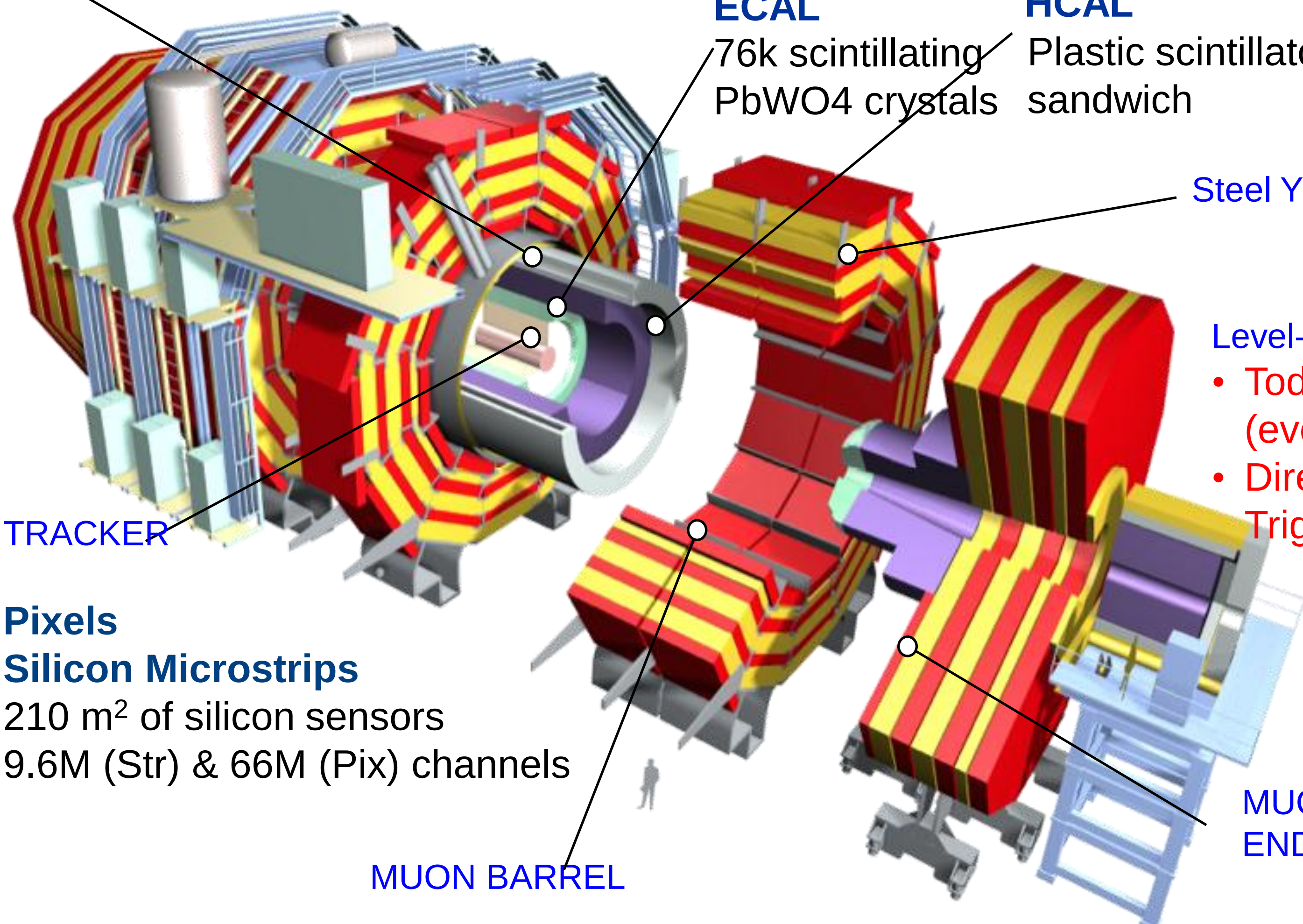

Superconducting Coil, 4 Tesla

CALORIMETERS

ECAL
76k scintillating
PbWO4 crystals

HCAL
Plastic scintillator/brass
sandwich

Steel YOKE

Level-1 Trigger Output
- Today: 50 kHz (eventually100 kHz)
- Directly feeds Higher Level Trigger CPU farm

TRACKER

Pixels
Silicon Microstrips
210 m^2 of silicon sensors
9.6M (Str) & 66M (Pix) channels

MUON BARREL

MUON ENDCAPS

Drift Tube Chambers (DT)

Resistive Plate Chambers (RPC)

Cathode Strip Chambers (CSC)
Resistive Plate Chambers (RPC)

LHCb:
Study of B decays and CP Violation
(indirect search for New Physics)

- Dipole magnet (4 T.m)
- Particle Identification (2 RICH)
- 21 layer of Si microstrip vertex locator (VELO)
- Tracking: Silicon + long straw tubes
- Shashlik (Pb/scint) em calorimeter
- HCAL (Fe/scint),
- MWPC muon system

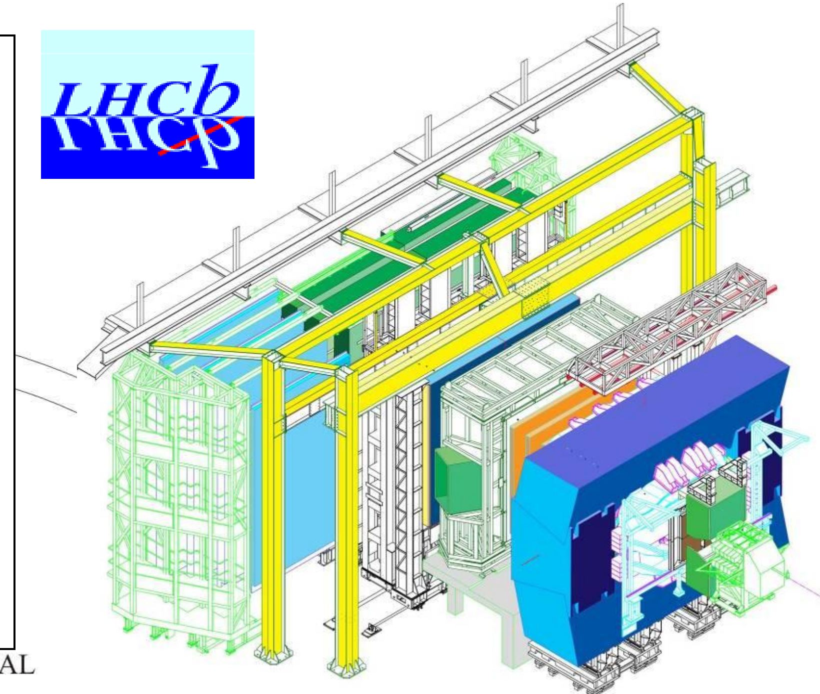

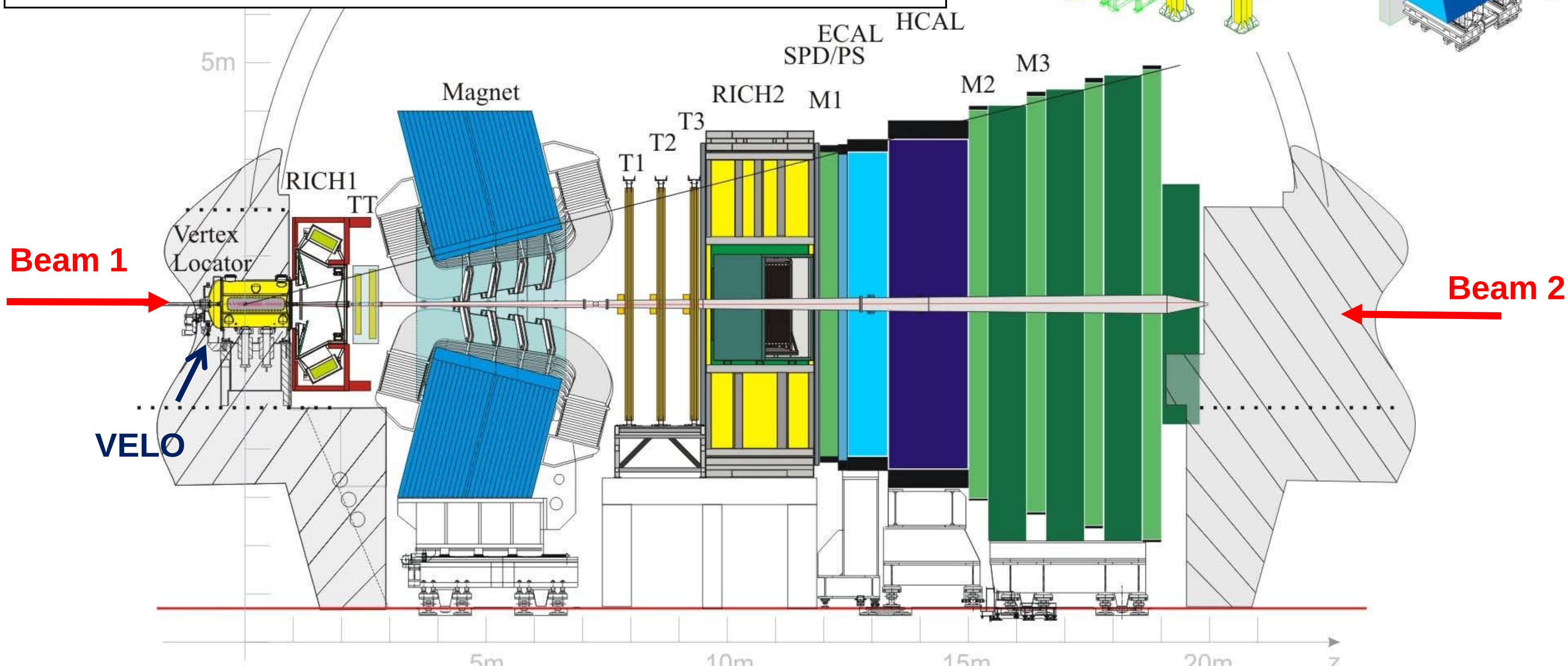

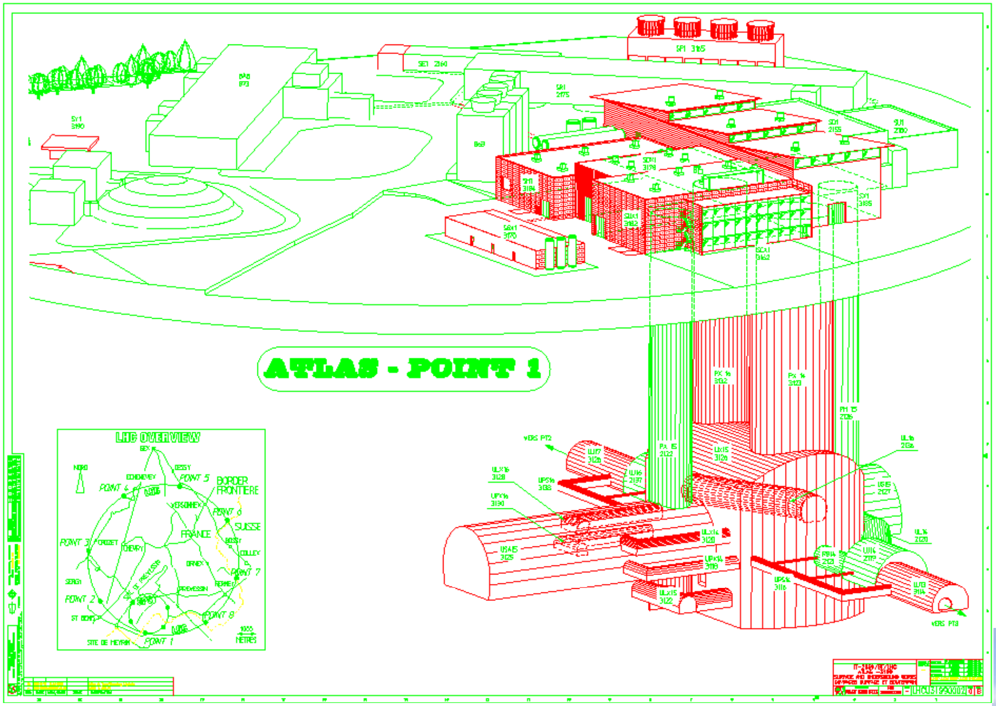

The Underground Cavern at Point-1 for the ATLAS Detector

Length = 55 m
Width = 32 m
Height = 35 m

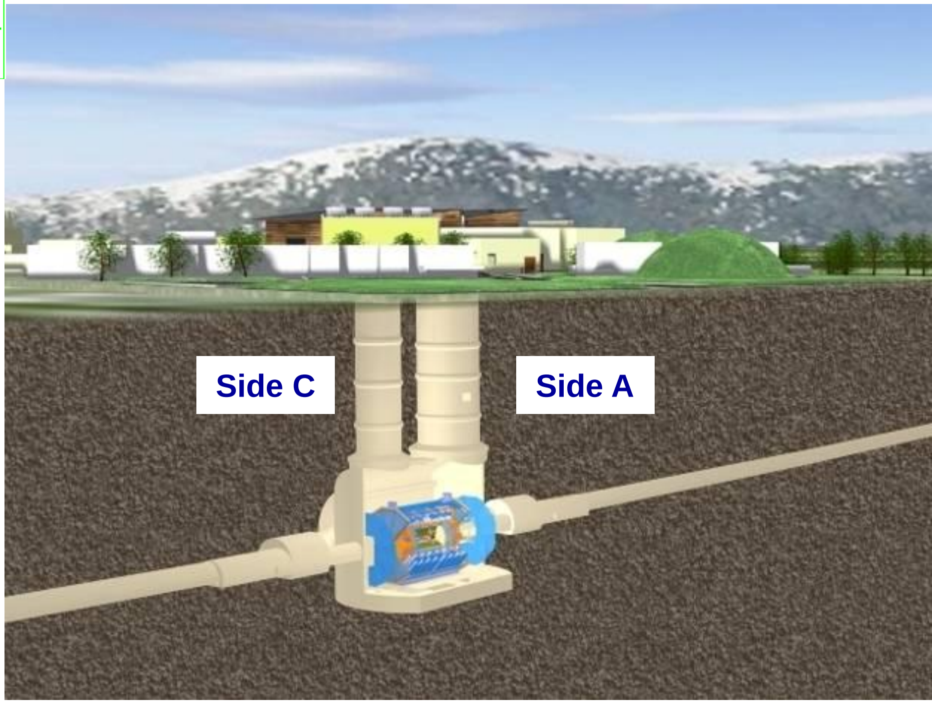

Collisions at LHC

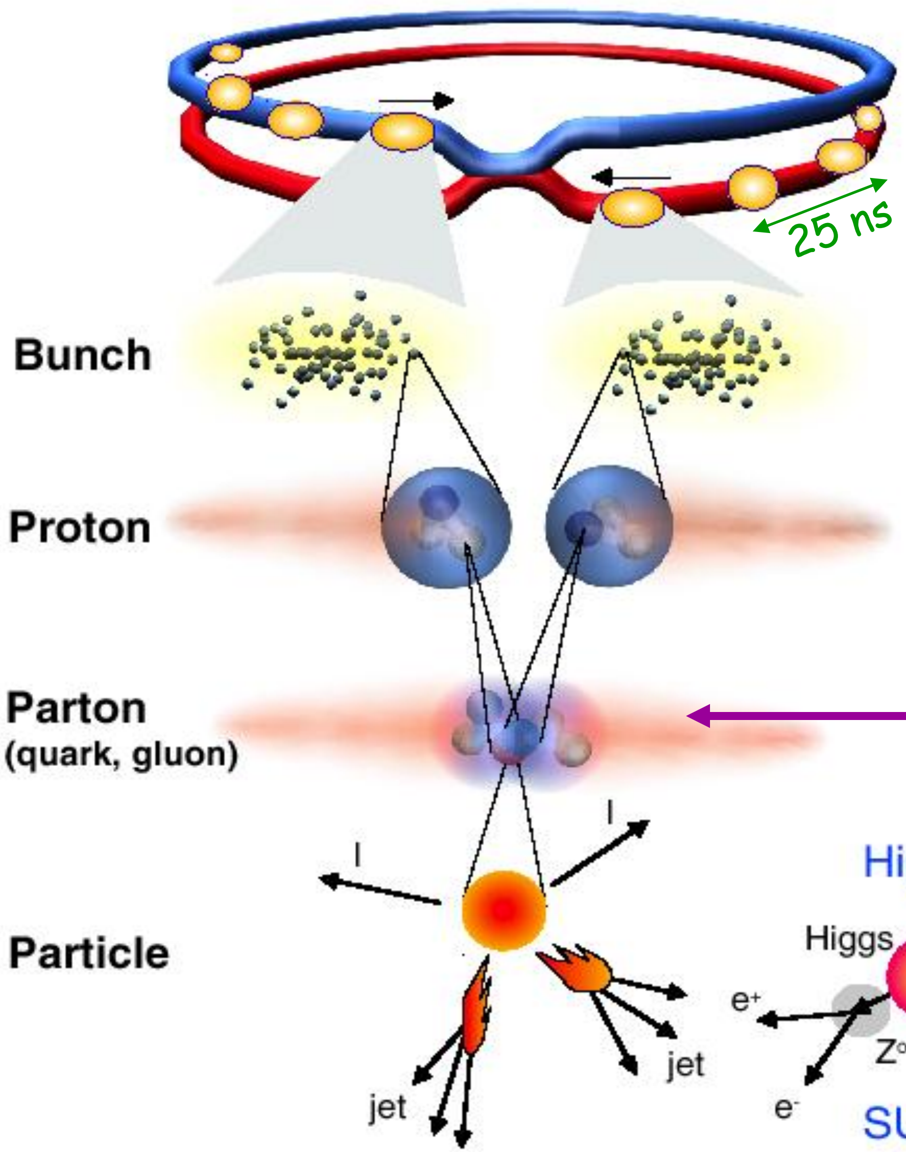

Proton-Proton	
Protons/bunch	10^{11}
Beam energy	7 TeV (7×10^{12} eV)
Luminosity	10^{34} cm^{-2} s^{-1}

Event rate:

N = L x σ (pp) ≈ 10^9 interactions/s

Mostly soft (low p_T) events

Interesting hard (high-p_T) events are rare

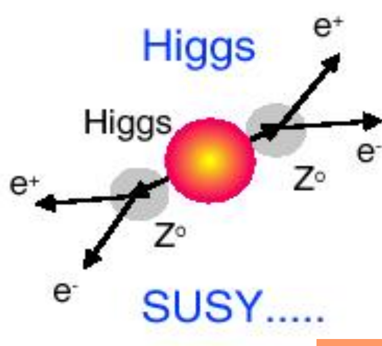

Selection of 1 in 10,000,000,000,000

→ very powerful detectors needed

Physics at the LHC: the challenge

Small x-sections
need highest luminosity
→ L= 10^{34-35} $cm^{-2}s^{-1}$

Orders of magnitude of event rates for various physics channels:

- **Inelastic :** 10^{10} Hz
- **W -> lν :** 10^{3} Hz
- **tt production :** 10^{2} Hz
- **Higgs (m=100 GeV) :** 1 Hz
- **Higgs (m=600 GeV) :** 10^{-1} Hz

(and include branching ratios: ~ 10^{-2})

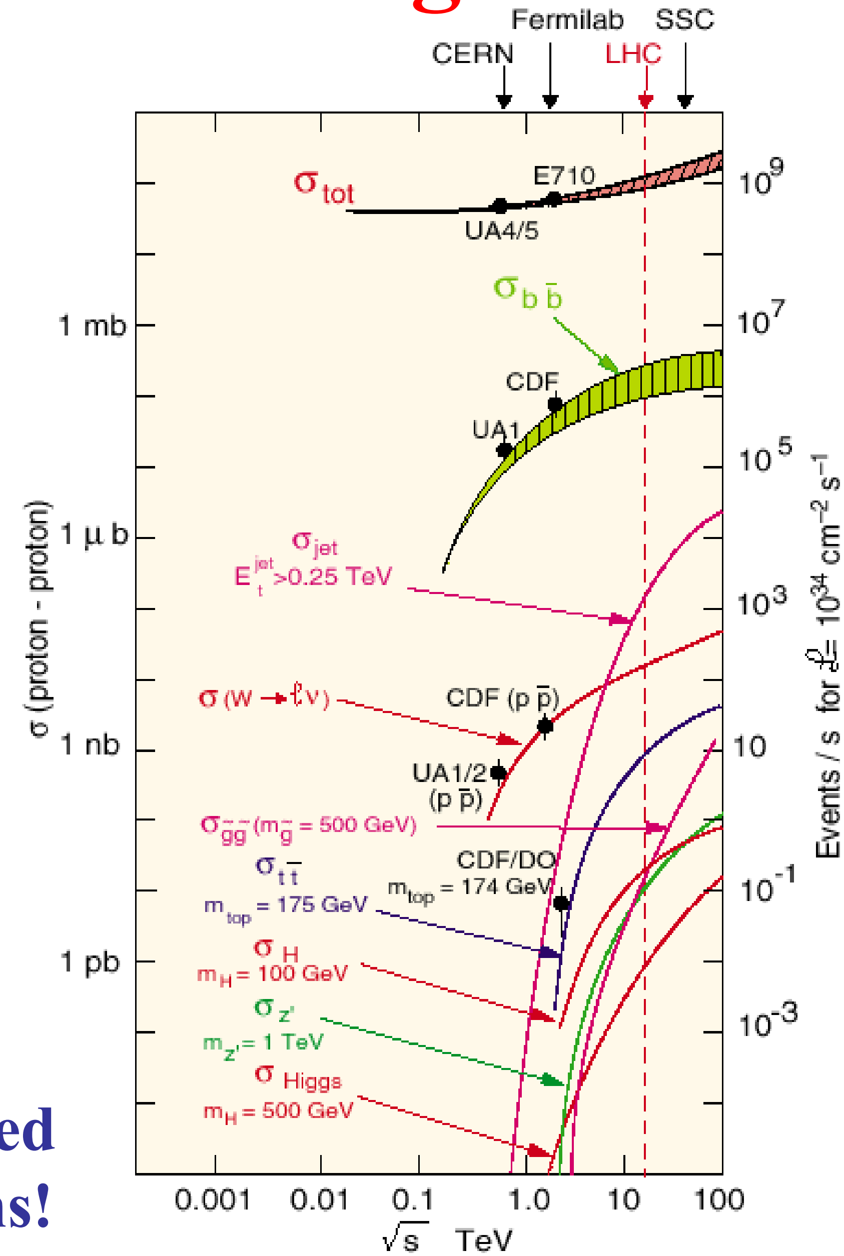

Selection power for Higgs discovery ≈ 10^{14-15}

i.e. 100 000 times better than achieved at Tevatron so far for high-p_T leptons!

Physics at the LHC: the challenge

LHC is a “factory” for top, W/Z, Higgs, SUSY, black holes ...

Expected event rates for representative (known and new) physics processes at “low” luminosity ($L=10^{33}$ cm^{-2} s^{-1}) in ATLAS/CMS

Process	Events/s	Events for 10 fb^{-1} (one year)	Total statistics collected elsewhere by 2008 (?)
$W \rightarrow e\nu$	30	10^8	10^4 LEP / 10^7 Tevatron
$Z \rightarrow ee$	3	10^7	10^6 LEP
Top	2	10^7	10^4 Tevatron
Beauty	10^6	$10^{12} - 10^{13}$	10^9 Belle/BaBar
H (m=130 GeV)	0.04	10^5	
Gluino (m= 1 TeV)	0.002	10^4	
Black holes m > 3 TeV	0.0002	10^3	

Physics at the LHC: the environment

What do we mean by particle reconstruction and identification at LHC?

Elementary constituents interact as such in "hard processes", namely:

Quarks and leptons as matter particles, and

Leptons	e (0.0005)	μ (0.105)	τ (1.777)
	ν_e	ν_μ	ν_τ
Quarks	u (< 0.005)	c (~ 1.25)	t (~ 175)
	d (< 0.005)	s (~ 0.1)	b (~ 4.2)

All masses in GeV

Gluons and EW bosons as gauge particles

Gluon(0) Colour octet	Photon (0)	W^+, W^- (80.42)	Z (91.188)

e, ν, γ : only rigorously stable particles

μ : at collider energies, do not decay in the detector

τ, c, b : Live long enough to travel a short distance, can see separated vertexes.

All other particles can only be seen through their stable decay products

Physics at the LHC: the environment

Which type of particles does one actually see in the final state?

LHC physics processes are dominated by strong interactions (QCD) :

- \+ **Jets : hard processes: quarks and gluons materialise as hadronic jets, which consist mostly of charged and neutral hadrons (pions, kaons, and to a lesser extent protons and neutrons, which at these energies can be all considered as stable).**
- \+ **"soup" : soft processes: non-perturbative QCD processes with soft gluons materialising as almost uniform soup of charged and neutral π, K, etc.**

- \+ **Heavy quarks with "long" lifetime are produced abundantly also**
- \+ **High-p_T (above ~ 10 GeV) leptons are produced mostly in c, b decays.**
- \+ **High-p_T isolated leptons may be found in fraction of J/ψ and Y decays**
- \+ **For p_T > 25 GeV, dominant source of high-p_T leptons: W/Z/tt decays**

Main challenge at LHC : **find e, γ, μ, τ, b amidst q/g soup**

Cross section, Luminosity, Reaction Rate

Fixed target experiment

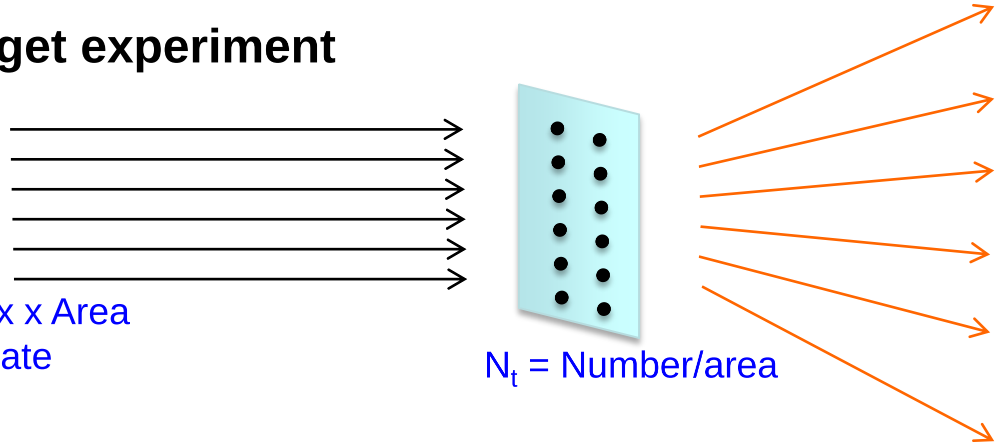

I_aA

Incident flux x Area
= Incident rate

N_t = Number/area

R = rate of reaction

$$R = I_a A N_t s$$

Collider experiment

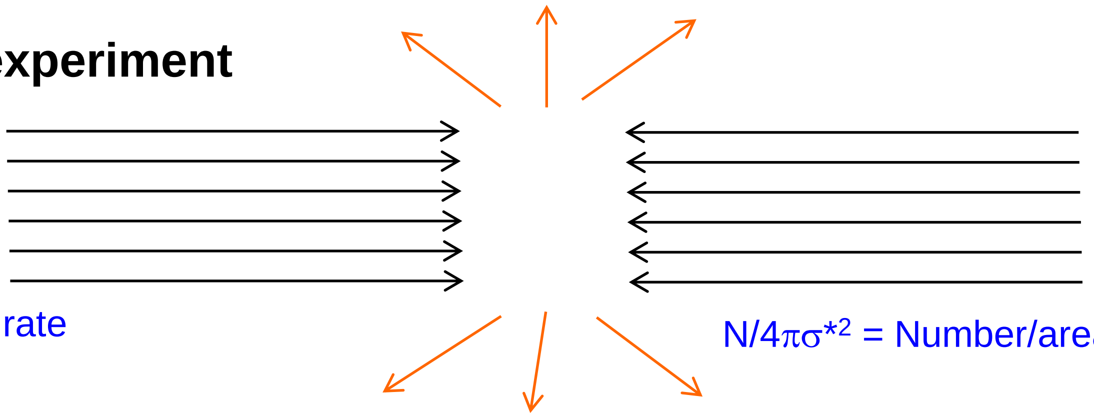

$Nf_{rev}n_b$

= Incident rate

$N/4\pi\sigma^{*2}$ = Number/area

R = rate of reaction

$$R = Ls$$

$$\mathcal{L} = \frac{N^2 f_{\text{rev}} n_b}{4\pi\sigma^{*2}}$$

Depends on f_{rev} revolution frequency
n_b number of bunches
N number of particles/bunch
σ^* beam size or rather overlap integral at IP

Luminosity

In scattering theory and accelerator physics, luminosity is the number of particles per unit area per unit time times the opacity of the target, usually expressed in cm−2 s−1. The integrated luminosity is the integral of the luminosity with respect to time. The luminosity is an important value to characterize the performance of an accelerator.

The following relations hold

$$\mathcal{L} = \frac{N^2 f_{\text{rev}}\, n_b}{4\pi\sigma^{*2}}$$

Depends on f_{rev} revolution frequency
n_b number of bunches
N number of particles/bunch
σ^* beam size or rather overlap integral at IP

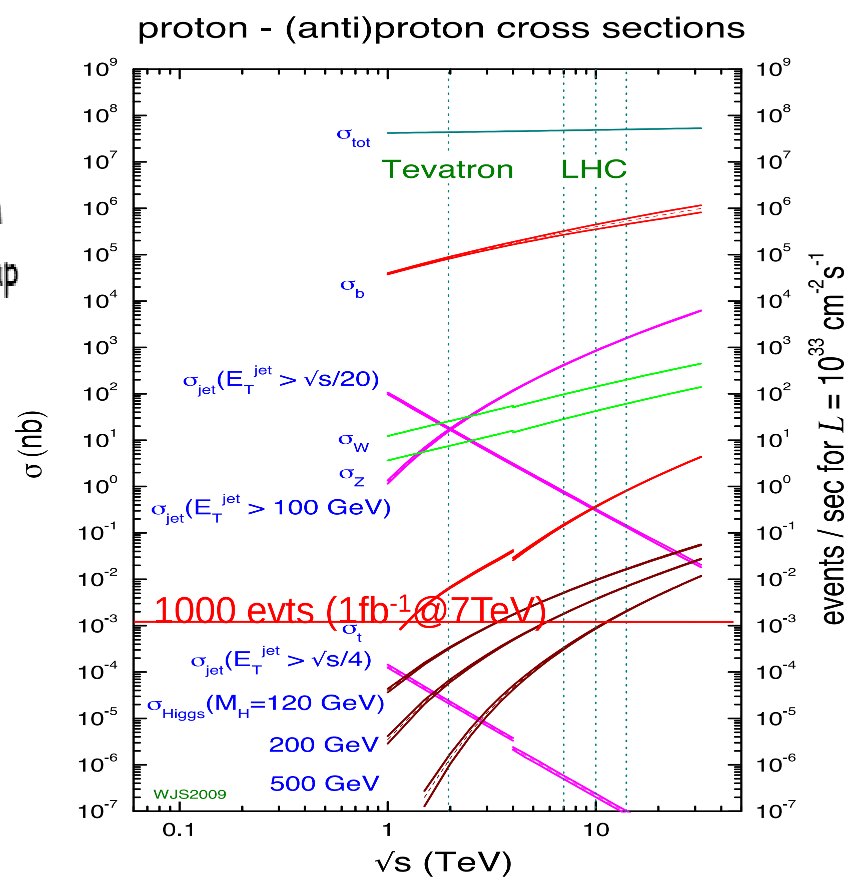

$$N = \sigma \int L \, dt$$ Number of measured events

$$\frac{dN}{dt} = L\sigma$$ Rate

$$\frac{d\sigma}{d\Omega} = \frac{1}{L}\frac{d^2N}{d\Omega\, dt}$$ Differential cross section

Luminosity measurements …

CMS/TOTEM and ATLAS forward detectors for forward physics, heavy ion, … and luminosity measurements … forward / high η physics (elastic scattering, diffractive processes …)

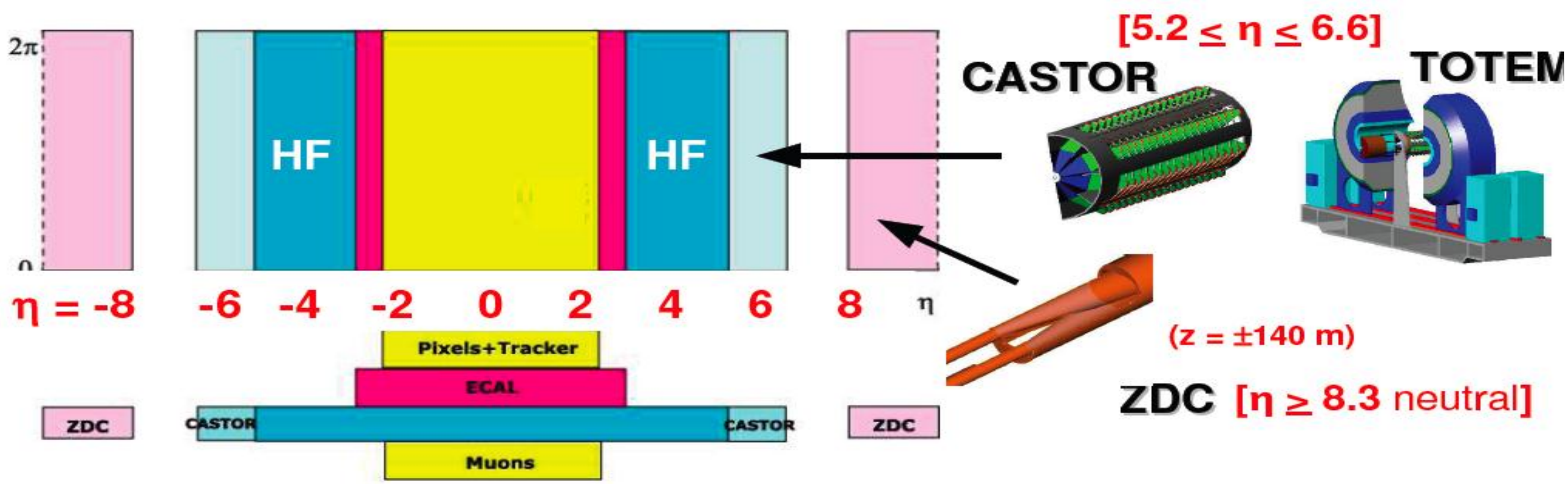

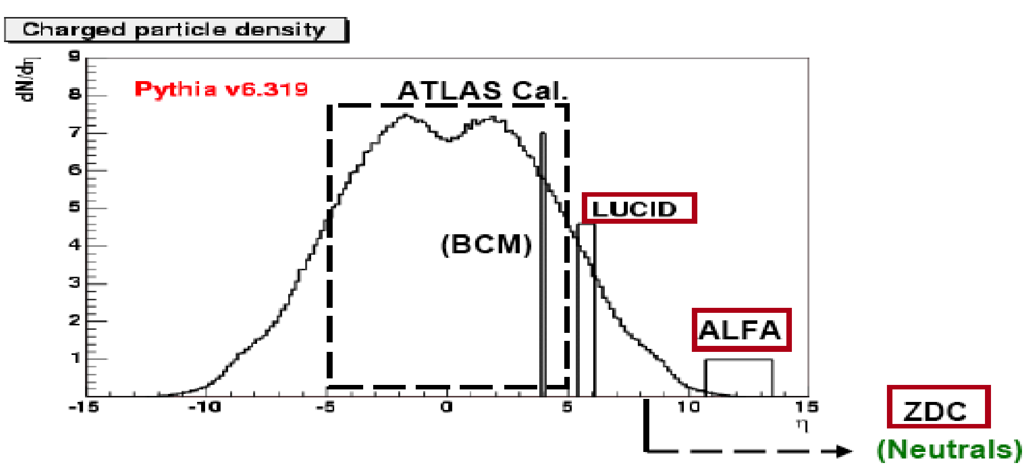

- Initially from machine parameters
  - Precision ~10-15%
- Medium term from physics processes: W/Z & $\mu\mu$/ee
  - Precision ~5-10%
- >= 2011 from Roman Pot detectors
  - Precision ~2-3%

Luminosity delivered to ATLAS since the beginning

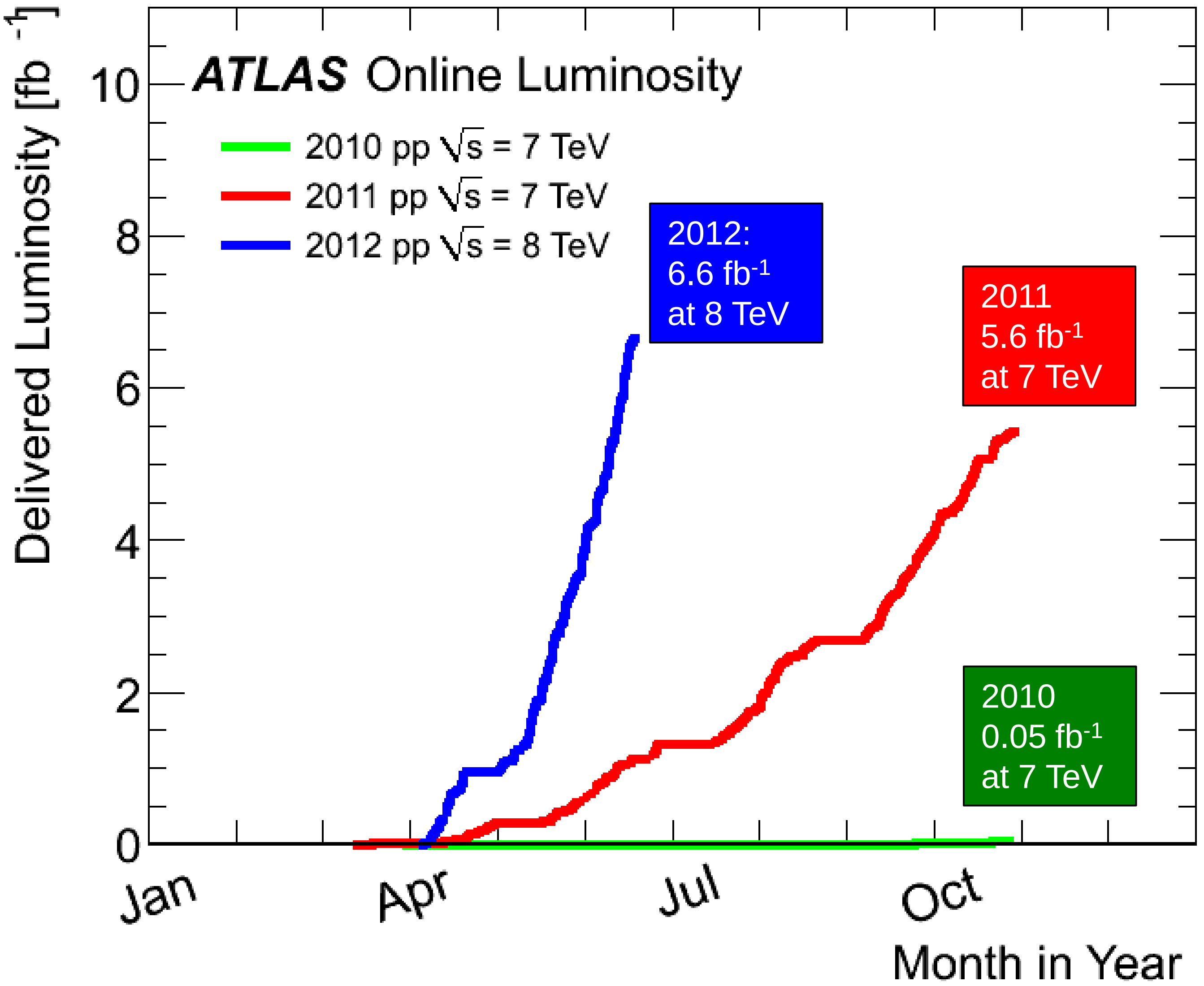

Physics at the LHC: the environment

Extract number of inelastic collisions per bunch crossing

$$\langle n \rangle = \sigma_{inel} \times L \times \Delta t / \varepsilon_{bunch}$$

LHC: $\langle n \rangle = 70 \text{ mb} \times 10^{34} \text{ cm}^{-2}\text{s}^{-1} \times 25 \text{ ns} / 0.8 = 23$

Big change compared to recent and current machines:

LEP:	$\Delta t = 22\ \mu s$	and	$\langle n \rangle \ll 1$
SppS:	$\Delta t = 3.3\ \mu s$	and	$\langle n \rangle \approx 3$
HERA:	$\Delta t = 96$ ns	and	$\langle n \rangle \ll 1$
Tevatron:	$\Delta t = 0.4\ \mu s$	and	$\langle n \rangle \approx 2$

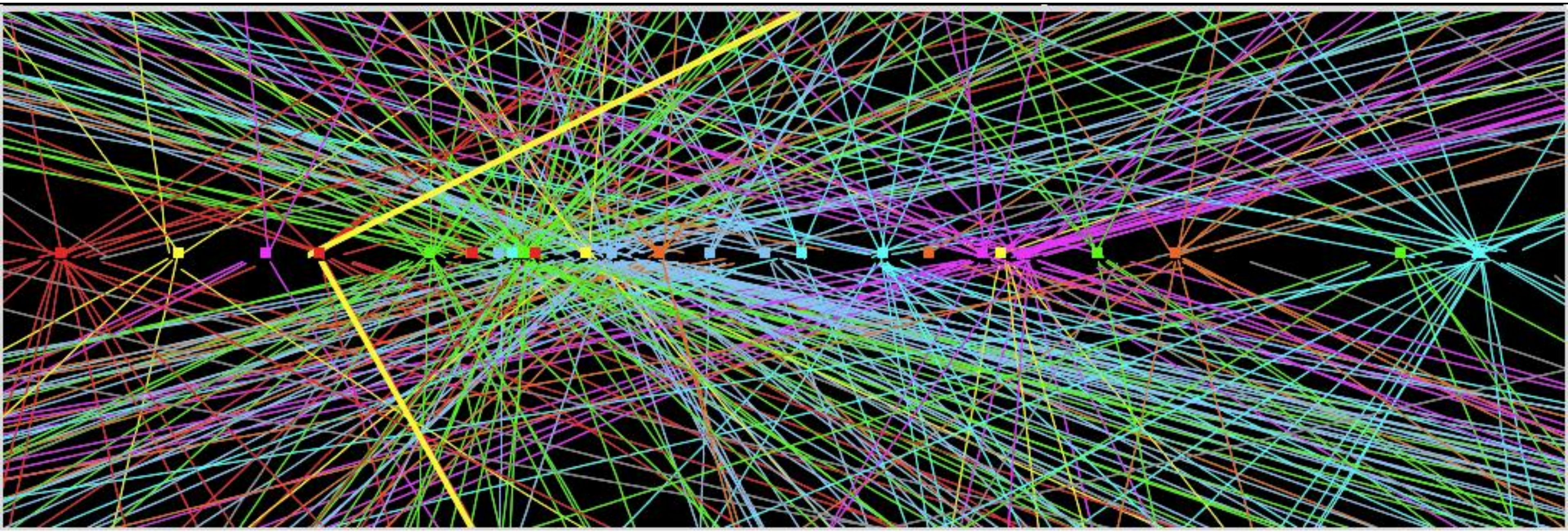

Rapidity, pseudo-rapidity

In experimental particle physics, pseudorapidity, η, is a commonly used spatial coordinate describing the angle of a particle relative to the beam axis. It is defined as

$$\eta = -\ln\left[\tan\left(\frac{\theta}{2}\right)\right],$$

where θ is the angle between the particle momentum p and the beam axis. In terms of the momentum, the pseudorapidity variable can be written as

$$\eta = \frac{1}{2}\ln\left(\frac{|\vec{p}|+p_L}{|\vec{p}|-p_L}\right),$$

In the limit where the particle is travelling close to the speed of light, or in the approximation that the mass of the particle is nearly zero, pseudorapidity is numerically close to the experimental particle physicist's definition of rapidity,

$$y = \frac{1}{2}\ln\left(\frac{E+p_L}{E-p_L}\right)$$

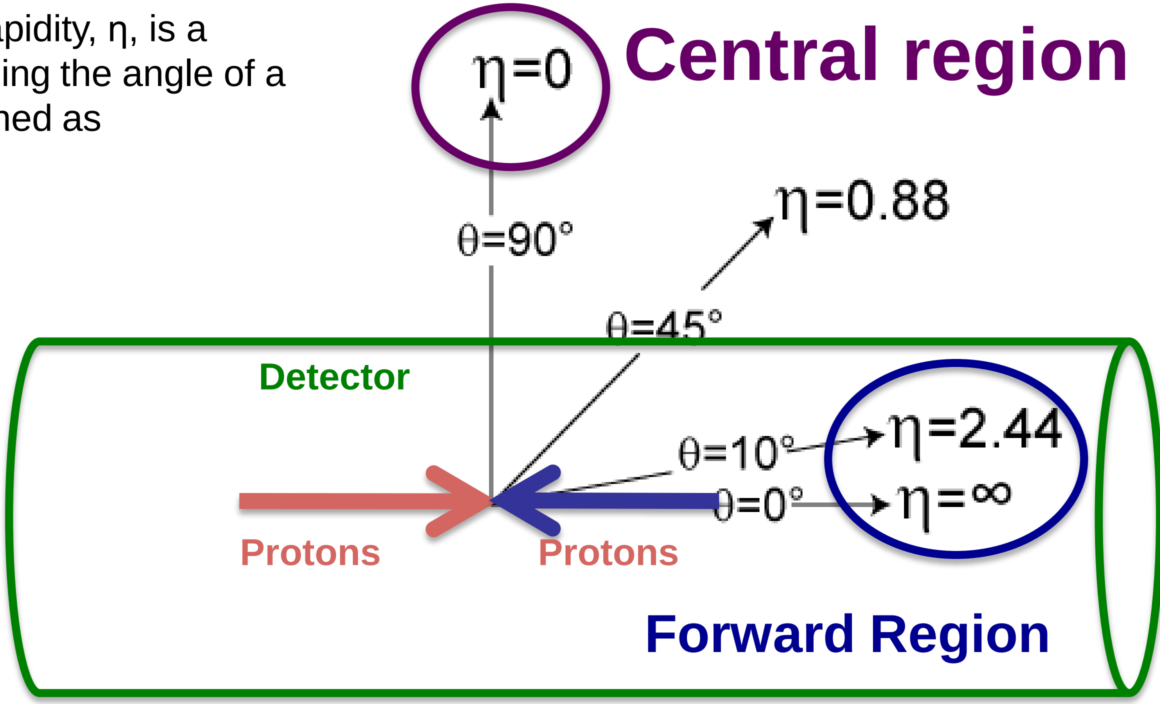

In hadron collider physics, the rapidity (or pseudorapidity) is preferred over the polar angle θ because, loosely speaking, particle production is constant as a function of rapidity. One speaks of the forward direction in a hadron collider experiment, which refers to regions of the detector that are close to the beam axis, at high |η|.

Physics at the LHC: the environment

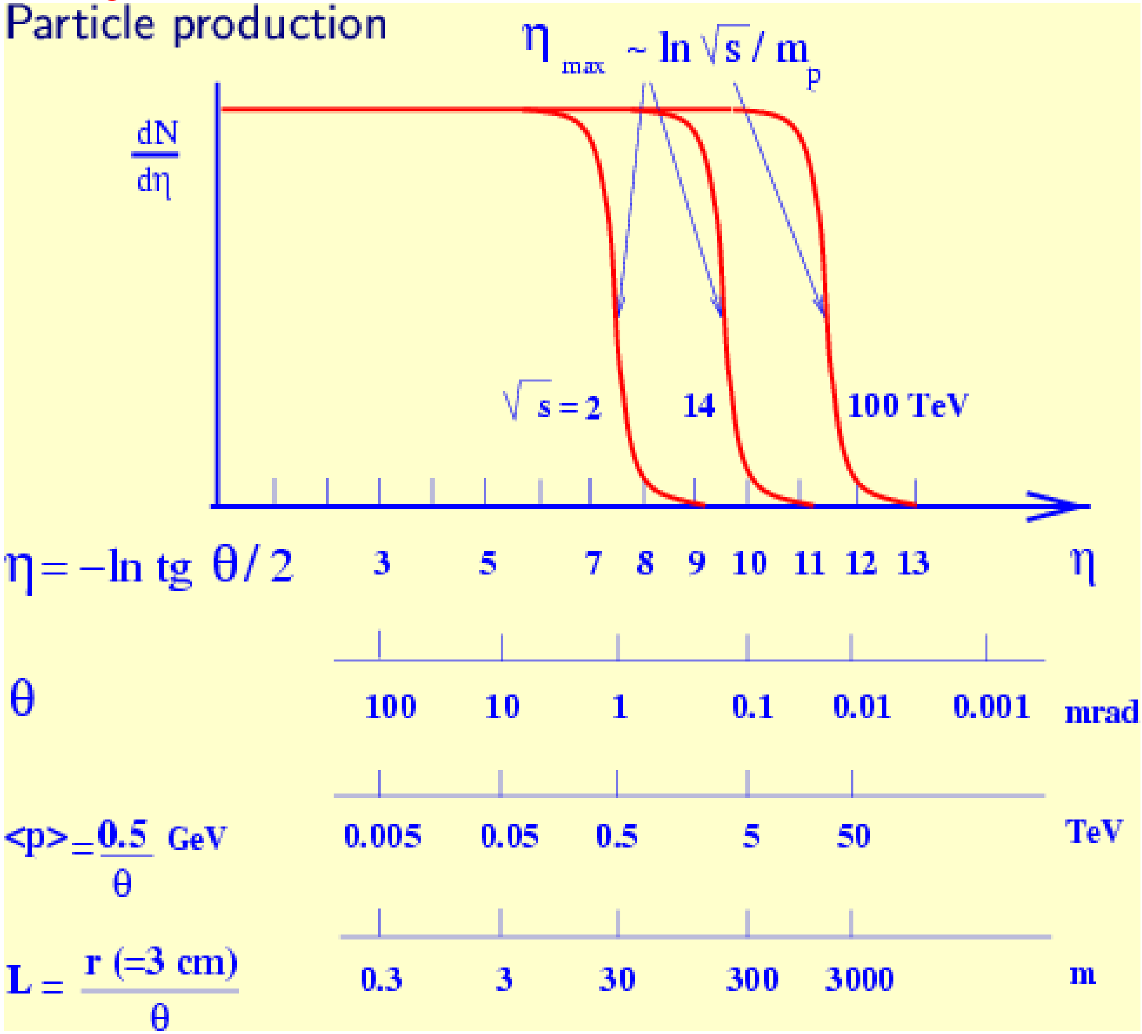

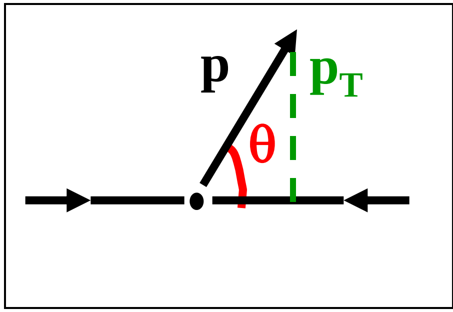

+ $d\sigma/dp_T dy$ is Lorentz-invariant

+$\eta = y$ for $m \approx 0$

+Physics is ~ constant versus η at fixed p_T

ATLAS/CMS: from design to reality

One word about neutrinos in hadron colliders:

- ✓ since most of the energy of the colliding protons escapes down the beam pipe, one can only use the energy-momentum balance in the transverse plane

→ concepts such as E_T^{miss}, missing transverse momentum and mass are often used (only missing component is E_z^{miss})

→ reconstruct "fully" certain topologies with neutrinos, e.g. $W \rightarrow l\nu$ and even better $H \rightarrow \tau\tau \rightarrow l\nu_l\nu_\tau\ h\nu_\tau$

- ✓ the detector must therefore be quite hermetic

→ transverse energy flow fully measured with reasonable accuracy

→ no neutrino escapes undetected

→ no human enters without major effort (fast access to some parts of ATLAS/CMS quite difficult)

Isolation

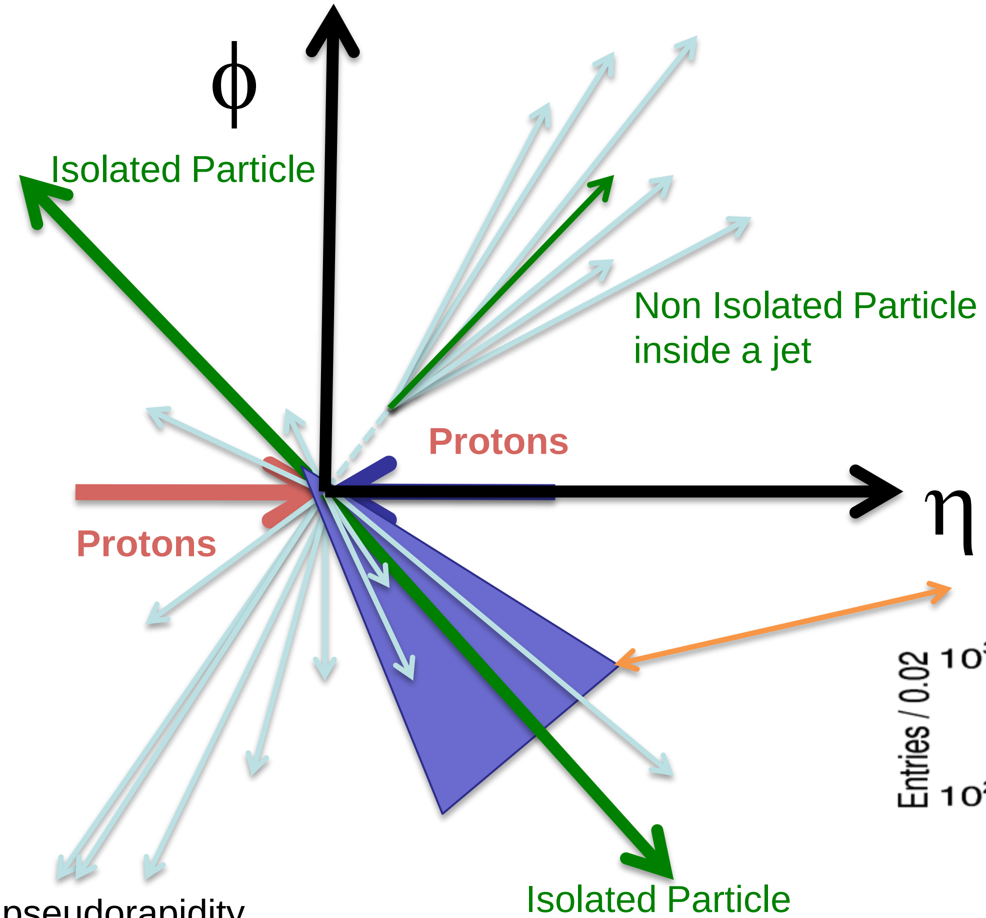

Isolation: track density or energy deposit in the vicinity of a particle of Interest. Important for Particle identification because Isolated particles are easier to Indentify.

The vicinity: $\Delta R = \sqrt{(\Delta\eta^2 + \Delta\phi^2)}$

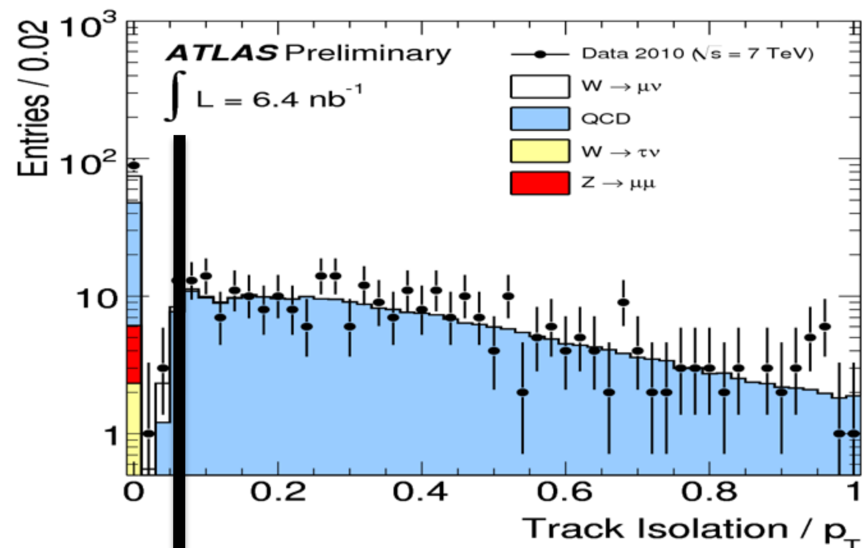

η= pseudorapidity
ϕ= azimuthal angle
p_T= transverse momentum= $\sqrt{(p_X^2+p_Y^2)}$
p_Z or p_L = longitudinal momentum
4-momentum (p_X, p_Y, p_Z, E)

Track Isolation: summed p_T of tracks in the specified ΔR
Calo isolation: summed calorimeter energy deposits in ΔR

An example from the ATLAS detector

Reconstruction of a 2e2μ candidate for the Higgs boson - with $m_{2e2\mu}$= 123.9 GeV

We need to understand the interaction of particles with matter in order to understand the design and operation of this detector, and the analysis of the data.

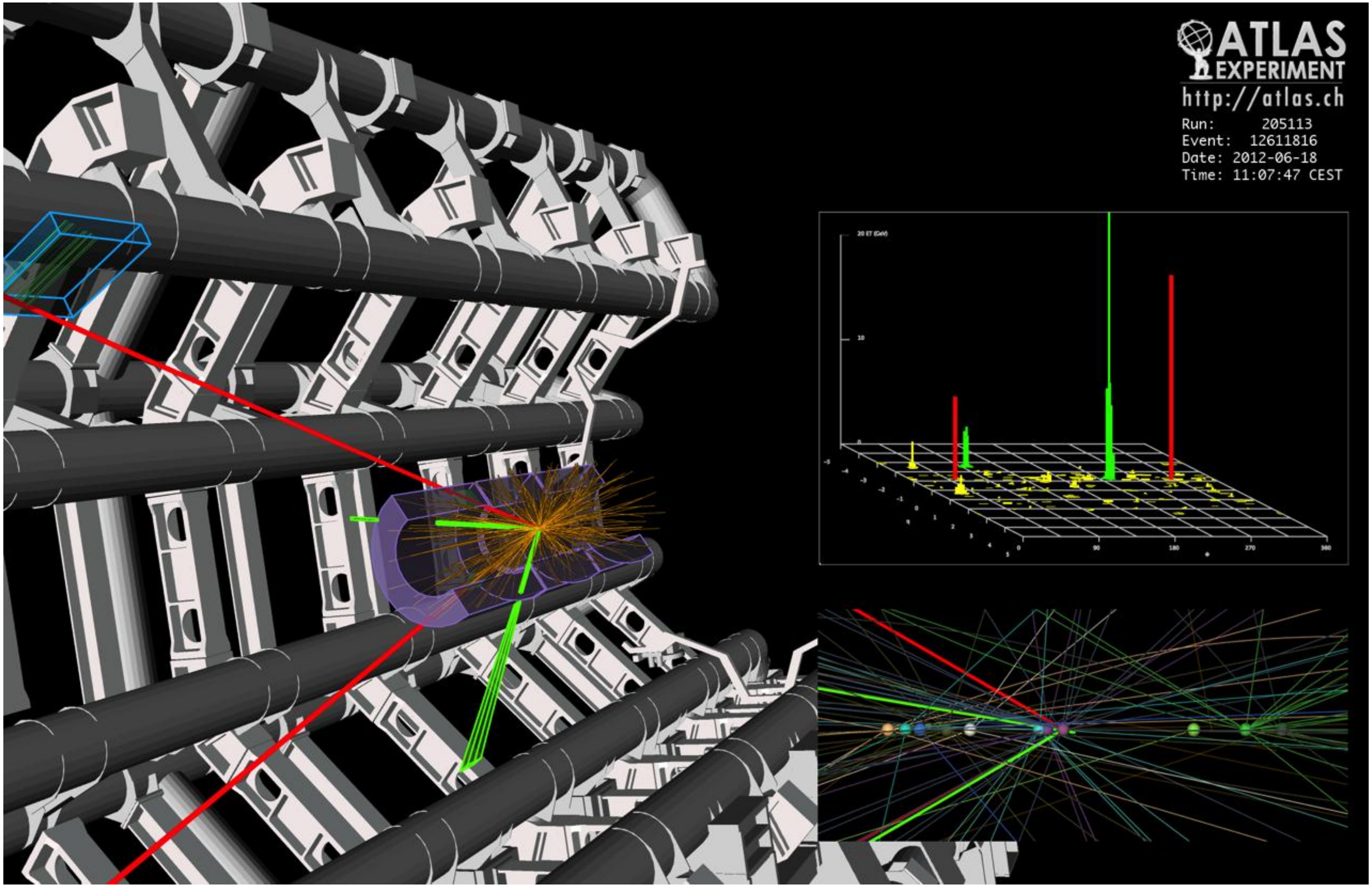

The ATLAS Inner Detector (barrel)

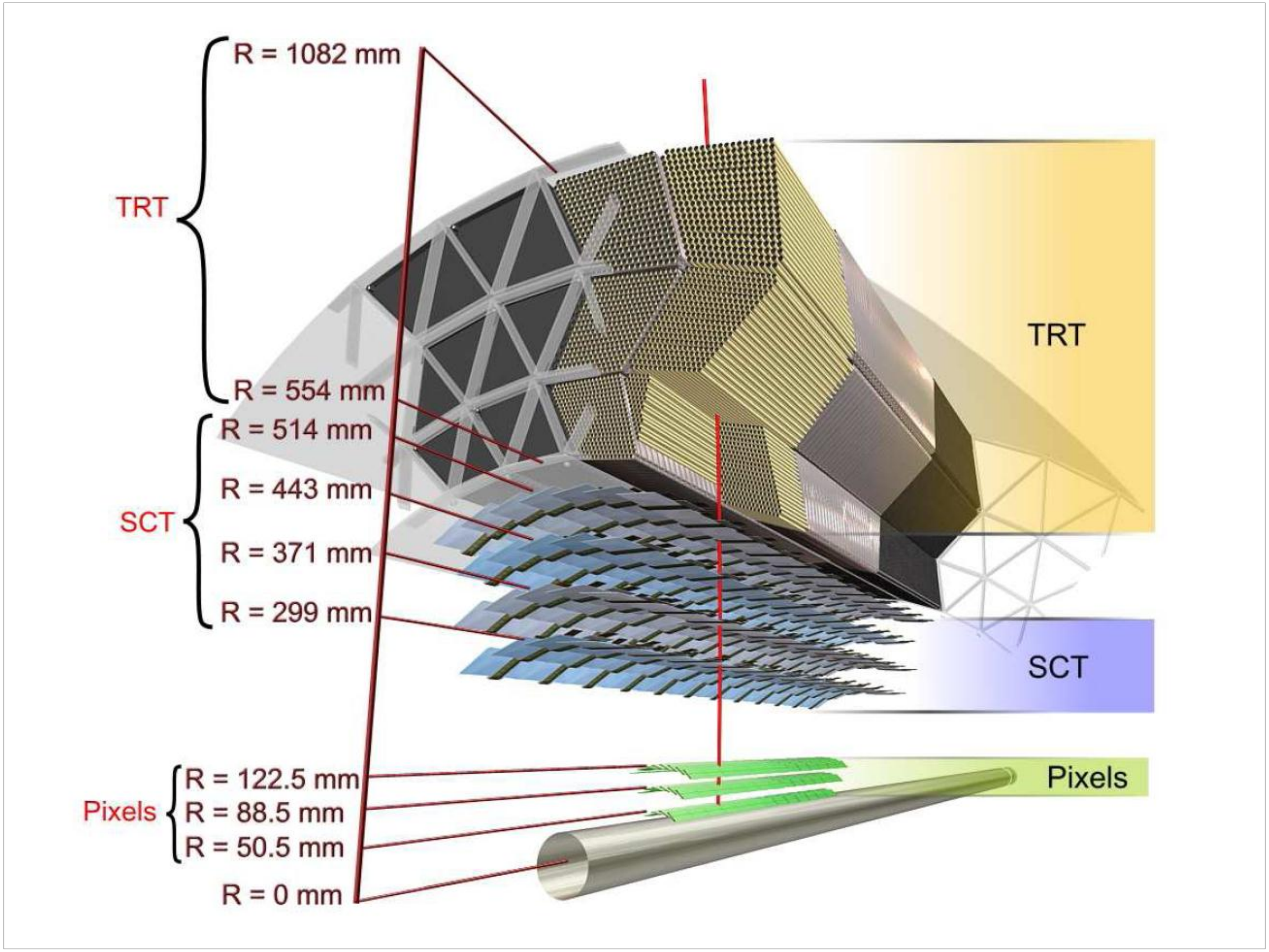

The ATLAS Inner Detector (one end-cap)

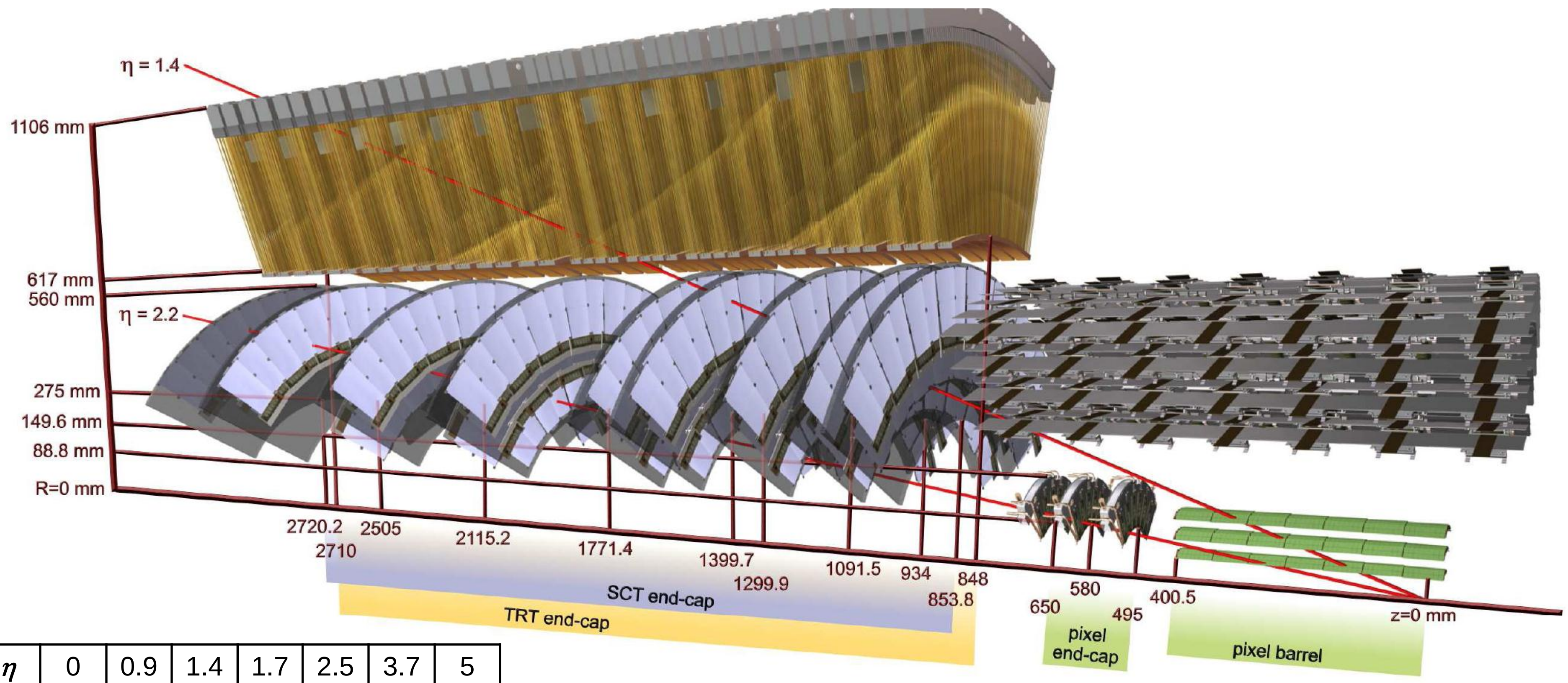

η	0	0.9	1.4	1.7	2.5	3.7	5
θ	90°	44°	28°	21°	9.4°	2.8°	0.8°

ATLAS Inner Detector

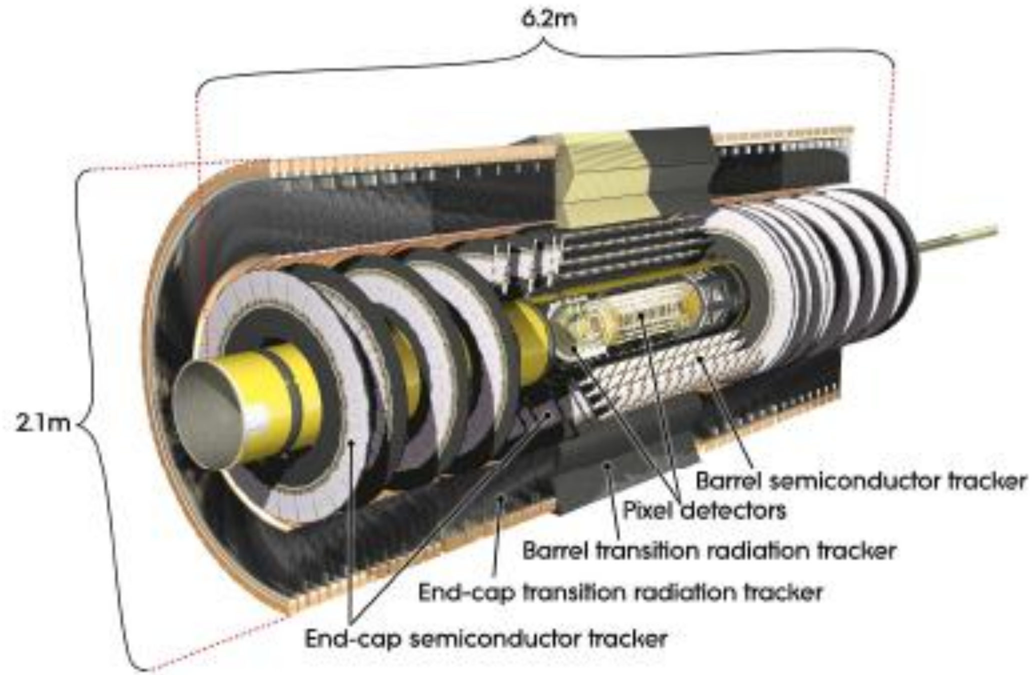

Figure 1.2: Cut-away view of the ATLAS inner detector.

Table 1.2: Main parameters of the inner-detector system.

Item		Radial extension (mm)	Length (mm)
Overall ID envelope		$0 < R < 1150$	$0 < \|z\| < 3512$
Beam-pipe		$29 < R < 36$	
Pixel	Overall envelope	$45.5 < R < 242$	$0 < \|z\| < 3092$
3 cylindrical layers	Sensitive barrel	$50.5 < R < 122.5$	$0 < \|z\| < 400.5$
2 × 3 disks	Sensitive end-cap	$88.8 < R < 149.6$	$495 < \|z\| < 650$
SCT	Overall envelope	$255 < R < 549$ (barrel)	$0 < \|z\| < 805$
		$251 < R < 610$ (end-cap)	$810 < \|z\| < 2797$
4 cylindrical layers	Sensitive barrel	$299 < R < 514$	$0 < \|z\| < 749$
2 × 9 disks	Sensitive end-cap	$275 < R < 560$	$839 < \|z\| < 2735$
TRT	Overall envelope	$554 < R < 1082$ (barrel)	$0 < \|z\| < 780$
		$617 < R < 1106$ (end-cap)	$827 < \|z\| < 2744$
73 straw planes	Sensitive barrel	$563 < R < 1066$	$0 < \|z\| < 712$
160 straw planes	Sensitive end-cap	$644 < R < 1004$	$848 < \|z\| < 2710$

1.2 Tracking

Approximately 1000 particles will emerge from the collision point every 25 ns within $|\eta| < 2.5$, creating a very large track density in the detector. To achieve the momentum and vertex resolution requirements imposed by the benchmark physics processes, high-precision measurements must be made with fine detector granularity. Pixel and silicon microstrip (SCT) trackers, used in conjunction with the straw tubes of the Transition Radiation Tracker (TRT), offer these features.

The Inner Detector is immersed in 2T magnetic field generated by a central Solenoid which extends over a length of 5.3 m with a diameter of 2.5 m

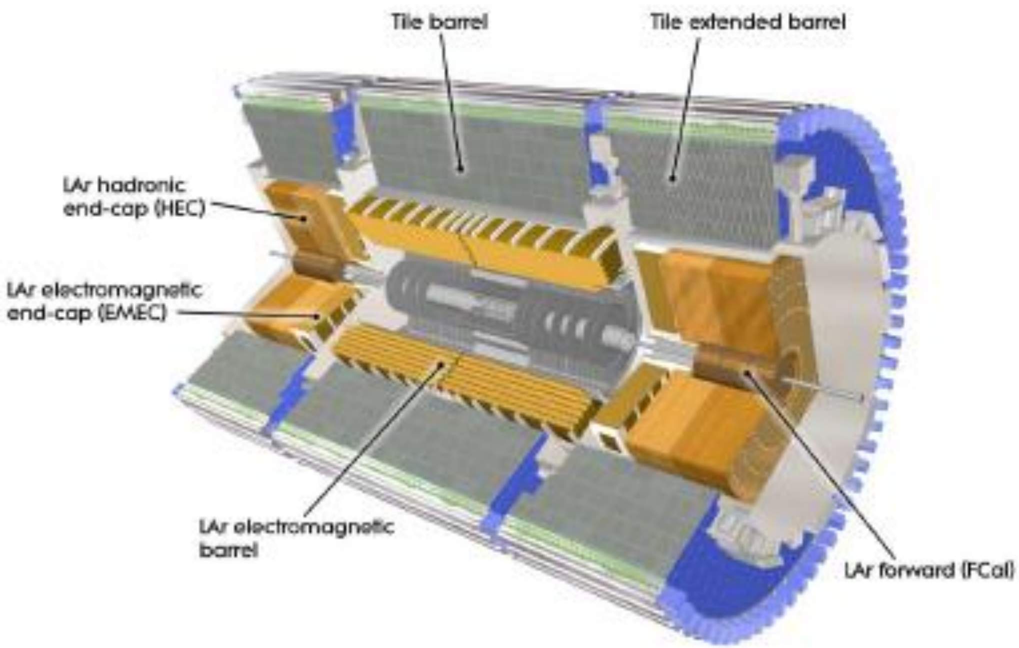

Figure 1.3: Cut-away view of the ATLAS calorimeter system.

A view of the sampling calorimeters is presented in figure 1.3, and the pseudorapidity coverage, granularity, and segmentation in depth of the calorimeters are summarised in table 1.3 (see also chapter 5). These calorimeters cover the range $|\eta| < 4.9$, using different techniques suited to the widely varying requirements of the physics processes of interest and of the radiation environment over this large η-range. Over the η region matched to the inner detector, the fine granularity of the EM calorimeter is ideally suited for precision measurements of electrons and photons. The coarser granularity of the rest of the calorimeter is sufficient to satisfy the physics requirements for jet reconstruction and E_T^{miss} measurements.

Table 1.3: Main parameters of the calorimeter system.

	Barrel		End-cap	
EM calorimeter				
Number of layers and $\|\eta\|$ coverage				
Presampler	1	$\|\eta\| < 1.52$	1	$1.5 < \|\eta\| < 1.8$
Calorimeter	3	$\|\eta\| < 1.35$	2	$1.375 < \|\eta\| < 1.5$
	2	$1.35 < \|\eta\| < 1.475$	3	$1.5 < \|\eta\| < 2.5$
			2	$2.5 < \|\eta\| < 3.2$
Granularity $\Delta\eta \times \Delta\phi$ versus $\|\eta\|$				
Presampler	0.025×0.1	$\|\eta\| < 1.52$	0.025×0.1	$1.5 < \|\eta\| < 1.8$
Calorimeter 1st layer	$0.025/8 \times 0.1$	$\|\eta\| < 1.40$	0.050×0.1	$1.375 < \|\eta\| < 1.425$
	0.025×0.025	$1.40 < \|\eta\| < 1.475$	0.025×0.1	$1.425 < \|\eta\| < 1.5$
			$0.025/8 \times 0.1$	$1.5 < \|\eta\| < 1.8$
			$0.025/6 \times 0.1$	$1.8 < \|\eta\| < 2.0$
			$0.025/4 \times 0.1$	$2.0 < \|\eta\| < 2.4$
			0.025×0.1	$2.4 < \|\eta\| < 2.5$
			0.1×0.1	$2.5 < \|\eta\| < 3.2$
Calorimeter 2nd layer	0.025×0.025	$\|\eta\| < 1.40$	0.050×0.025	$1.375 < \|\eta\| < 1.425$
	0.075×0.025	$1.40 < \|\eta\| < 1.475$	0.025×0.025	$1.425 < \|\eta\| < 2.5$
			0.1×0.1	$2.5 < \|\eta\| < 3.2$
Calorimeter 3rd layer	0.050×0.025	$\|\eta\| < 1.35$	0.050×0.025	$1.5 < \|\eta\| < 2.5$
Number of readout channels				
Presampler	7808		1536 (both sides)	
Calorimeter	101760		62208 (both sides)	
LAr hadronic end-cap				
$\|\eta\|$ coverage			$1.5 < \|\eta\| < 3.2$	
Number of layers			4	
Granularity $\Delta\eta \times \Delta\phi$			0.1×0.1	$1.5 < \|\eta\| < 2.5$
			0.2×0.2	$2.5 < \|\eta\| < 3.2$
Readout channels			5632 (both sides)	
LAr forward calorimeter				
$\|\eta\|$ coverage			$3.1 < \|\eta\| < 4.9$	
Number of layers			3	
Granularity $\Delta x \times \Delta y$ (cm)			FCal1: 3.0×2.6	$3.15 < \|\eta\| < 4.30$
			FCal1: $\sim$ four times finer	$3.10 < \|\eta\| < 3.15$,
				$4.30 < \|\eta\| < 4.83$
			FCal2: 3.3×4.2	$3.24 < \|\eta\| < 4.50$
			FCal2: $\sim$ four times finer	$3.20 < \|\eta\| < 3.24$,
				$4.50 < \|\eta\| < 4.81$
			FCal3: 5.4×4.7	$3.32 < \|\eta\| < 4.60$
			FCal3: $\sim$ four times finer	$3.29 < \|\eta\| < 3.32$,
				$4.60 < \|\eta\| < 4.75$
Readout channels			3524 (both sides)	
Scintillator tile calorimeter				
	Barrel		Extended barrel	
$\|\eta\|$ coverage	$\|\eta\| < 1.0$		$0.8 < \|\eta\| < 1.7$	
Number of layers	3		3	
Granularity $\Delta\eta \times \Delta\phi$	0.1×0.1		0.1×0.1	
Last layer	0.2×0.1		0.2×0.1	
Readout channels	5760		4092 (both sides)	

Muon Spectrometer

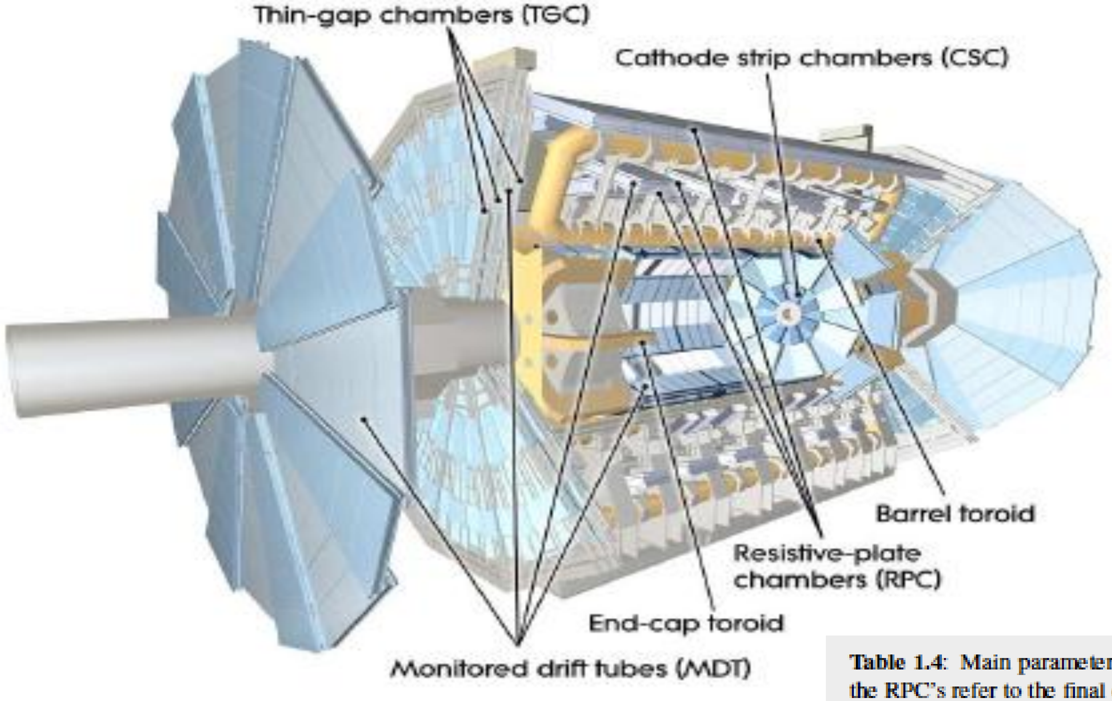

Table 1.4: Main parameters of the muon spectrometer. Numbers in brackets for the MDT's and the RPC's refer to the final configuration of the detector in 2009.

Monitored drift tubes	**MDT**
- Coverage	$\|\eta\| < 2.7$ (innermost layer: $\|\eta\| < 2.0$)
- Number of chambers	1088 (1150)
- Number of channels	339 000 (354 000)
- Function	Precision tracking
Cathode strip chambers	**CSC**
- Coverage	$2.0 < \|\eta\| < 2.7$
- Number of chambers	32
- Number of channels	31 000
- Function	Precision tracking
Resistive plate chambers	**RPC**
- Coverage	$\|\eta\| < 1.05$
- Number of chambers	544 (606)
- Number of channels	359 000 (373 000)
- Function	Triggering, second coordinate
Thin gap chambers	**TGC**
- Coverage	$1.05 < \|\eta\| < 2.7$ (2.4 for triggering)
- Number of chambers	3588
- Number of channels	318 000
- Function	Triggering, second coordinate

The conceptual layout of the muon spectrometer is shown in figure 1.4 and the main parameters of the muon chambers are listed in table 1.4 (see also chapter 6). It is based on the magnetic deflection of muon tracks in the large superconducting air-core toroid magnets, instrumented with separate trigger and high-precision tracking chambers. Over the range $|\eta| < 1.4$, magnetic bending is provided by the large barrel toroid. For $1.6 < |\eta| < 2.7$, muon tracks are bent by two smaller end-cap magnets inserted into both ends of the barrel toroid. Over $1.4 < |\eta| < 1.6$, usually referred to as the transition region, magnetic deflection is provided by a combination of barrel and end-cap fields. This magnet configuration provides a field which is mostly orthogonal to the muon trajectories, while minimising the degradation of resolution due to multiple scattering. The anticipated high level of particle flux has had a major impact on the choice and design of the spectrometer instrumentation, affecting performance parameters such as rate capability, granularity, ageing properties, and radiation hardness.

Particle ID and Kinematics

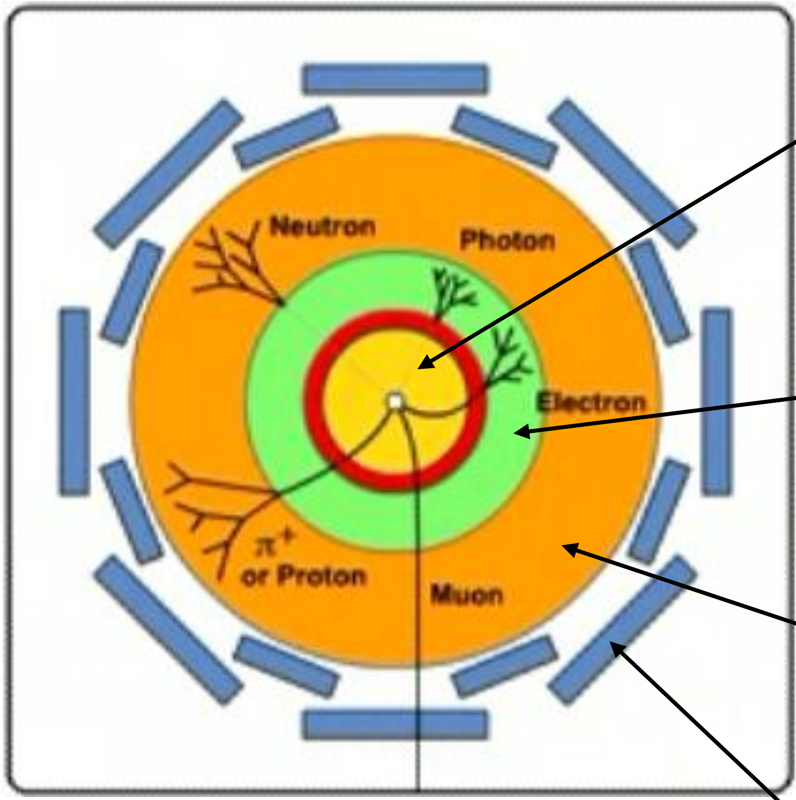

Tracking detector

−Measure charge and momentum of charged particles in magnetic field

Electro-magnetic calorimeter

−Measure energy of electrons, positrons and photons

Hadronic calorimeter

−Measure energy of hadrons (particles containing quarks), such as protons, neutrons, pions, etc.

Muon detector

−Measure charge and momentum of muons

Neutrinos are only detected indirectly via 'missing energy' not recorded in the calorimeters

Alignment

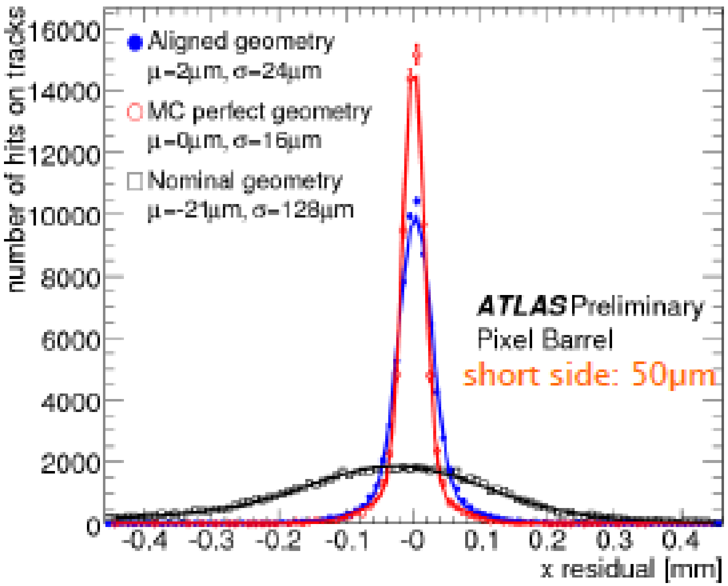

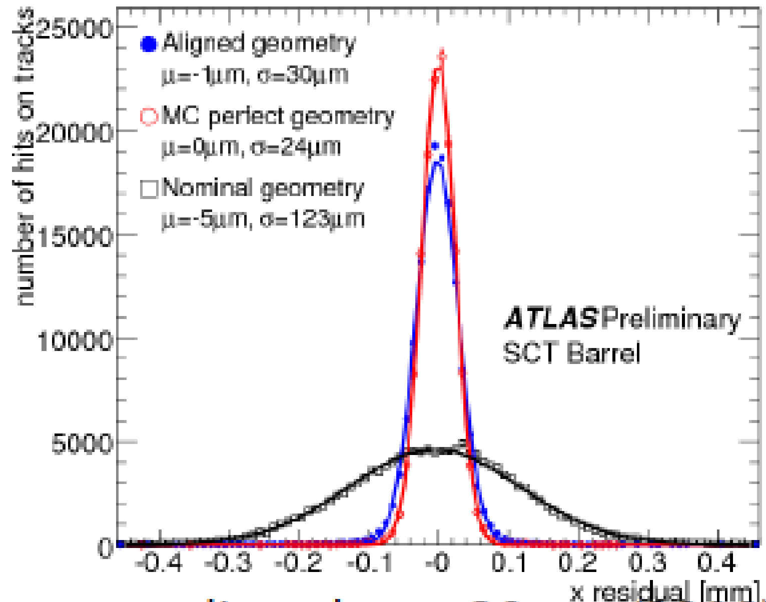

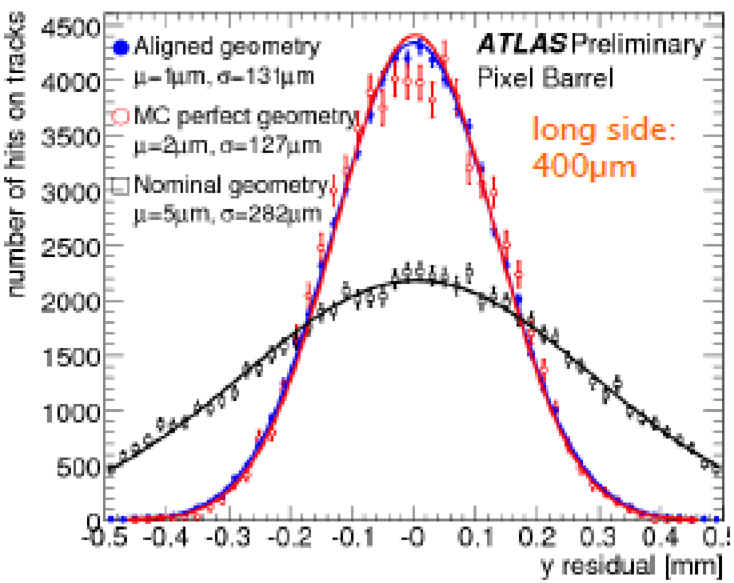

➔ Si detectors aligned at ≲ 20 µm (2008)

➔ stable in 2009

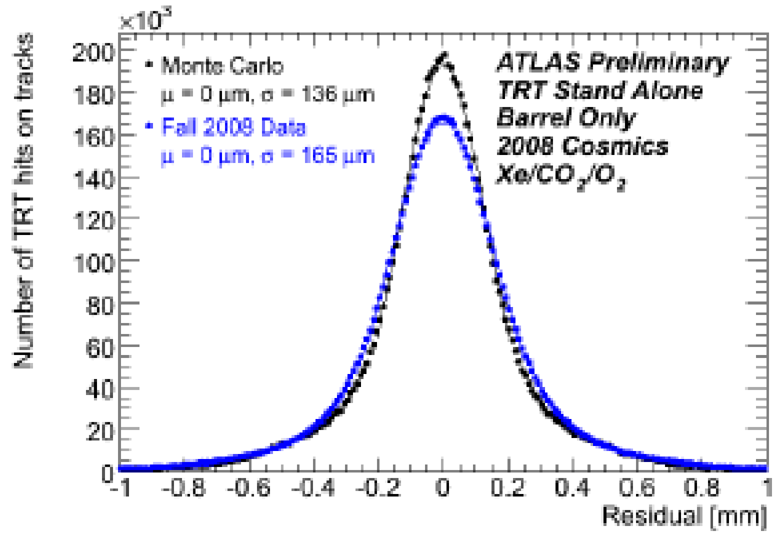

Laurent Vacavant

Materials in the front of the ATLAS calorimeter

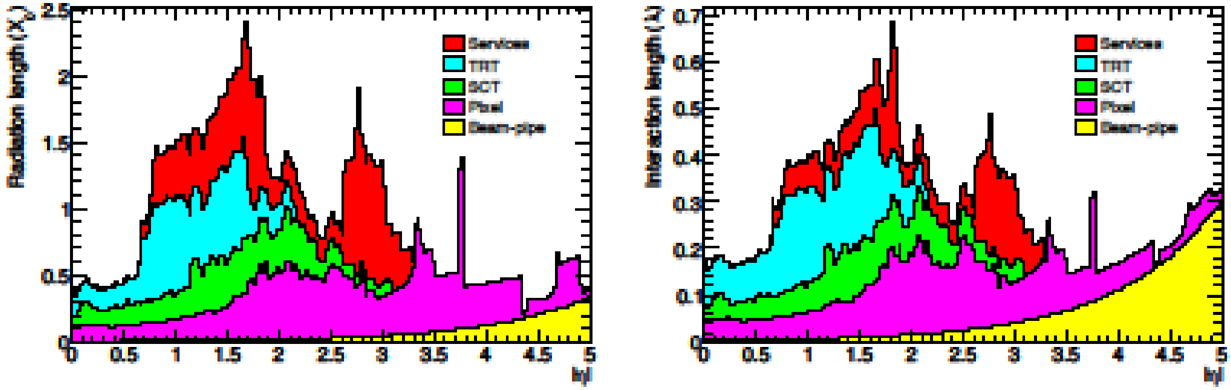

Figure 4.45: Material distribution (X_0, λ) at the exit of the ID envelope, including the services and thermal enclosures. The distribution is shown as a function of $|\eta|$ and averaged over ϕ. The break-down indicates the contributions of external services and of individual sub-detectors, including services in their active volume.

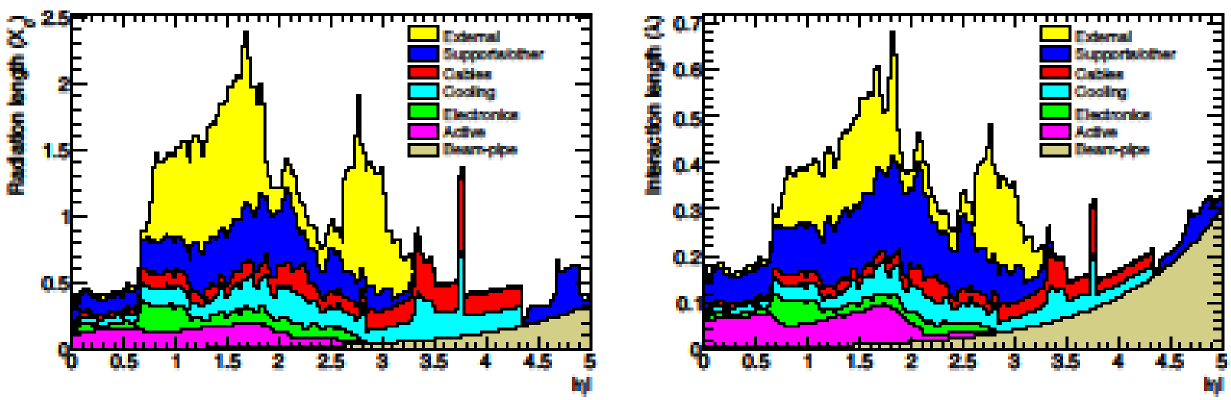

Figure 4.46: Material distribution (X_0, λ) at the exit of the ID envelope, including the services and thermal enclosures. The distribution is shown as a function of $|\eta|$ and averaged over ϕ. The breakdown shows the contributions of different ID components, independent of the sub-detector.

Electron identification: Track/Cluster matching

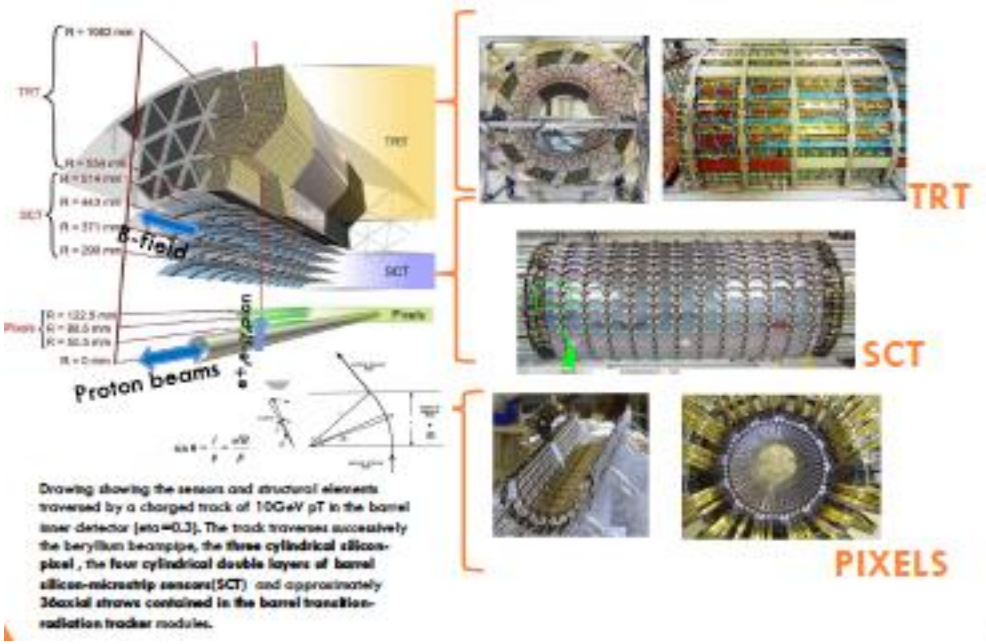

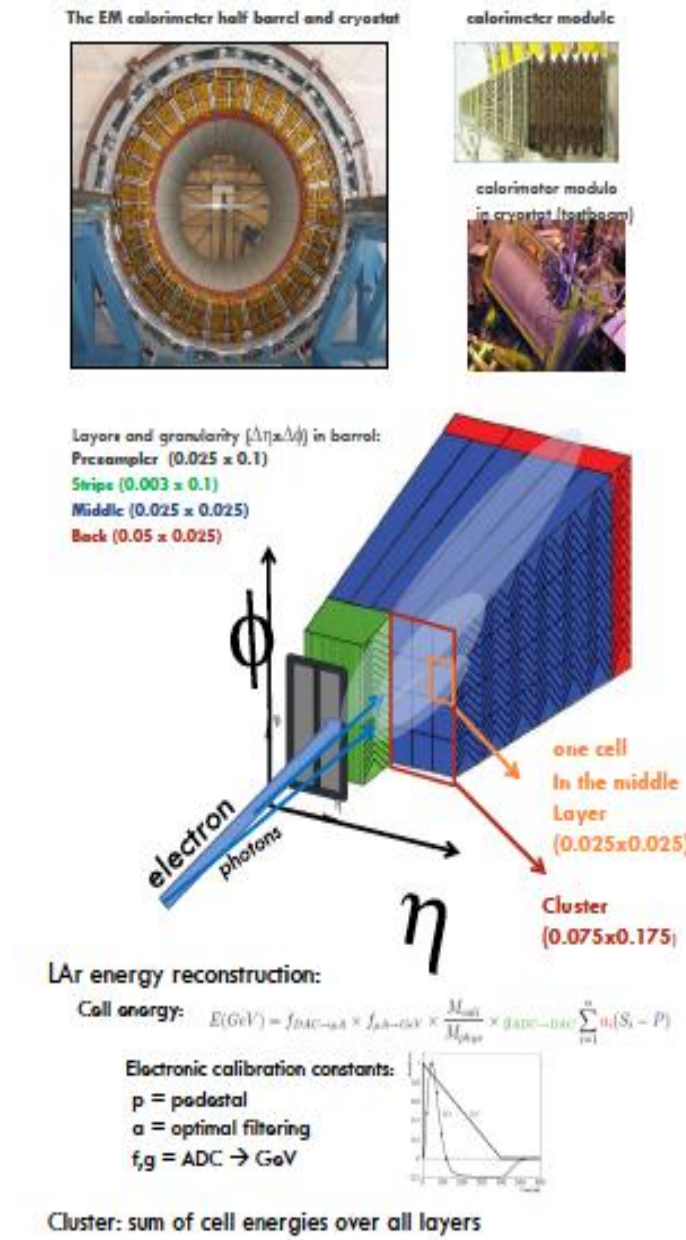

Electron = track in the Inner Detector (direction measurement)
Matched to an EM cluster in the calorimeter (energy measurement). Need to know:

- material distribution in the Inner detector in the front of the EM calorimeter
- calibration of the energy response of the calorimeter
- rejection against jet faking electrons

Electron identification

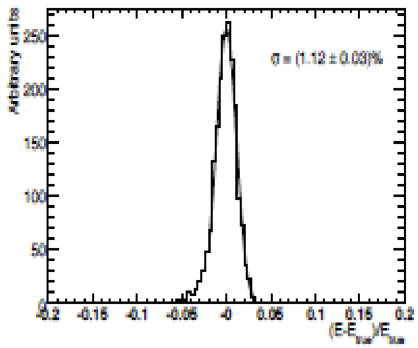

Figure 10.46: Difference between measured and true energy normalised to true energy for electrons with an energy of 100 GeV at $\eta = 0.325$.

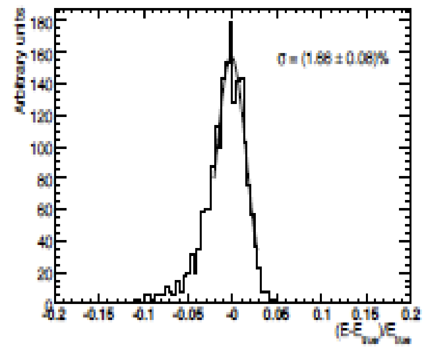

Figure 10.47: Difference between measured and true energy normalised to true energy for electrons with an energy of 100 GeV at $\eta = 1.075$.

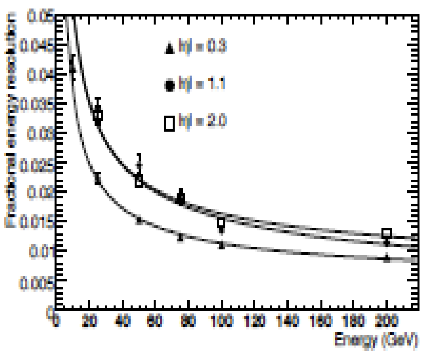

Figure 10.50: Expected relative energy resolution as a function of energy for electrons at $|\eta| = 0.3$, 1.1, and 2.0. The curves represent fits to the points at the same $|\eta|$ by a function containing a stochastic term, a constant term and a noise term.

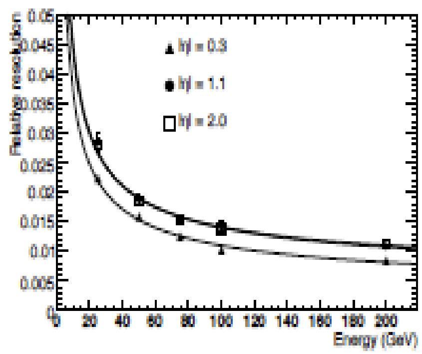

Figure 10.51: Expected relative energy resolution as a function of energy for photons at $|\eta| = 0.3$, 1.1, and 2.0. The curves represent fits to the points at the same η by a function containing a stochastic term, a constant term and a noise term.

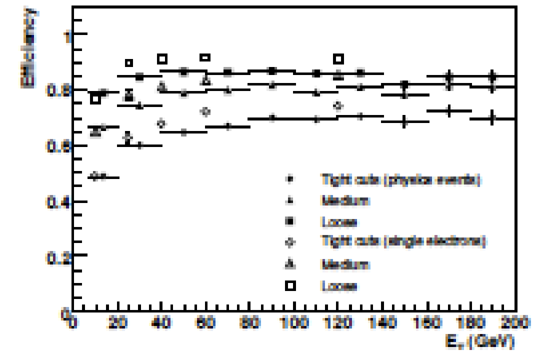

Figure 10.56: Overall reconstruction and identification efficiency of various levels of electron cuts: loose, medium, and tight isol. as a function of E_T for single electrons (open symbols) and for isolated electrons in a sample of physics events with a busy environment (full symbols).

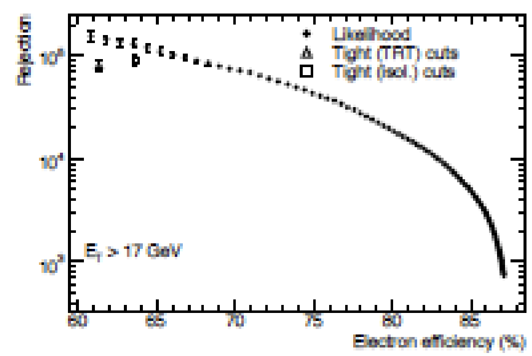

Figure 10.57: Jet rejection as a function of overall reconstruction and identification efficiency for electrons, as obtained using a likelihood method (full circles). The results obtained with the standard cut-based method are also shown in the case of tight TRT (open triangle) and tight isol. (open square) cuts.

Photon identification

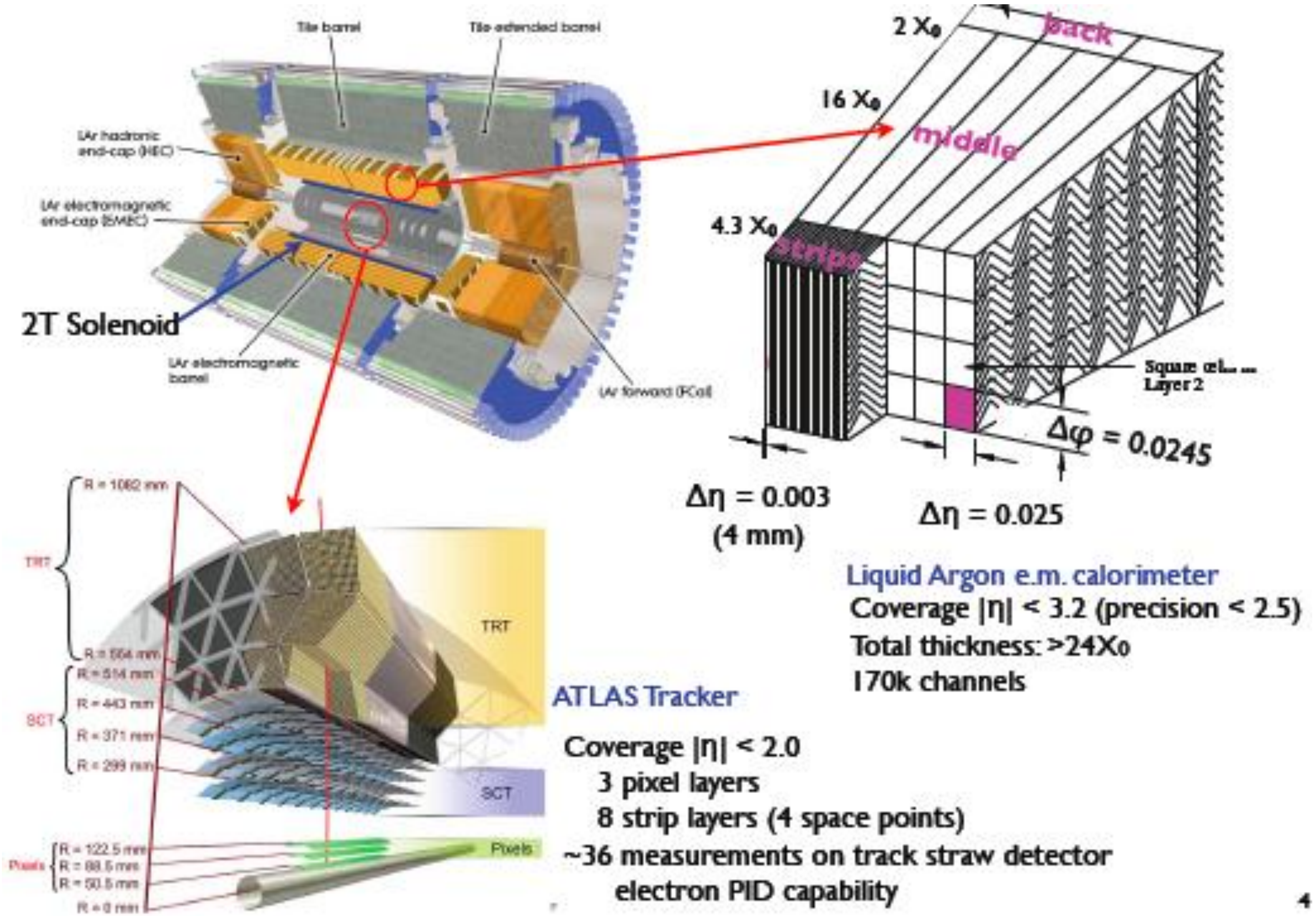

Photon = no track in the Inner Detector and an EM cluster in the calorimeter
However: because of materials in the Inner Detector and in front of the calorimeter,
Photon may convert into e-e+ pair. → photon may be reconstructed as single or double
Track conversion

Photon identification

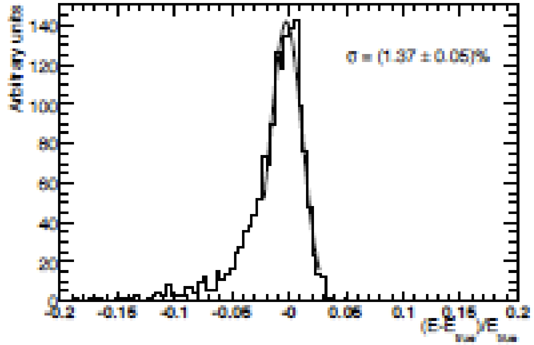

Figure 10.48: Difference between measured and true energy normalised to true energy for all photons with an energy of 100 GeV at $\eta = 1.075$.

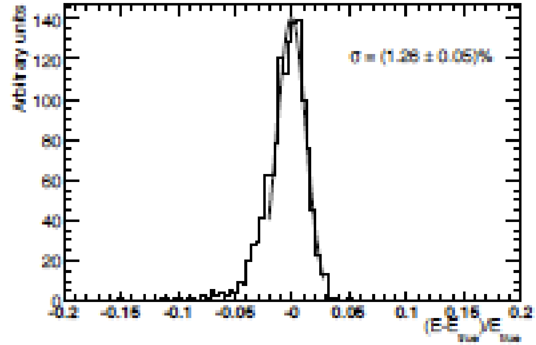

Figure 10.49: Difference between measured and true energy normalised to true energy for unconverted photons with an energy of 100 GeV at $\eta = 1.075$.

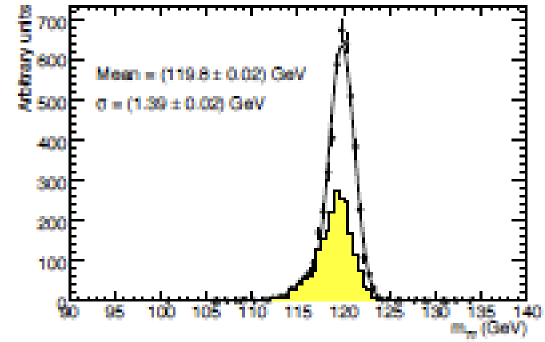

Figure 10.61: Expected distribution for the invariant mass of the two photons from Higgs-boson decays with $m_H = 120$ GeV. The shaded plot corresponds to events in which at least one of the two photons converted at a radius below 80 cm.

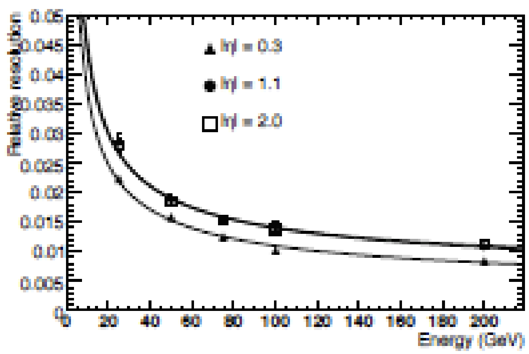

Figure 10.51: Expected relative energy resolution as a function of energy for photons at $|\eta| = 0.3$, 1.1, and 2.0. The curves represent fits to the points at the same η by a function containing a stochastic term, a constant term and a noise term.

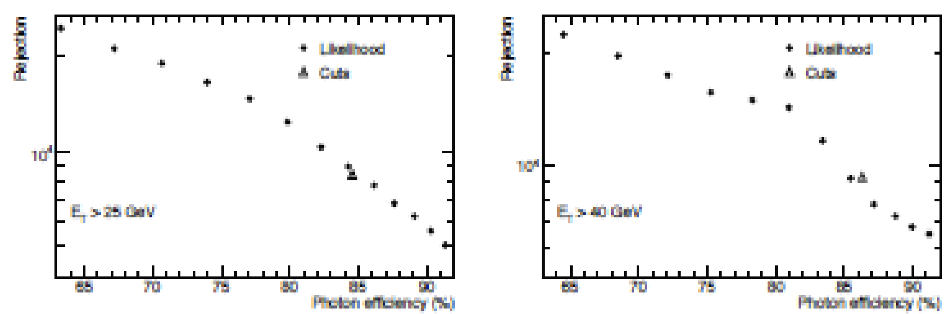

Figure 10.59: For reconstructed photon candidates with $E_T > 25$ GeV (left) and with $E_T > 40$ GeV (right), jet rejection as a function of photon efficiency, as obtained using a likelihood method. The results obtained with the standard cut-based method are also shown for reference.

Muon identification

Muon: identified as tracks in the
Inner Detector and the Muon Spectrometer.
For muon with enough energy to pass
through the calorimeter, then energy loss
in the calorimeter must be corrected for.

Internal alignment of Muon chambers
important and relative alignment of the
inner Detector and Muon Spectrometer
also important to match track segments
From both detectors.

Magnetic field mapping also
important

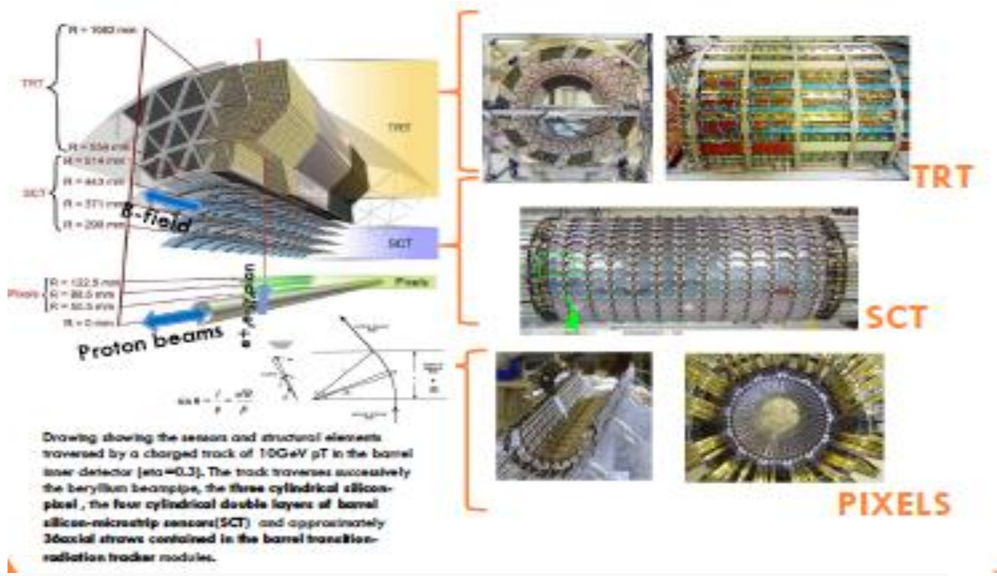

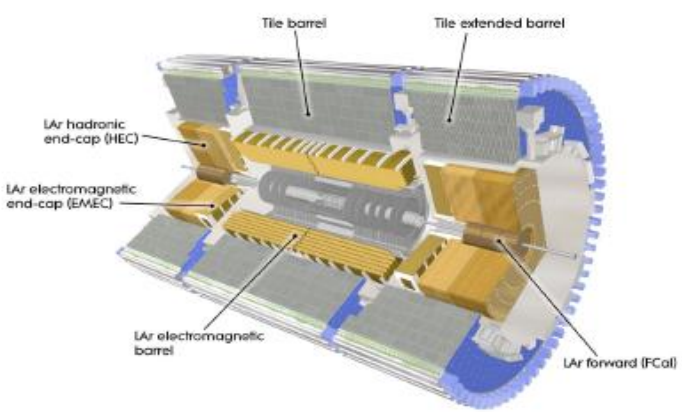

Figure 1.3: Cut-away view of the ATLAS calorimeter system.

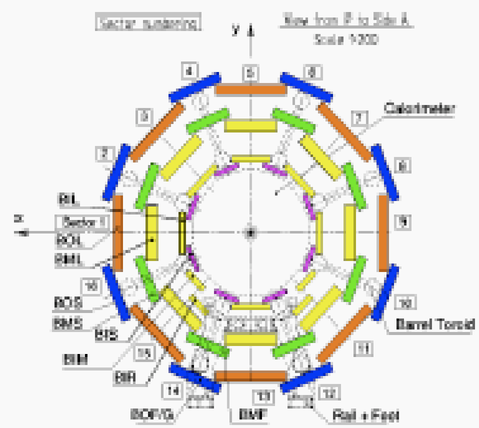

Figure 6.1: Cross-section of the barrel muon system perpendicular to the beam axis (non-bending plane), showing three concentric cylindrical layers of eight large and eight small chambers. The outer diameter is about 20 m.

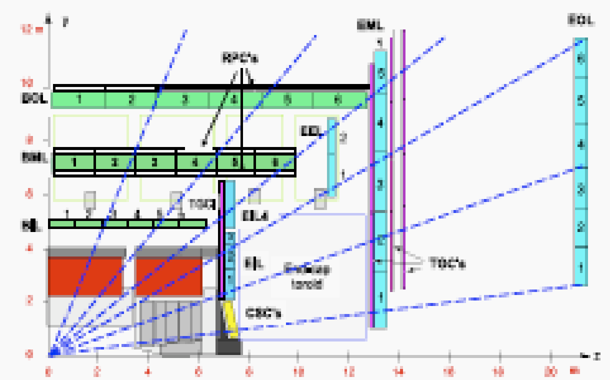

Figure 6.2: Cross-section of the muon system in a plane containing the beam axis (bending plane). Infinite-momentum muons would propagate along straight trajectories which are illustrated by the dashed lines and typically traverse three muon stations.

Muon Identification

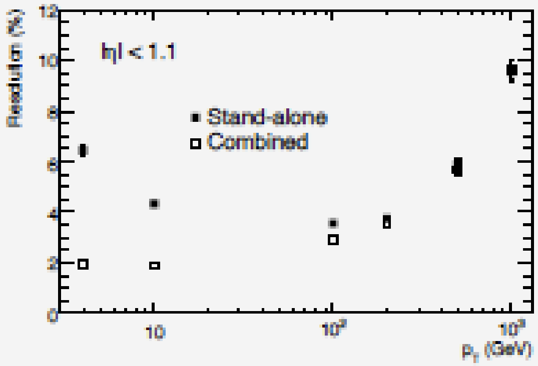

Figure 10.35: Expected stand-alone and combined fractional momentum resolution as a function of p_T for single muons with $|\eta| < 1.1$.

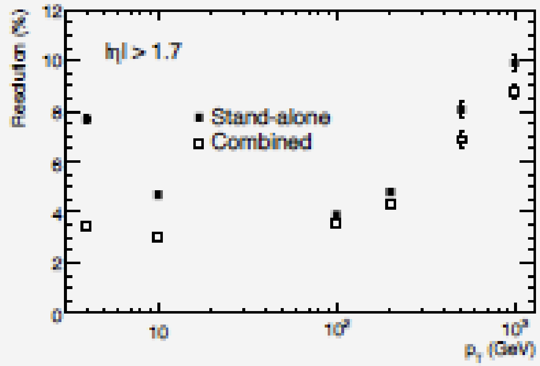

Figure 10.36: Expected stand-alone and combined fractional momentum resolution as a function of p_T for single muons with $|\eta| > 1.7$.

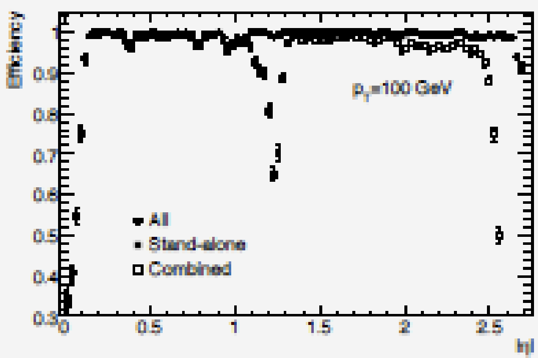

Figure 10.37: Efficiency for reconstructing muons with $p_T = 100$ GeV as a function of $|\eta|$. The results are shown for stand-alone reconstruction, combined reconstruction and for the combination of these with the segment tags discussed in the text.

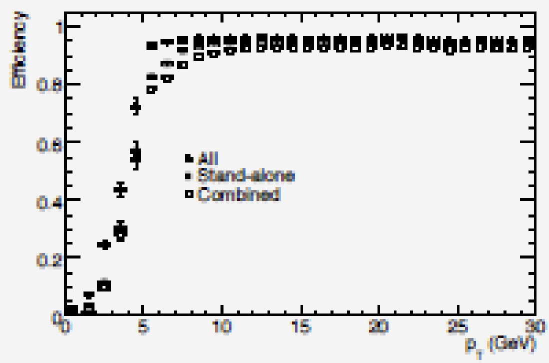

Figure 10.38: Efficiency for reconstructing muons as a function of p_T. The results are shown for stand-alone reconstruction, combined reconstruction and for the combination of these with the segment tags discussed in the text.

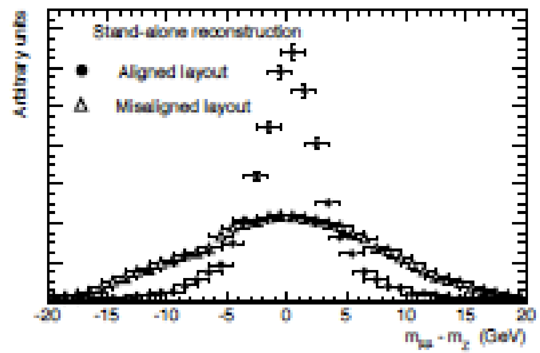

Figure 10.39: For stand-alone muon reconstruction, reconstructed invariant mass distribution of dimuons from $Z \rightarrow \mu\mu$ decays for an aligned layout of the chambers and for a misaligned layout, where all chambers are displaced and rotated randomly by typically 1 mm and 1 mrad.

Muon Identification

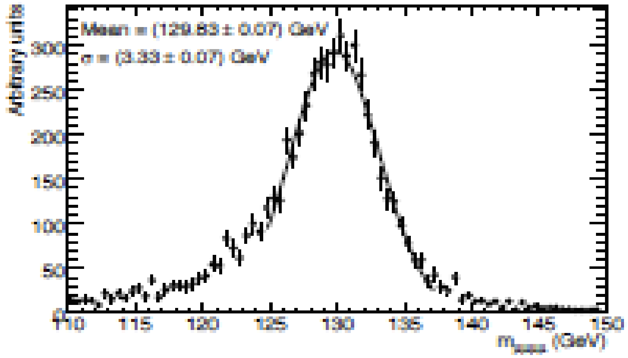

Figure 10.40: For $H \rightarrow \mu\mu\mu\mu$ decays with $m_H = 130$ GeV, reconstructed mass of the four muons using stand-alone reconstruction. The results do not include a Z-mass constraint.

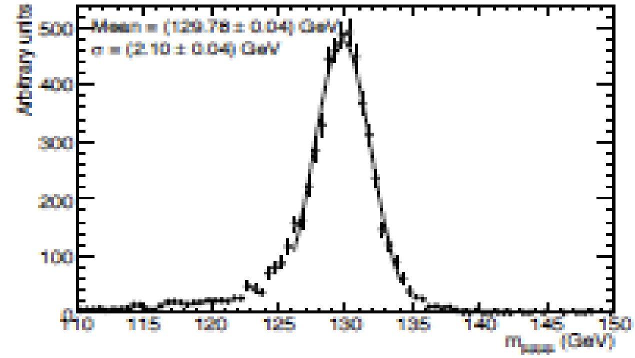

Figure 10.41: For $H \rightarrow \mu\mu\mu\mu$ decays with $m_H = 130$ GeV, reconstructed mass of the four muons using combined reconstruction. The results do not include a Z-mass constraint.

Correlation between Muon Spectrometer and Inner Detector track parameters

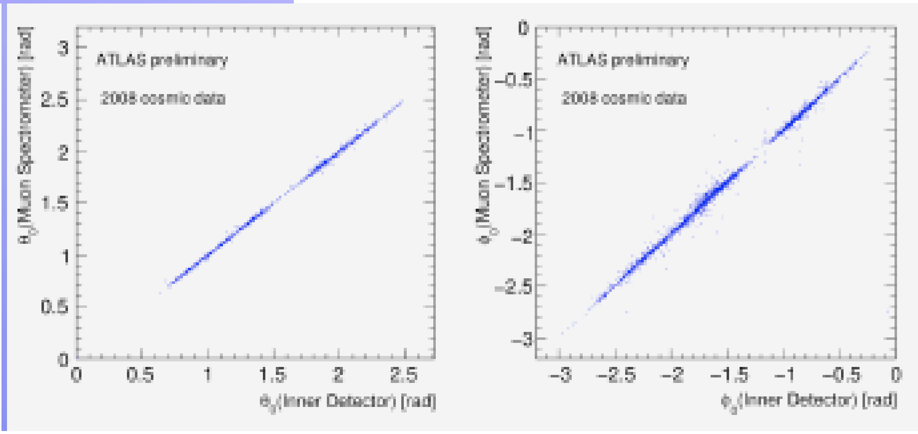

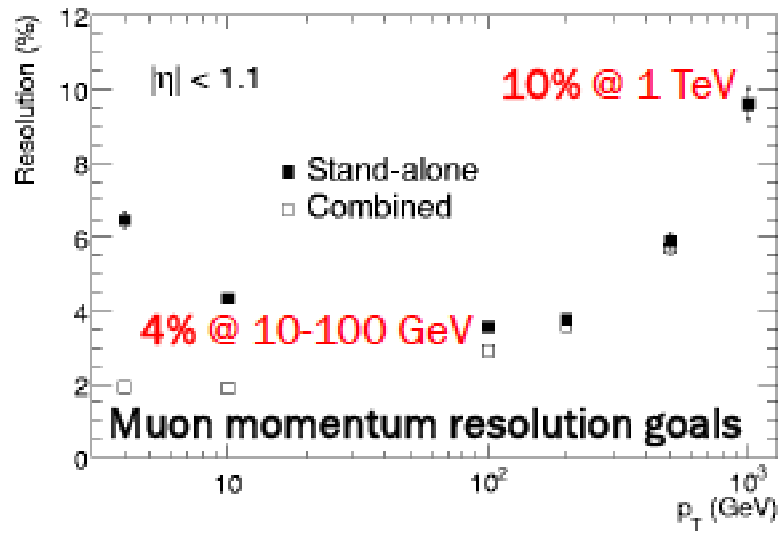

Hadronic tau identification

The transverse momentum range of interest spans from below 10 GeV up to 500 GeV. τ leptons decay hadronically in 64.8% of all cases, while in $\sim$ 17.8% (17.4%) of the cases they decay to an electron (muon) [1]. From the detection point of view, hadronic modes are divided by the number of charged πs among the decay products into single-prong (one charged π) and three-prong (three charged πs) decays. The small fraction (0.1%) of five-prong decays is usually too hard to detect in a jet environment. The $\tau \rightarrow \pi^{\pm}\nu$ mode contributes 22.4% to single-prong hadronic decays and the $\tau \rightarrow n\pi^{0}\pi^{\pm}\nu$ modes 73.5%. For three-prong decays, the $\tau \rightarrow 3\pi^{\pm}\nu$ decay contributes 61.6%, and the $\tau \rightarrow n\pi^{0}3\pi^{\pm}\nu$ mode only 33.7%. In general, one- and three-prong modes are dominated by final states consisting of $\pi^{\pm}$ and π^{0}.

Properties of hadronically decaying τ-leptons:

- Collimated energy deposition in calorimeter
- 1 or 3 charged decay products ($\pi^{\pm}$)
- Isolated EM clusters corresponding to π^{0} in τ-decay
- Modest but significant proper lifetime
- BR ($\tau \rightarrow$ hadrons) = 64.8%

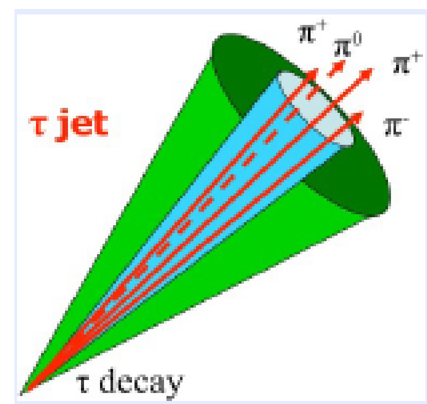

Thus also needs the tracks (Inner Detector) associated to a narrow Cluster. Need a strong rejection against jets, electrons, while maintaining high tau-jet reconstruction efficiency

Hadronic tau identification

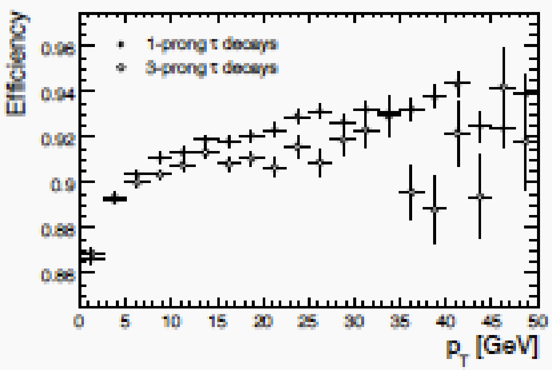

Figure 10.89: Reconstruction efficiency for charged-pion tracks as a function of the pion transverse momentum for single- and three-prong hadronic τ-decays from $W \to \tau\nu$ and $Z \to \tau\tau$ signal samples.

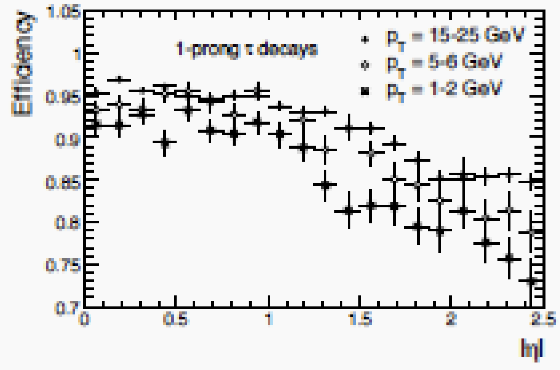

Figure 10.90: Reconstruction efficiency for the charged-pion track as a function of $|\eta|$ for three different ranges of pion p_T, for single-prong hadronic τ-decays from $W \to \tau\nu$ and $Z \to \tau\tau$ signal samples.

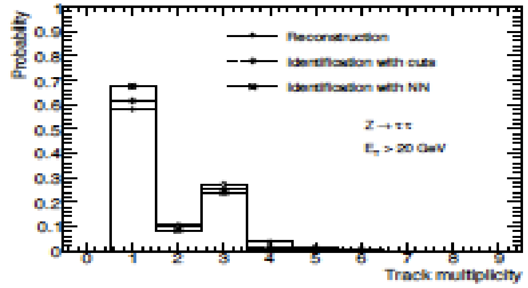

Figure 10.95: Track multiplicity distributions obtained for hadronic τ-decays with visible transverse energy above 20 GeV using the track-based τ-identification algorithm. The distributions are shown after reconstruction, after cut-based identification and finally after applying the neural network (NN) discrimination technique for an efficiency of 30% for the signal.

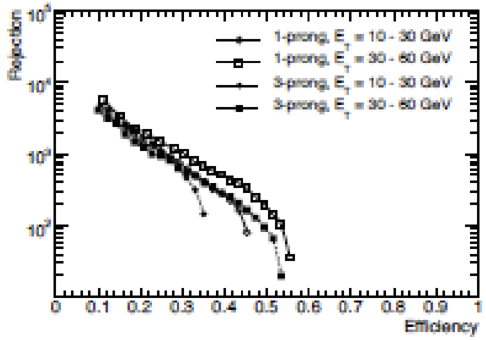

Figure 10.93: Expected rejection against hadronic jets as a function of the efficiency for hadronic τ- decays for the track-based algorithm using a neural-network selection. The results are shown separately for single- and three-prong decays and for two ranges of visible transverse energy.

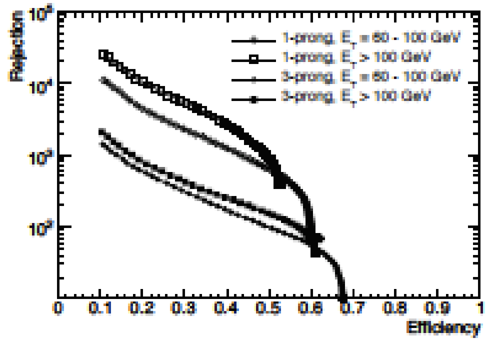

Figure 10.94: Expected rejection against hadronic jets as a function of the efficiency for hadronic τ- decays for the calorimeter-based algorithm using a likelihood selection. The results are shown separately for single- and three-prong decays and for two ranges of visible transverse energy.

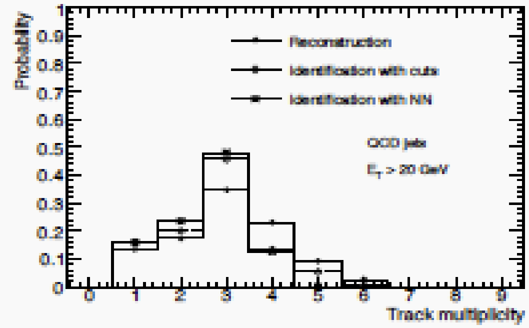

Figure 10.96: Track multiplicity distributions obtained for the background from QCD jets with visible transverse energy above 20 GeV using the track-based τ-identification algorithm. The distributions are shown after reconstruction, after cut-based identification and finally after applying the neural network (NN) discrimination technique for an efficiency of 30% for the signal.

Jet and Missing ET identification

ATLAS calorimeters

Main features for jet and E_T^{Miss} reconstruction and calibration:

- Non compensating (e/h >1) :
  - Response to hadrons is lower than that to electrons and photons
  - Developed specific calibrations
- Dead material:
  - Energy loss before EM calorimeter and between EM and HAD barrel calorimeters:
    - dead material corrections
- Different technologies and many transition regions:
  - "Crack" regions: $\eta \approx 1.4, 3.2$
- Magnetic field bending

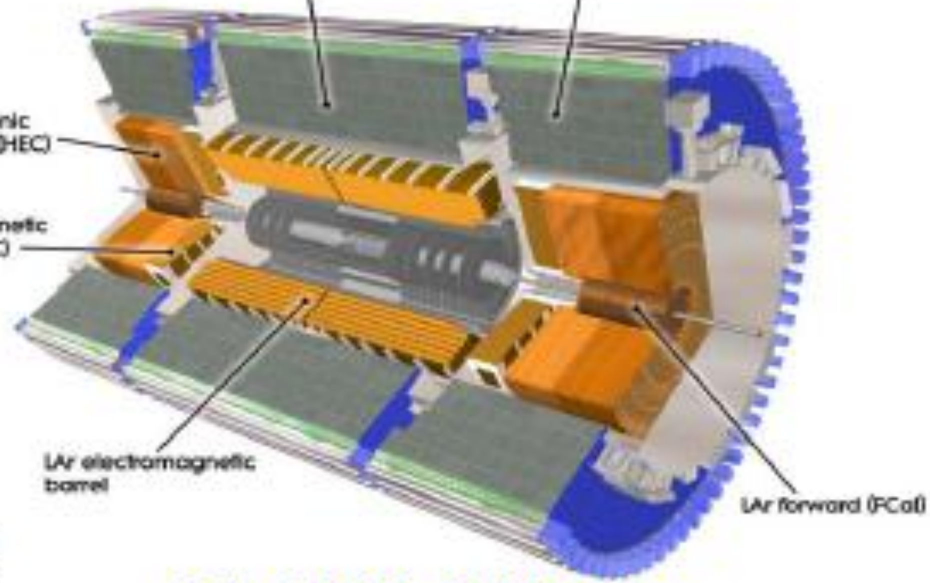

ATLAS Fiducial Regions

- Hadronic Calorimeter:
  - Barrel: $|\eta| < 1.7$
  - Endcap: $1.5 < |\eta| < 3.2$
- Electromagnetic Calorimeters
  - Barrel: $|\eta| < 1.4$
  - Endcap: $1.375 < |\eta| < 3.2$
- Forward: $3.2 < |\eta| < 4.9$

3

$\eta = -\log(\tan(\theta/2))$

Jet and Missing ET identification

- Topo-Clusters: group of calorimeter cells topologically connected
  - Noise suppression via noise-driven clustering thresholds:
    - Seed, Neighbour, Perimeter cells (S,N,P) = (4,2,0)
      - seed cells with $|E_{cell}| > S\sigma_{noise}$ ($S = 4$)
      - expand in 3D; add neighbours with $|E_{cell}| > N\sigma_{noise}$ ($N = 2$)
        - » merge clusters with common neighbours (N < S)
      - add perimeter cells with $|E_{cell}| > P\sigma_{noise}$ ($P = 0$)
  - Attempt to reconstruct single particles in calorimeter
- Towers: thin radial slice of calorimeters of fixed size
- Topo-Tower: selecting only the cells in the tower with a significant signal

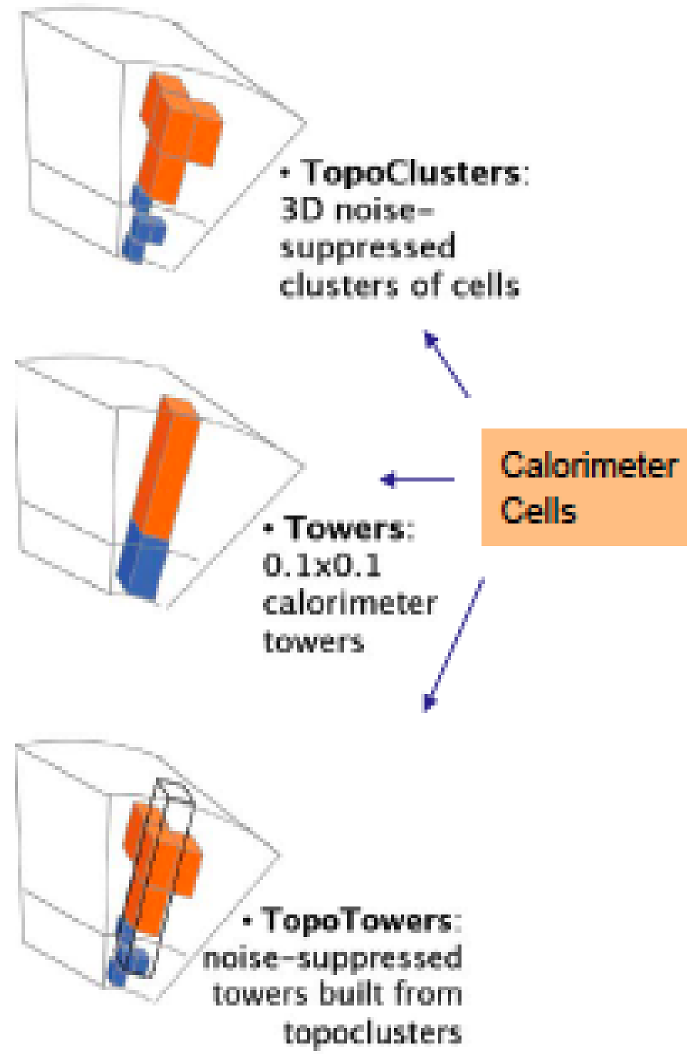

Jet Reconstruction

Sequential process:

- Input signal selection:
  - TopoClusters, Towers, TopoTowers
- Jet finding:
  - The jet finding algorithm groups the collection of clusters(towers) according to geometrical and/or kinematic criteria.
  - Many algorithms studied in ATLAS: ⇒ recently concentrated on AntiKt algorithm
- Jet calibration:
  - depending on detector input signal definition, jet finder choices…
- Jet selection:
  - apply cuts on kinematics to select jets of interest

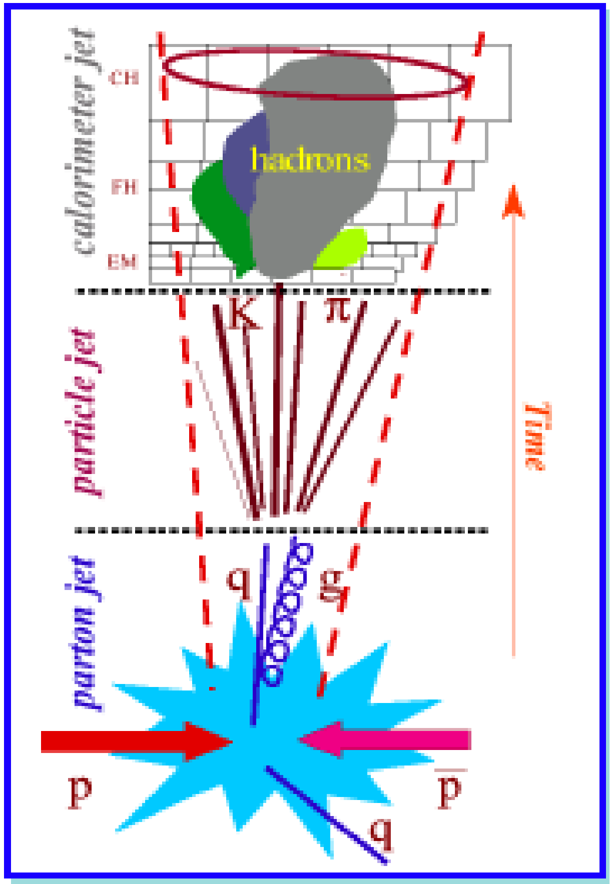

Track jets use tracks as input to the jet finding and reconstruction. This would Miss the neutral component of the jet. However track jets are useful in a Number of applications

Missing ET Reconstruction

Transverse Missing Energy:

$$E_T miss = \sqrt{E_x miss^2 + E_y miss^2}$$

$E_x miss = -\Sigma Ex$

$E_y miss = -\Sigma Ey$

$SumE_T = \Sigma E_T$

Sum of energy of all particles seen in the detector

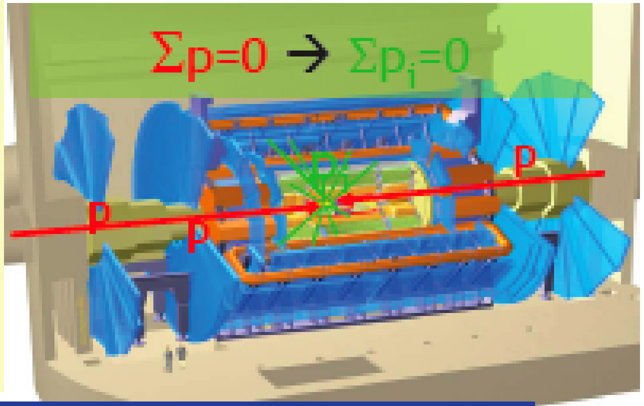

E_T^{miss} is a complex event quantity:

– It is calculated adding all significant signals from all detectors:
  - Calorimeter input signals (Cells, TopoClusters):
    – in physics objects
    – not used in physics objects
  - Muons
  - Tracks in regions where Calorimeter/Muon Spectrometer are inefficient
  - Correction for energy lost in dead material

Fake Missing ET

- Fake muons can be caused by jet punch-through detected as excess activity in Muon Chambers.
- Cleaning criteria: count of muon hits and of muon segments within a cone around jet axes.

- Missing muons due to detector features
    - η=0: holes in Muon Spectrometer for cables, services to Inner Detector & Calorimeter.
    - $|\eta|$ ~1.2: middle muon station missing for initial data taking
    - $|\eta|$>2.7: no muon coverage
- use calorimeter and track information to recover missing muons used in E_T^{miss} calculation

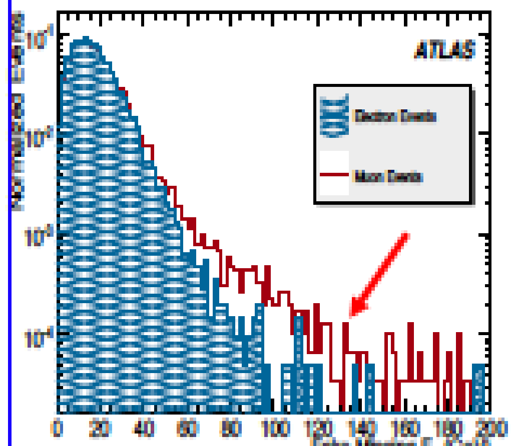

E_T^{miss} Fake in ttbar events in the electron and muon channel: ⇒large tails due to missed or fake muons

$E_{x,y}^{miss}$ Fake= $E_{x,y}^{miss}$ - $E_{x,y}^{miss}$True

Fake Missing ET

Fake E_T^{miss} in calorimeter can also be produced by mis-measurements of jets due to cracks, gaps, transition regions used for services.

Crack" regions: $\eta \approx 1.4, 3.2$

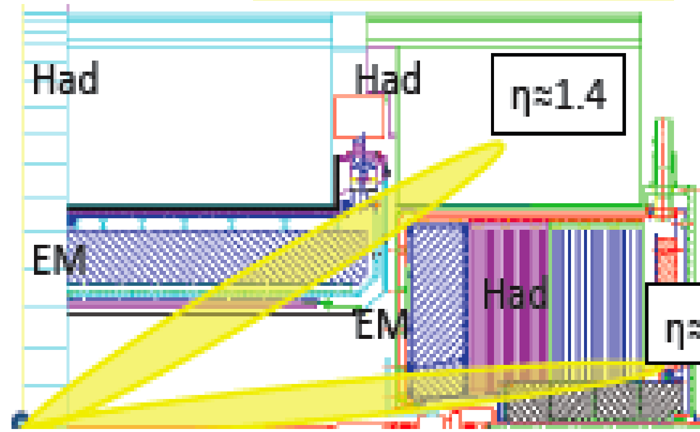

- Leakage of jets entering 'crack' region $1.3<|\eta|<1.6$ can be detected:
  - looking for large deposits in the outermost layers of the calorimeter
  - checking the E_T^{miss} calculated from tracks found in the Inner Detector that can provide a complementary information
  - checking if E_T^{miss} is closely associated with one of the leading jets in the transverse (φ) plane
- Cleaning cuts based on those criteria could be applied⇒ analysis dependent

Di-jet QCD sample 560 GeV<p_T<1120 GeV

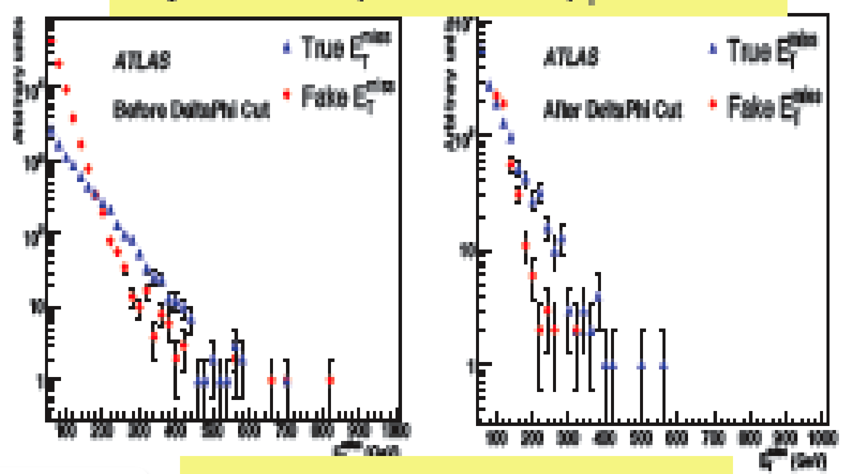

$\Delta\varphi(\text{jet-}E_T^{miss})$

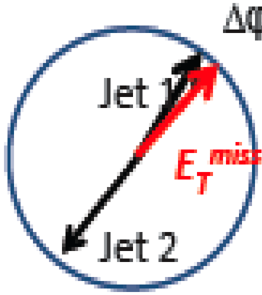

$E_{x,y}^{miss}$ Fake= $E_{x,y}^{miss}$ - $E_{x,y}^{miss}$True

12

Jet energy scale

- **Factorized multi-step approach**
  - Flexibility to understand corrections individually and use different techniques as they become validated with data within a same framework
  - Combination of "in-situ" and Monte Carlo (MC) methods

Hadronic Calibration:
- correct for calorimeter effects: non-compensation, dead material
- ATLAS developped two different strategies: **Global and Local calibration**

Jet Energy Scale

Offset correction for pile-up:
- subtract the average contribution to the jet energy not originating from the primary interaction

Response correction:
- **Eta intercalibration**: equalization of the jet response as a function of η
- **Absolute energy scale**: in-situ correction from gamma/Z-jet balance

Other optional corrections to improve resolution (scale unchanged):
- **Layer Fraction**: EM-scale jets + layer fraction, exploit longitudinal shower development
- **Tracking corrections**: fraction of jet momentum carried by charged tracks associated with the jet

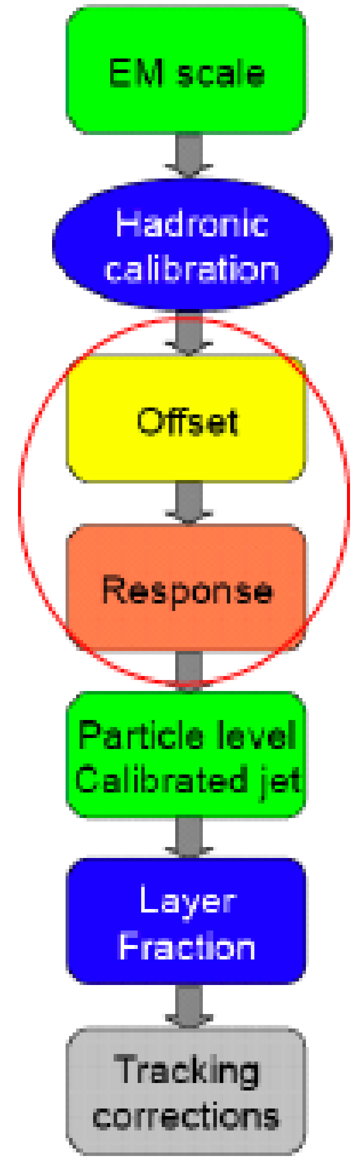

Jet Reconstruction

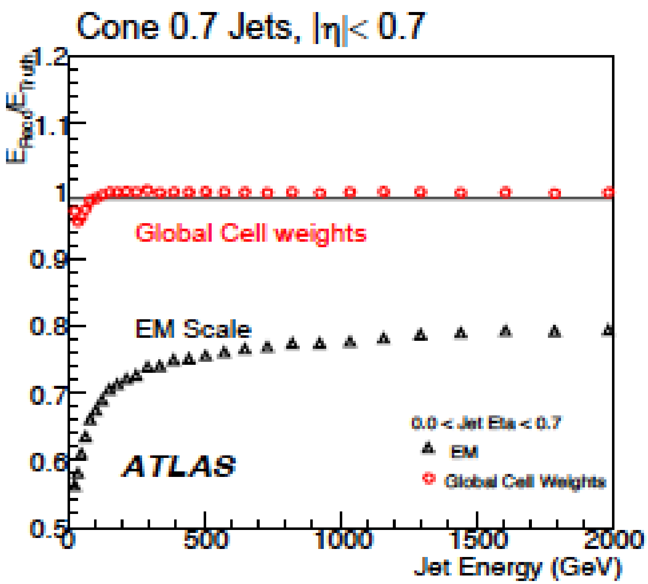

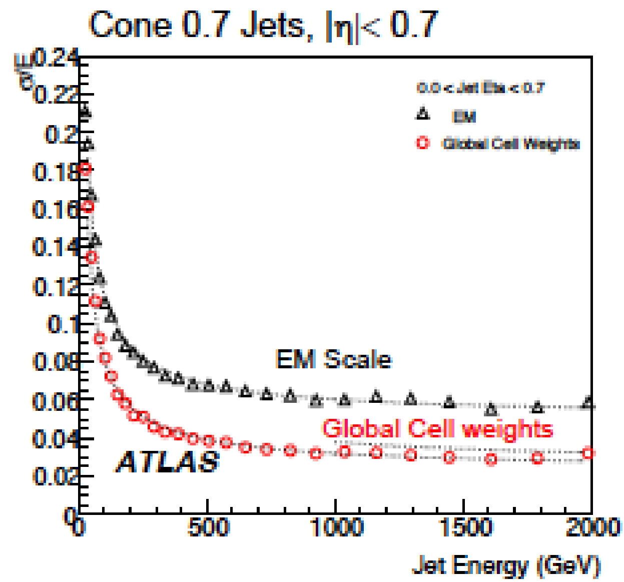

Jet energy response linearity

- Global Cell weights within 2%
- largest non linearity coming from low energies

Jet energy resolution

- Global Cell weights ~ 4% at high energy

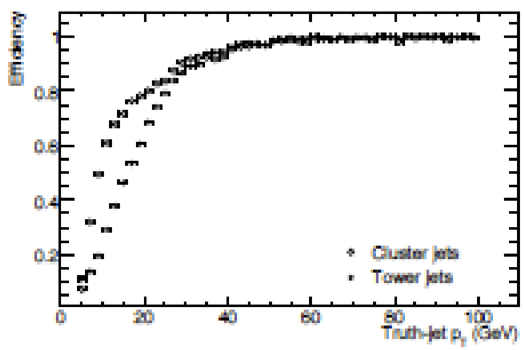

Figure 10.76: Efficiency of jet reconstruction in VBF-produced Higgs-boson events as a function of p_T of the truth-particle jet for cone-tower and cone-cluster jets with $\Delta R = 0.7$.

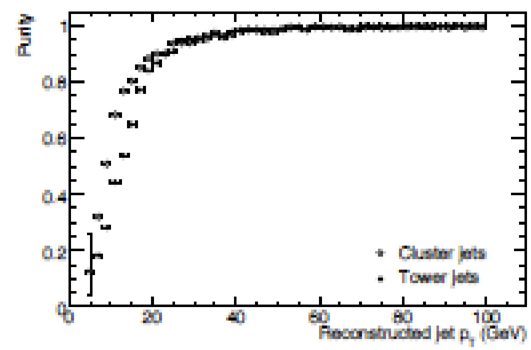

Figure 10.77: Purity of jet reconstruction in VBF-produced Higgs-boson events as a function of p_T of the reconstructed jet for cone-tower and cone-cluster jets with $\Delta R = 0.7$.

Missing ET Reconstruction

Basic E_T^{miss} from all calorimeter cells applying two possible noise suppression approaches:

- from all Cells with $|E|>2\sigma$ noise
- from all Cells inside TopoClusters

$\Rightarrow$ NO calibration, usable since day 1

Final E_T^{miss} obtained adding:

- Calibration step: two different calibrations approaches (coherent with jets):
  - Global cell energy density calibration and local hadron calibration applied
- Contribution from muons: $E_{x,y}^{Muon} = -\sum_{RecMuons} E_{x,y}$.
- Correction for energy lost in cryostat between EM and Had calorimeters from jets:

$$E_{jet}^{cryo} = w^{cryo}\sqrt{E_{EM}\times E_{HAD}}$$

Refined E_T^{miss} original approach by ATLAS based on event signal ambiguity resolution:

- sequential decomposition of reconstructed objects: *electrons, photons, taus, jet, muons* into basic constituents (calorimeter cells or TopoClusters) and veto of multiple contribution to guarantee no double counting in E_T^{miss} calculation
- Calibration weights applied to basic constituents depend on the type of reconstructed object
- Also TopoClusters not associated with any reconstructed objects taken into account

$\Rightarrow$ Most complex schema, usable after validation of reconstructed objects

Missing ET performance

Linearity = (Truth E_T^{miss} – Reco E_T^{miss})/Truth E_T^{miss}

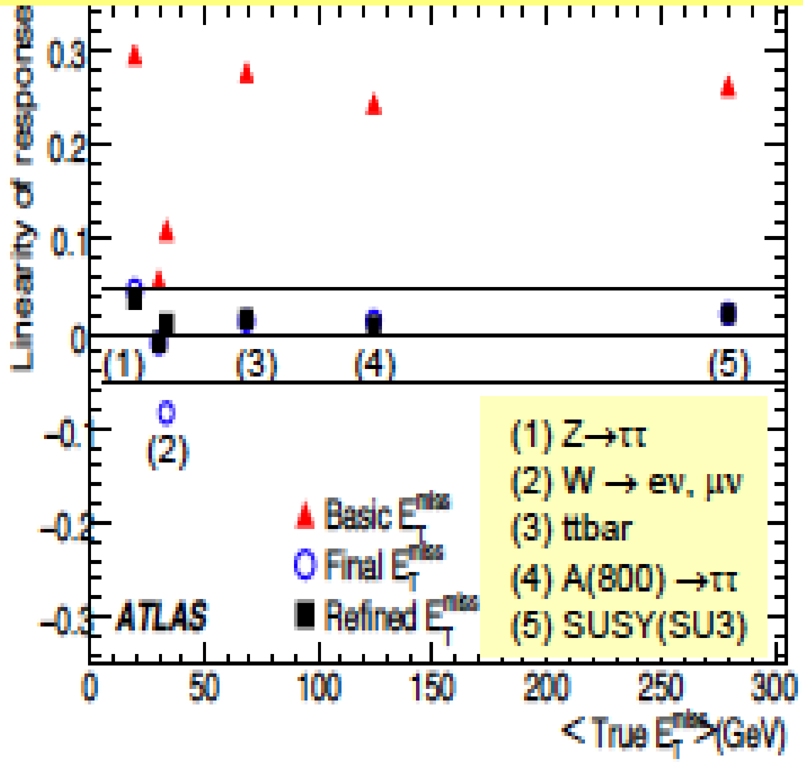

Resolution = σ(Truth $E_{x,y}^{miss}$ – Reco $E_{x,y}^{miss}$)

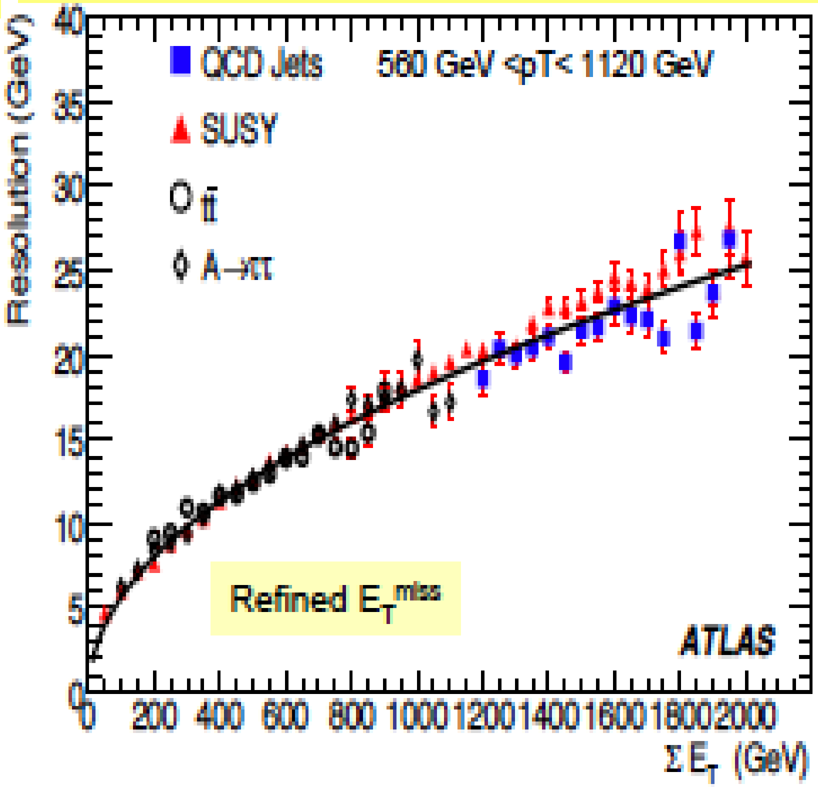

E_T^{miss} Refined Calibration provides best performances in terms of Linearity and Resolution (resolution less sensitive to calibration):

- E_T^{miss} Linearity within ~ 3% over wide E_T^{miss} range for different processes
- E_T^{miss} Resolution: mainly depend on ΣET in calorimeters,
  well described by: Resolution = $k * \sqrt{\Sigma E_T}$ (k ~ 0.5)

Flavor tagging

For example:
tt → wb wb → jjb evb

You want to tag these jets a b-jet to reduce backgrounds

Hard fragmentation of b quarks $x_B \sim 70\%$

High mass $m_B \sim 5$ GeV

Lifetime of B hadrons:

$c\tau \sim 470\ \mu m$ (mixture $B^+/B^0/B_s$) , $\sim 390\ \mu m$ (Λ_b)

for E(B) ~ 50 GeV, flight length ~ 5 mm, $d_0 \sim 500\ \mu m$

→ Spatial tagging:

- Signed impact parameter of tracks (or significance)
- Secondary vertex

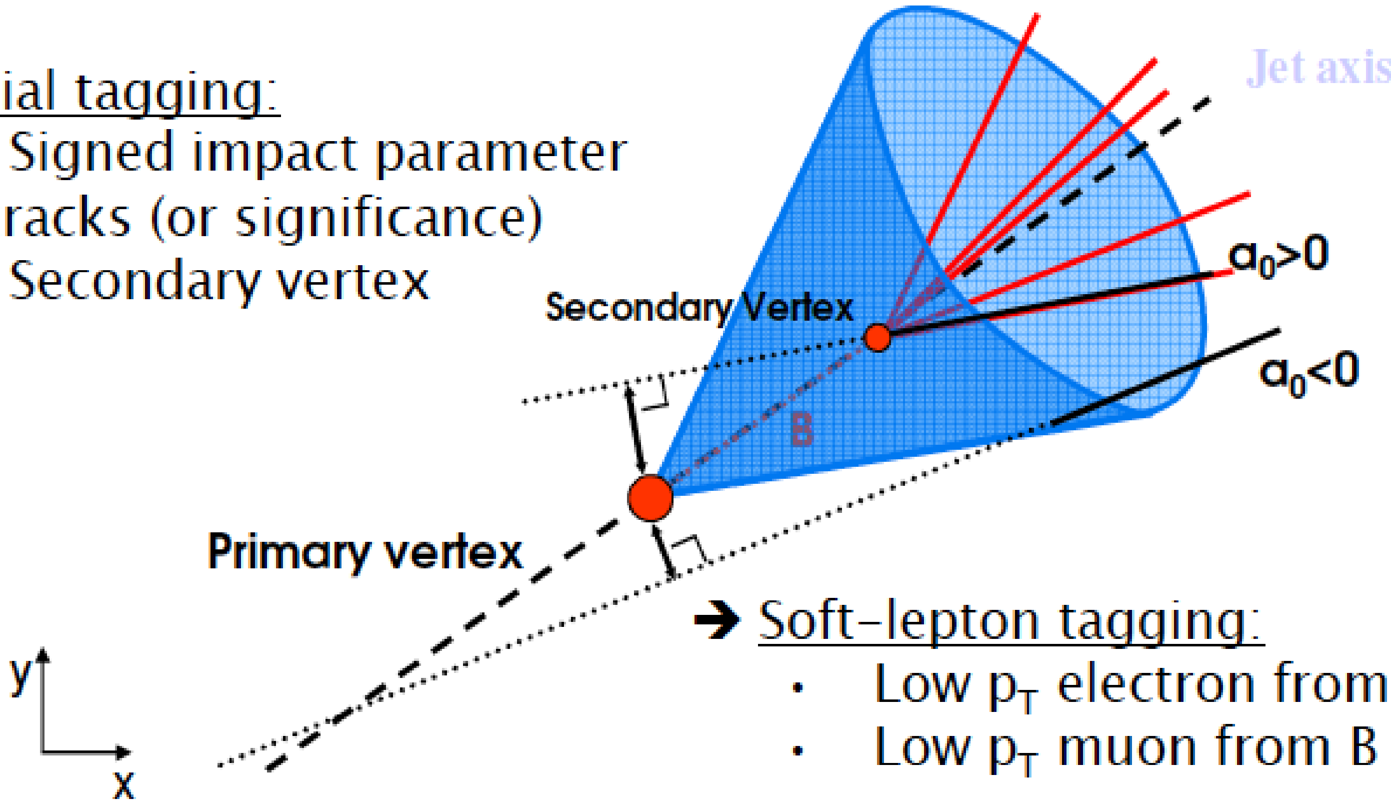

→ Soft-lepton tagging:

- Low p_T electron from B (D)
- Low p_T muon from B (D)

(limited by Br: around 20% each)

Vertexing and b-jet tagging

- The innermost silicon detector must provide the required b-tagging efficiency

Good vertex resolution is achieved by placing the **innermost (*B*) layer close to the beam pipe**, and **the next layer farer to it** (lever arm), and by an excellent *B*-layer resolution

Small multiple scattering term: $\sigma_{MS} \sim \frac{1}{p}\sqrt{X/X_0}$

Expected transverse IP resolution ~13 μm for 100 GeV track

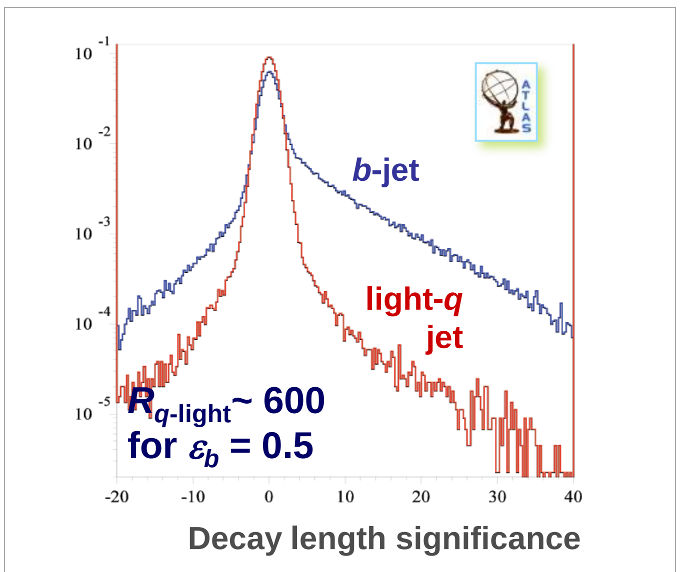

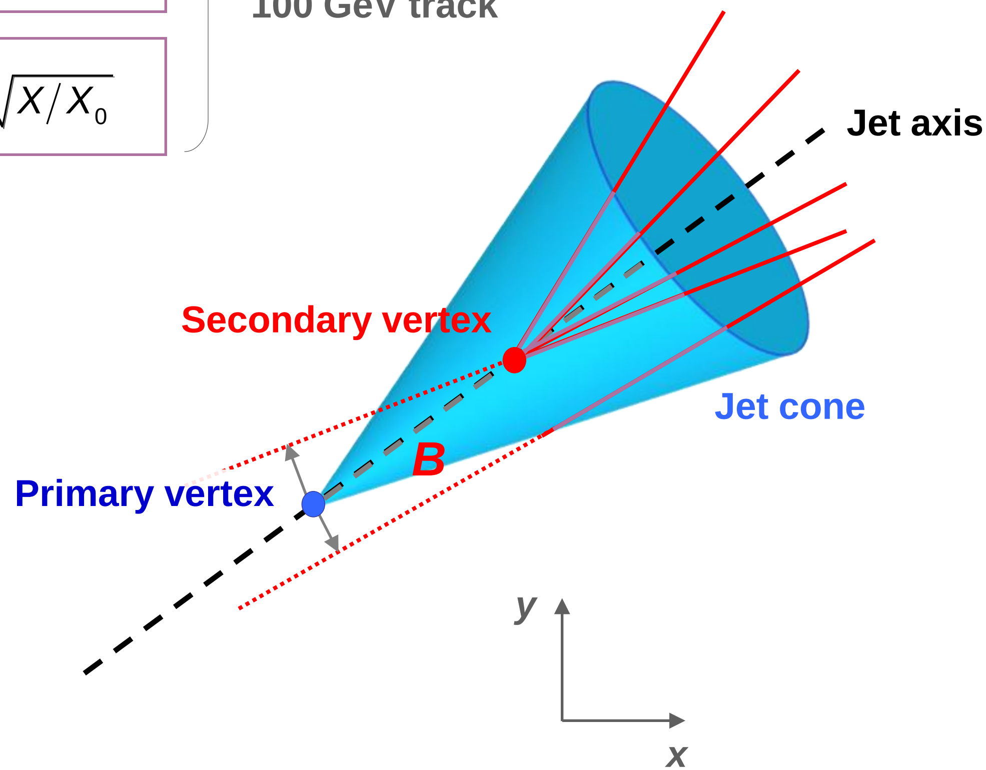

Simpler b-taggers

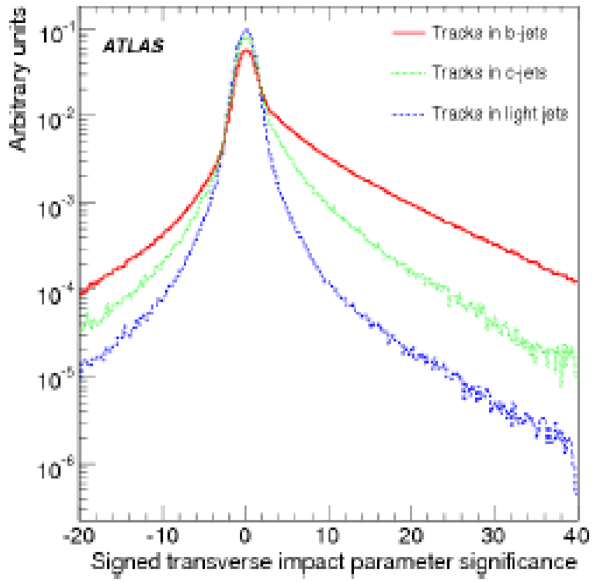

➔Relying on transverse impact parameter:

➔ TrackCounting: # of tracks with large d_0/σ

➔ JetProb: measuring compatibility of tracks with primary vertex, using a resolution function derived from data: it can be derived already with the 900 GeV data.

➔Relying on secondary vertex:

– inclusive secondary vertex

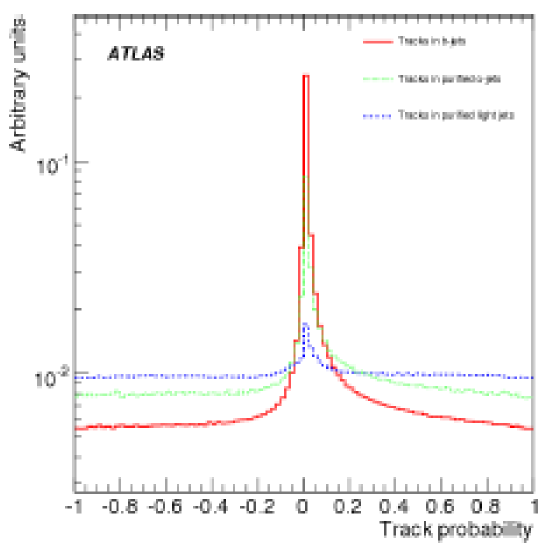

Track compatibility with primary vertex

Normalized distance PV-SV

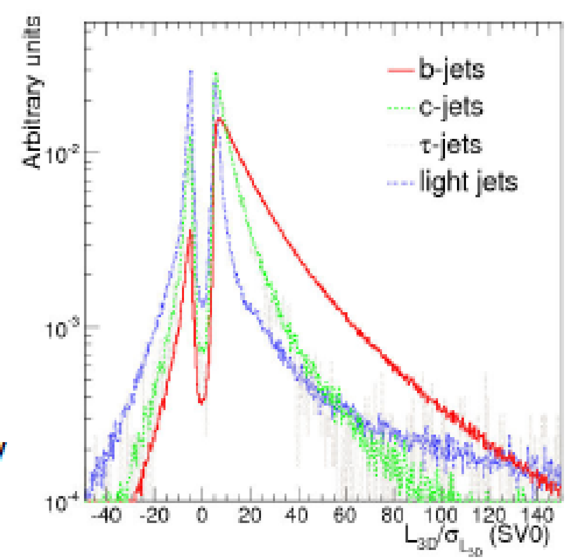

Simpler b-taggers

<u>Test sample:</u>
- 500k ttbar events (10 TeV)
- rather central jets
- average p_T:
  - 70 GeV for b-jets
  - 55 GeV for light jets
- selection: p_T>15 GeV, $|\eta|$<2.5

<u>Estimators:</u> light jet rejection (inverse of mis-tagging rate) vs b-tagging efficiency.

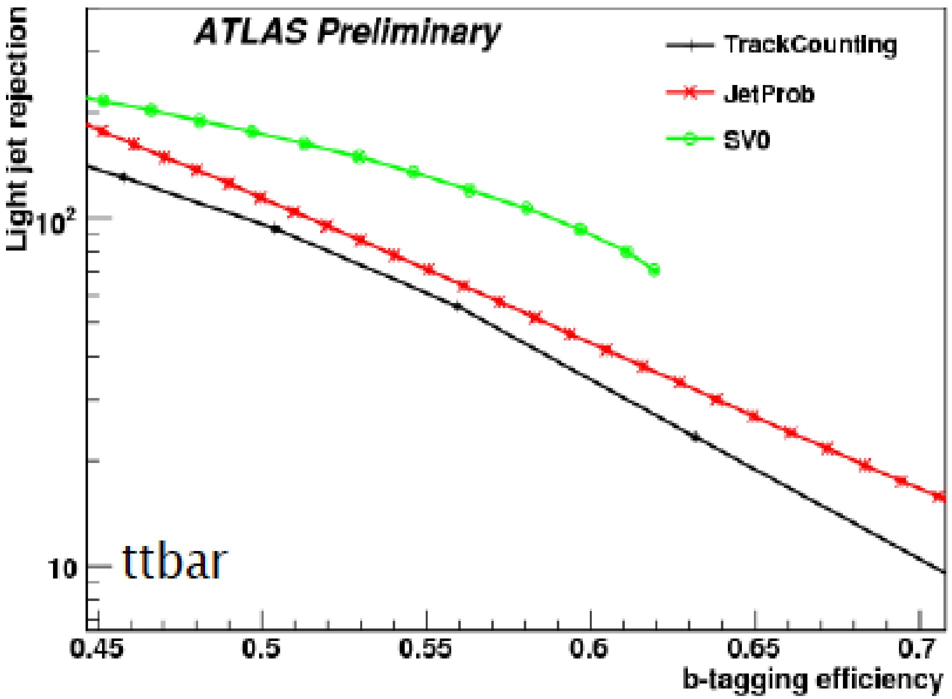

	ϵ_b= 50%	ϵ_b = 60%
TrackCounting	96	38
JetProb	114	44
SV0	173	89

(errors stat.: ±1)

Combining Tracking with PID: the ATLAS TRT

- e/π separation via transition radiation: polymer (PP) fibres/foils interleaved with DTs

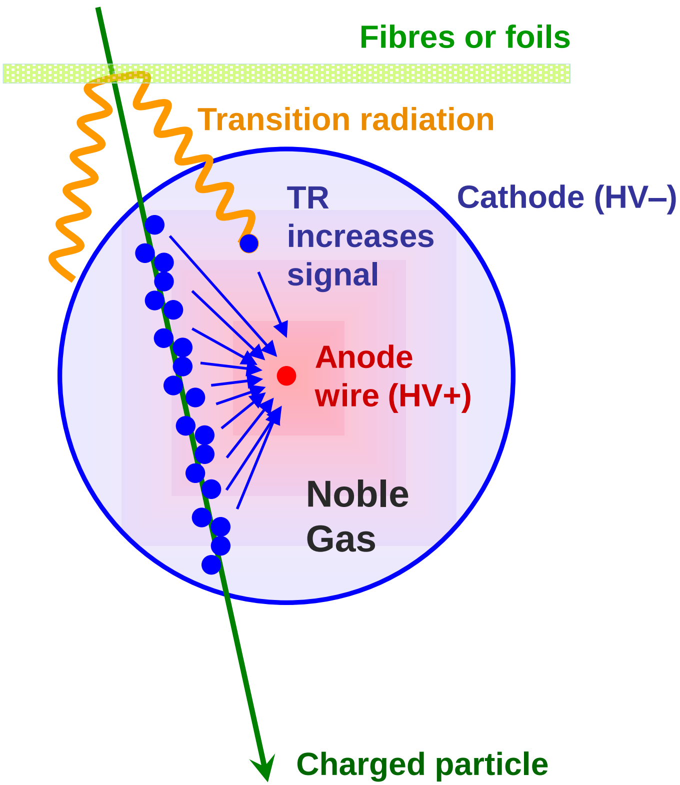

Electrons radiate → higher signal
PID info by counting high-threshold hits

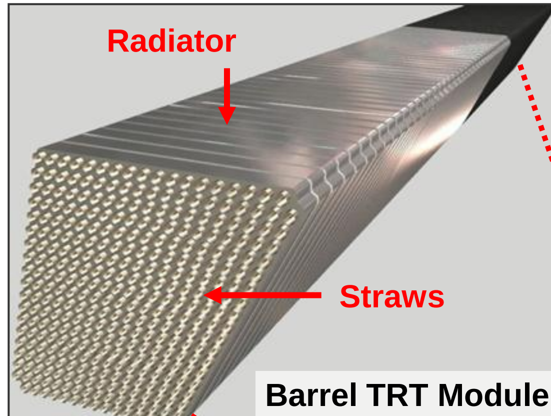

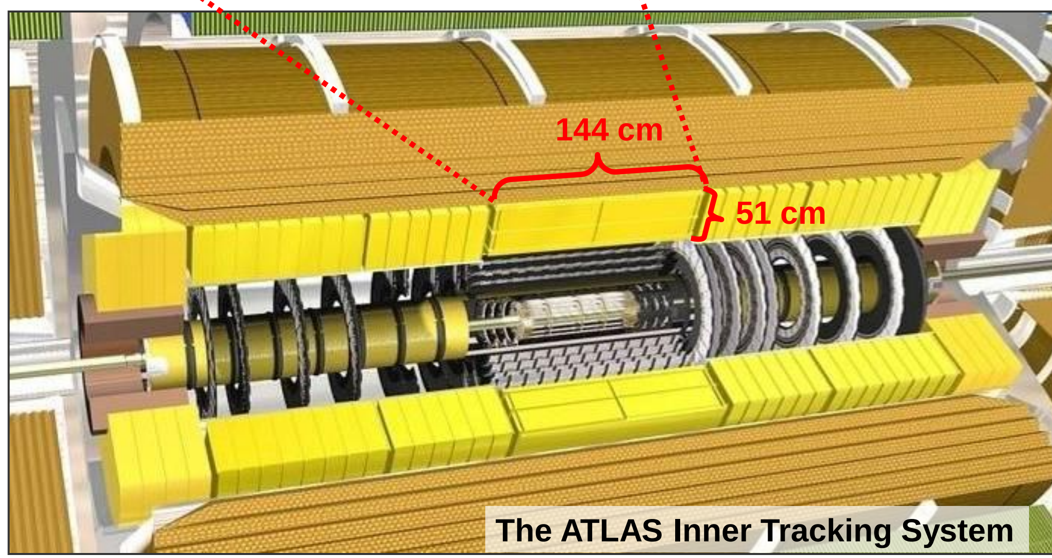

Total: 370k straws

Barrel ($|\eta| < 0.7$): 36 r-ϕ measurements / track
Resolution ~130 μm / straw

18 end-cap wheels ($|\eta| < 2.5$): 40 or less z-ϕ points

Momentum Measurement in Tracking Device

- Charged particles deflection in magnetic field:
  - Lorentz force ⊥ to *B*-field and to particle direction
  - Particle trajectory projected onto plane ⊥ to *B*-field is *circle* with radius: $r\,[\mathrm{m}] = \dfrac{p_T\,[\mathrm{GeV}]}{0.3 \cdot B\,[\mathrm{T}]}$
  - ➡ For p_T = 10 … 1000 GeV and B = 2 T → R = 17 … 1700 m (*cf*, R_{ID} ~ 1 m)
  - ➡ … and if p_T < 0.5 GeV, the particle is trapped in solenoi
- Obtain r and p_T from measurement of sagitta:

$$r \approx \frac{L}{8s} \quad (\text{if } s \ll L) \quad \Rightarrow \quad p_T \propto \frac{1}{s} \quad \text{and} \quad \frac{\sigma(p_T)}{p_T} \propto p_T$$

- Track fitting in LHC environment challenging
  - Must handle ambiguities, hit overlaps, multiple scattering, bremsstrahlung, multiple vertices, …
  - Track fitters take Gaussian noise (Kalman) and non-Gaussian noise (GSF) into account
  - Fitter must be fast, used in high-level trigger

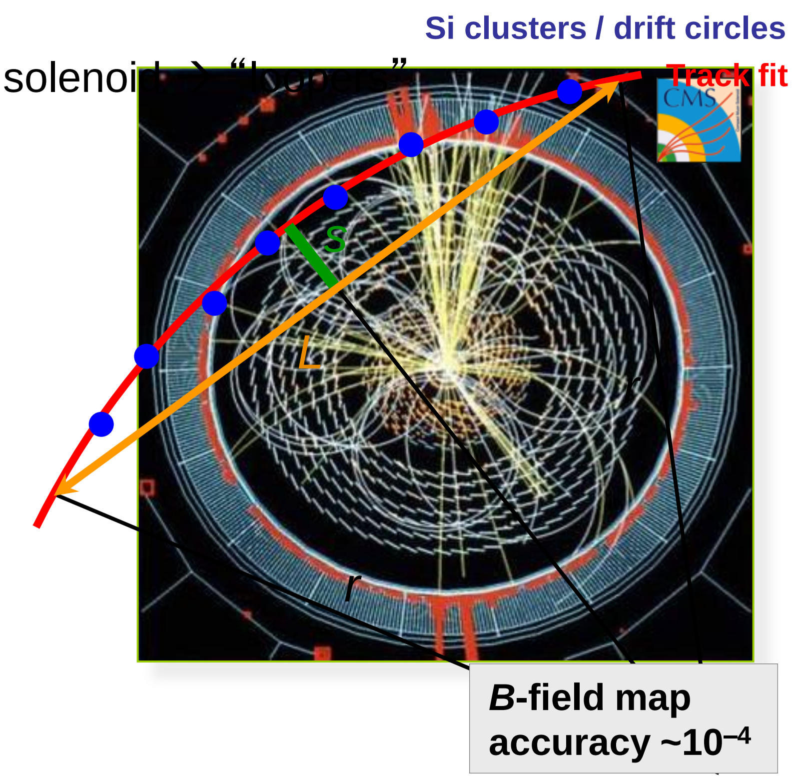

The ATLAS Muon Spectrometer (Active Material)

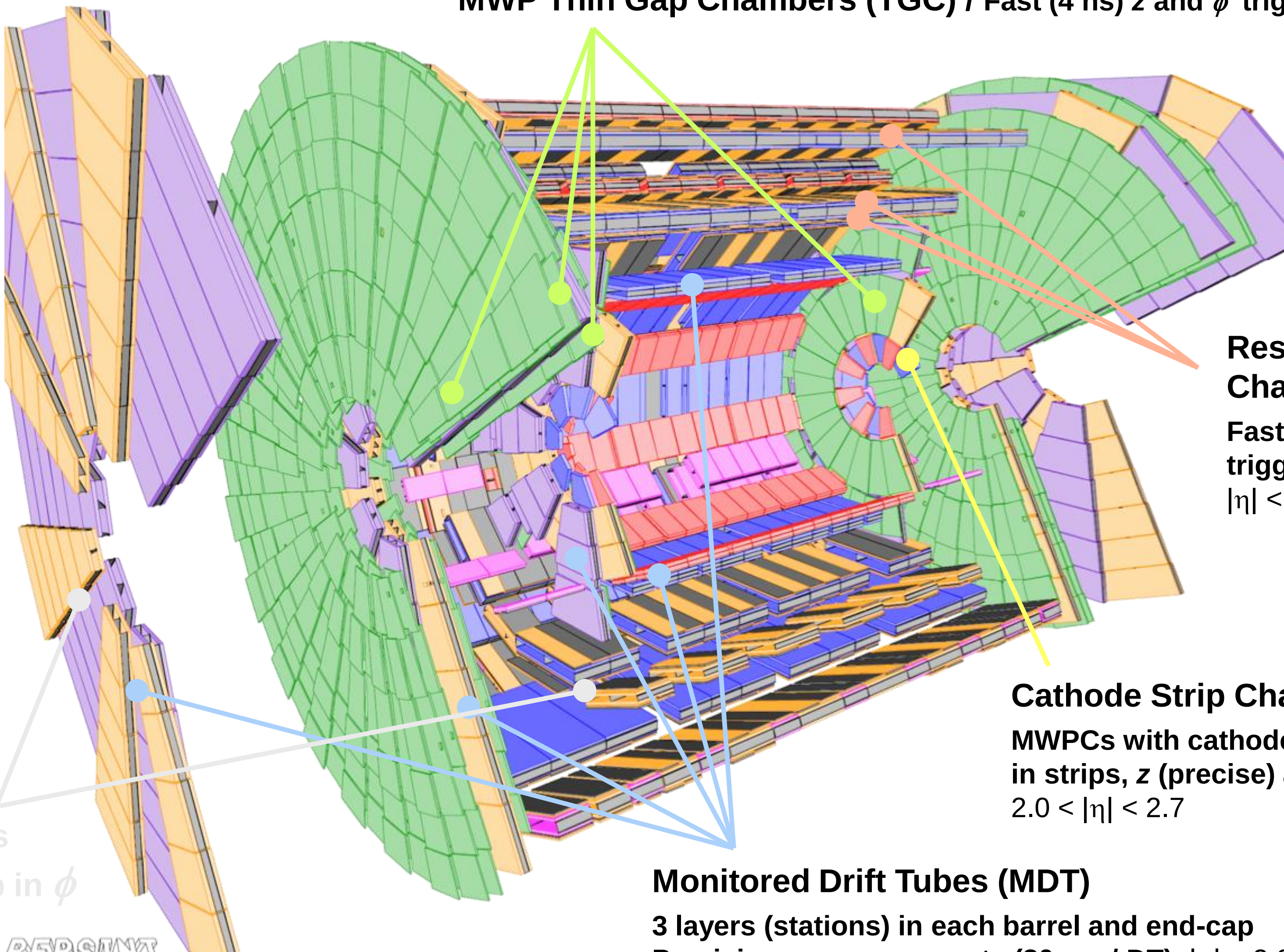

The ATLAS Muon Spectrometer

- Outer layer of LHC detectors, only reached by WI(M)Ps (ν, χ) or EM MIPs (μ)
  - Good containment of jets requires ~11 λ before muon systems
  - ATLAS opted for good stand-alone tracking if too high-backgrounds in ID
- Huge magnetic volume
  - ATLAS has 8 (barrel) 3 T_{max} and 2×8 (endcap) 6 T_{max} superconducting toroid magnets

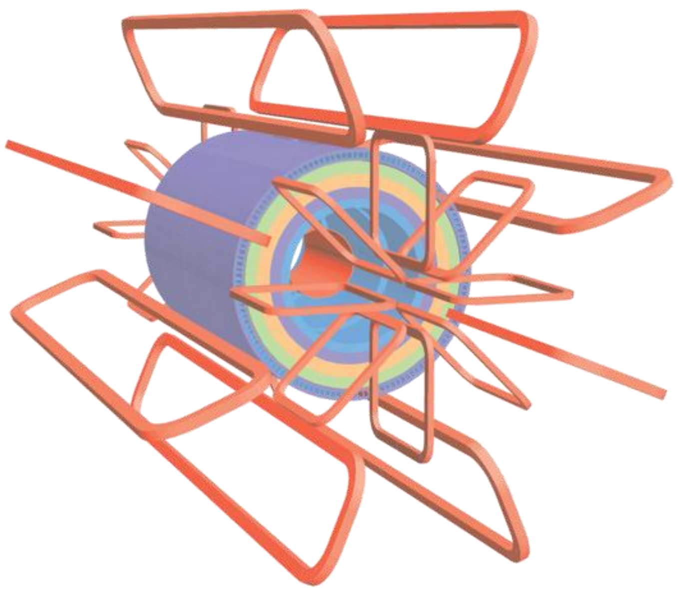

- Huge active detectors area
  - Open structure minimises multiple scattering
  - Dedicated trigger chambers
- Huge mechanical structure
  - Challenging tolerances for mechanical stability, positioning and alignment (optical sensors)

ATLAS Toroid Fields

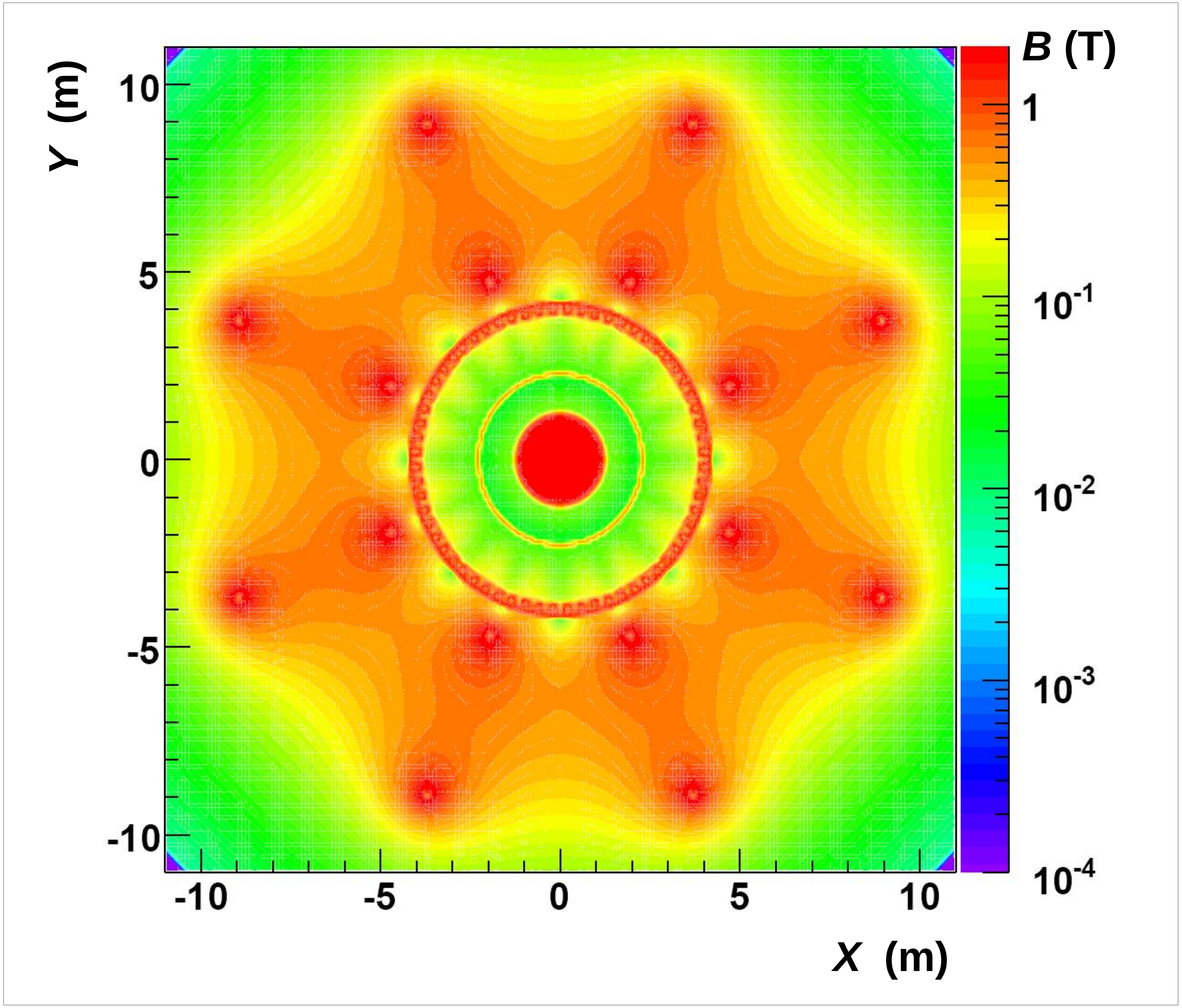

Momentum Measurement

- Toroid fields bend tracks in ***z* direction**, instead of R -ϕ as in the inner detector

  $\sigma(z)$ = 35 μm per chamber → $\sigma(s) \approx (3/2)^{1/2} \cdot \sigma(z)$ = 43 μm

  → 1 TeV track has s = 500 μm at $\eta \approx 0$ → < 10 % precision on momentum measurement

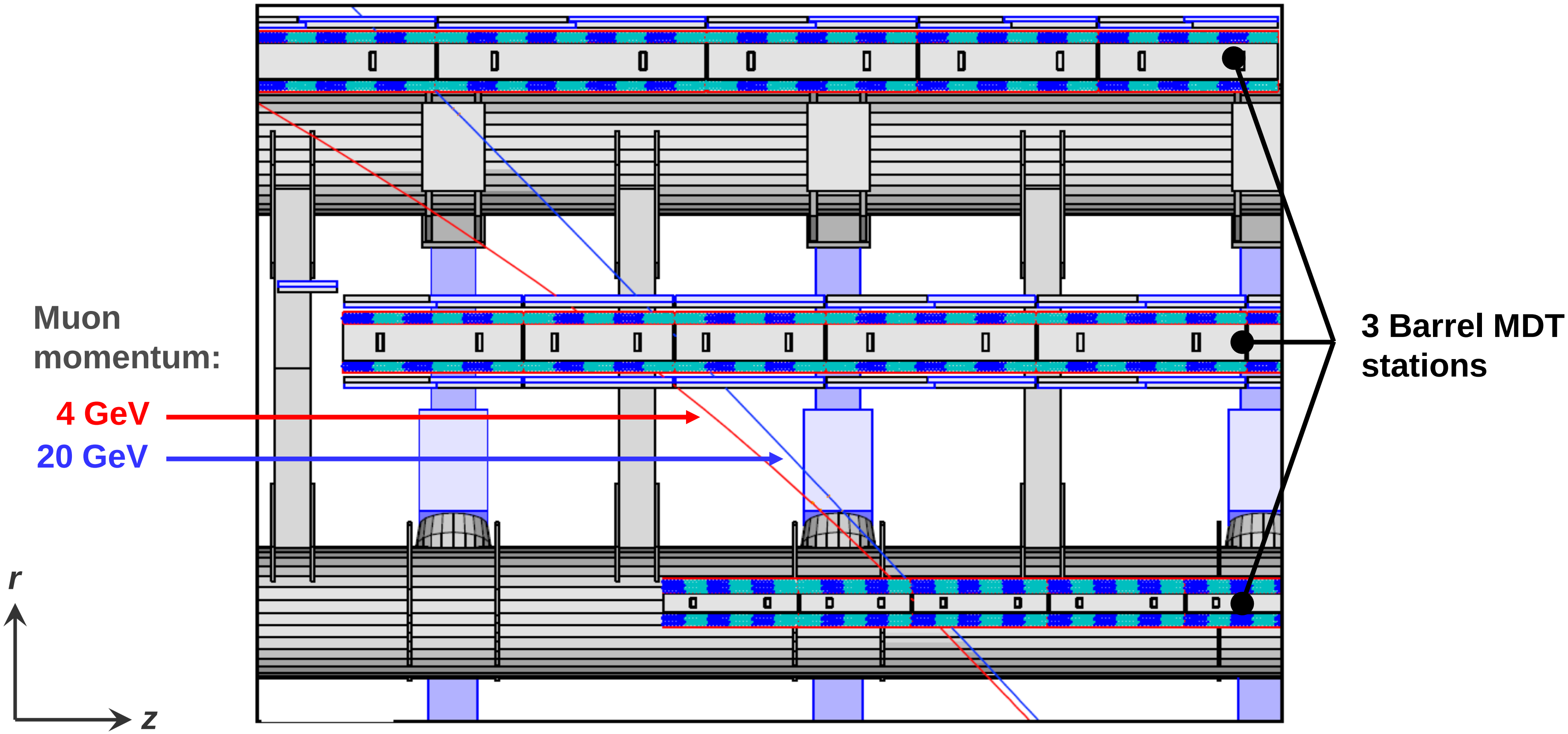

Triggering Muons

- Ultra-fast L1 trigger requires coincident hits in 3 RPC (barrel) or 3 TGC (end-caps) layers within "roads" corresponding to predefined momenta (thresholds)

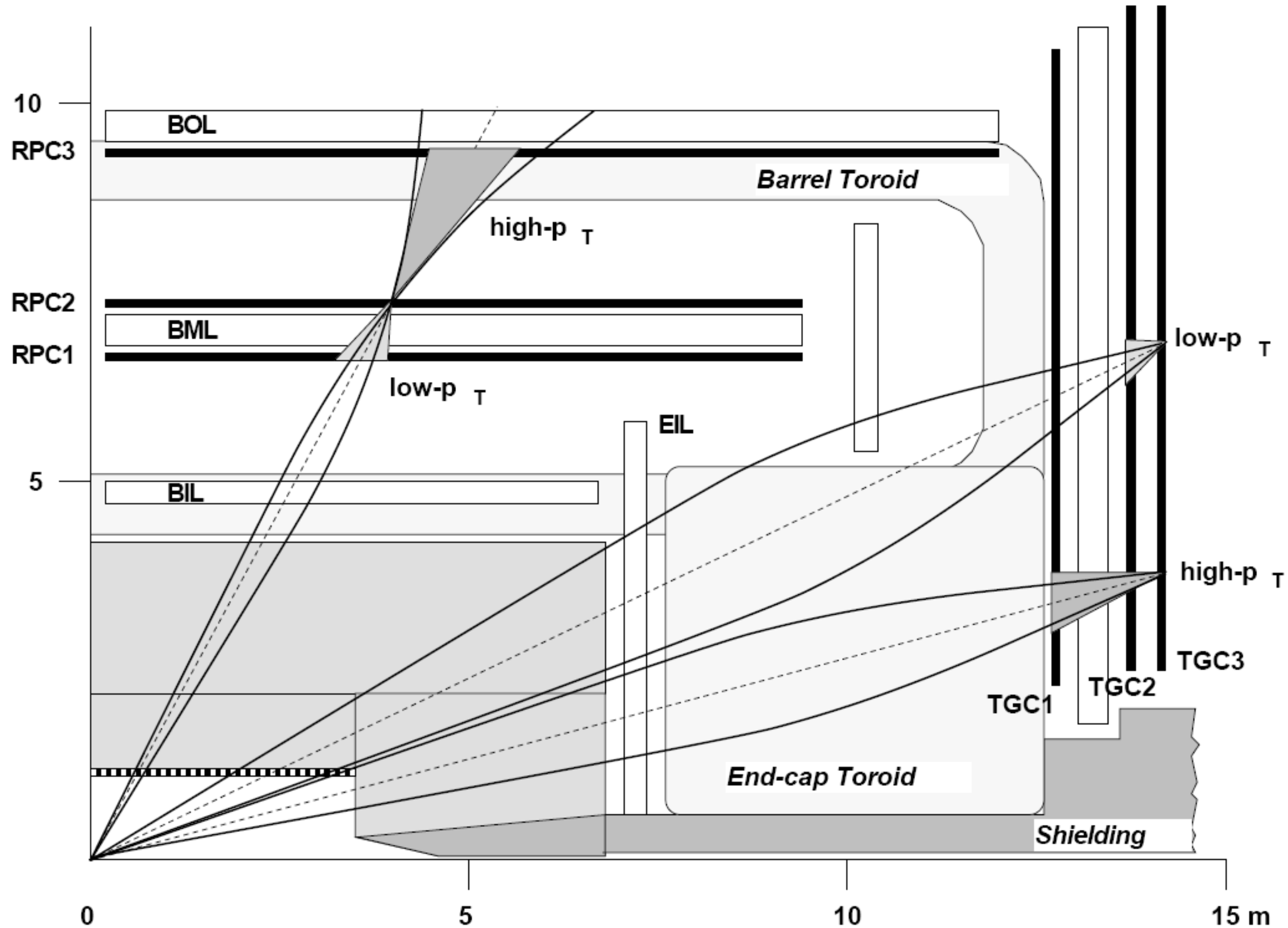

Cosmic Commissioning of ATLAS, CMS, ALICE and LHC-b

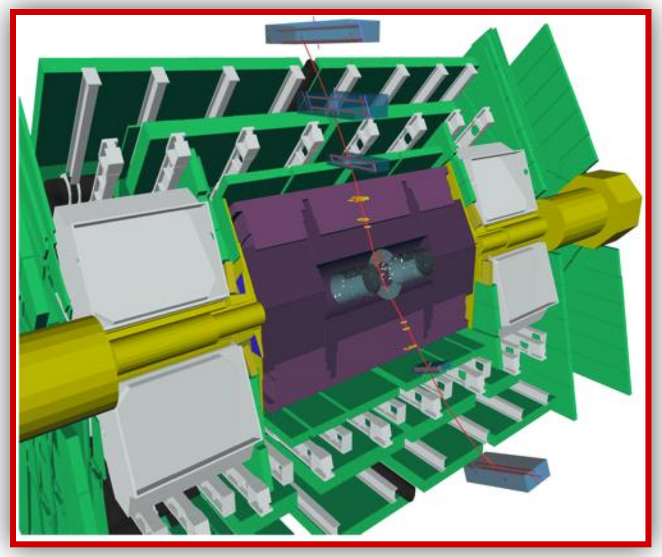

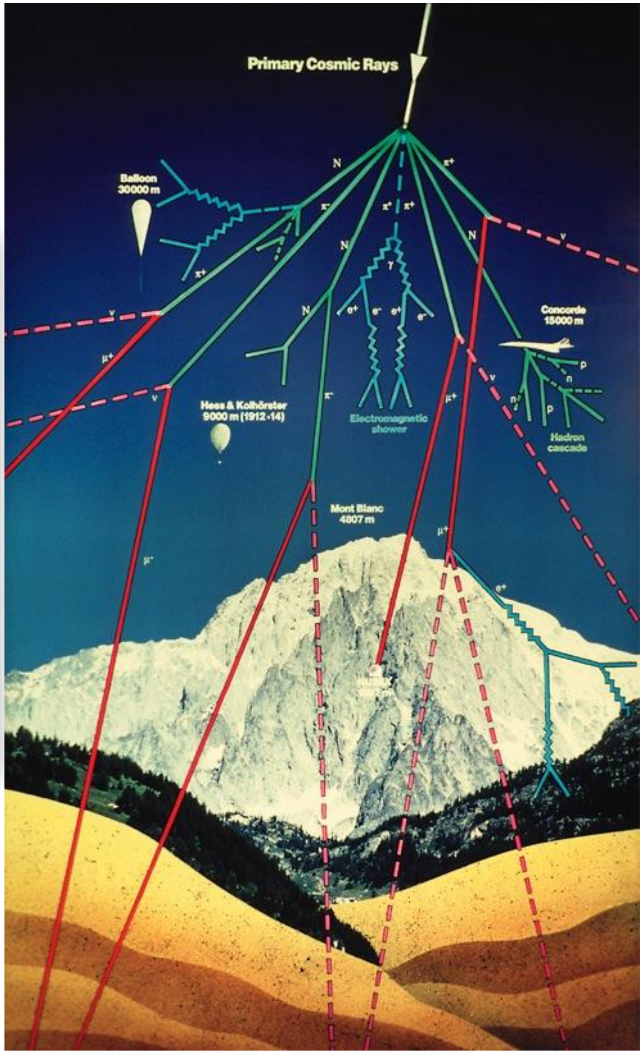

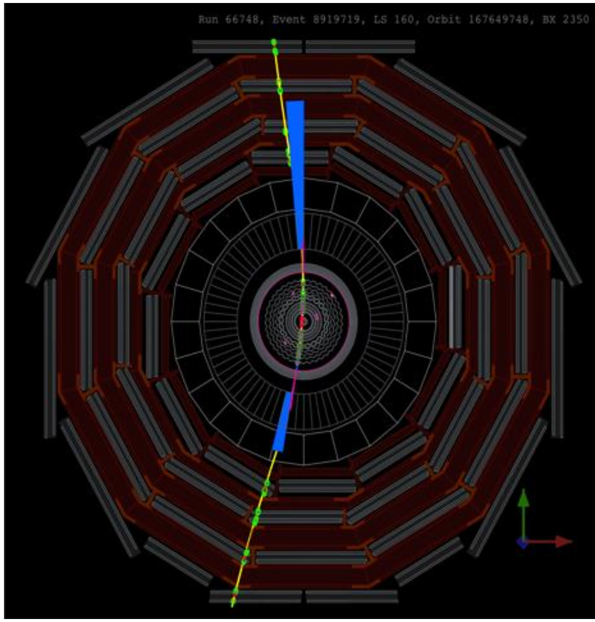

Commissioning Example: CMS – 25 Performance papers published

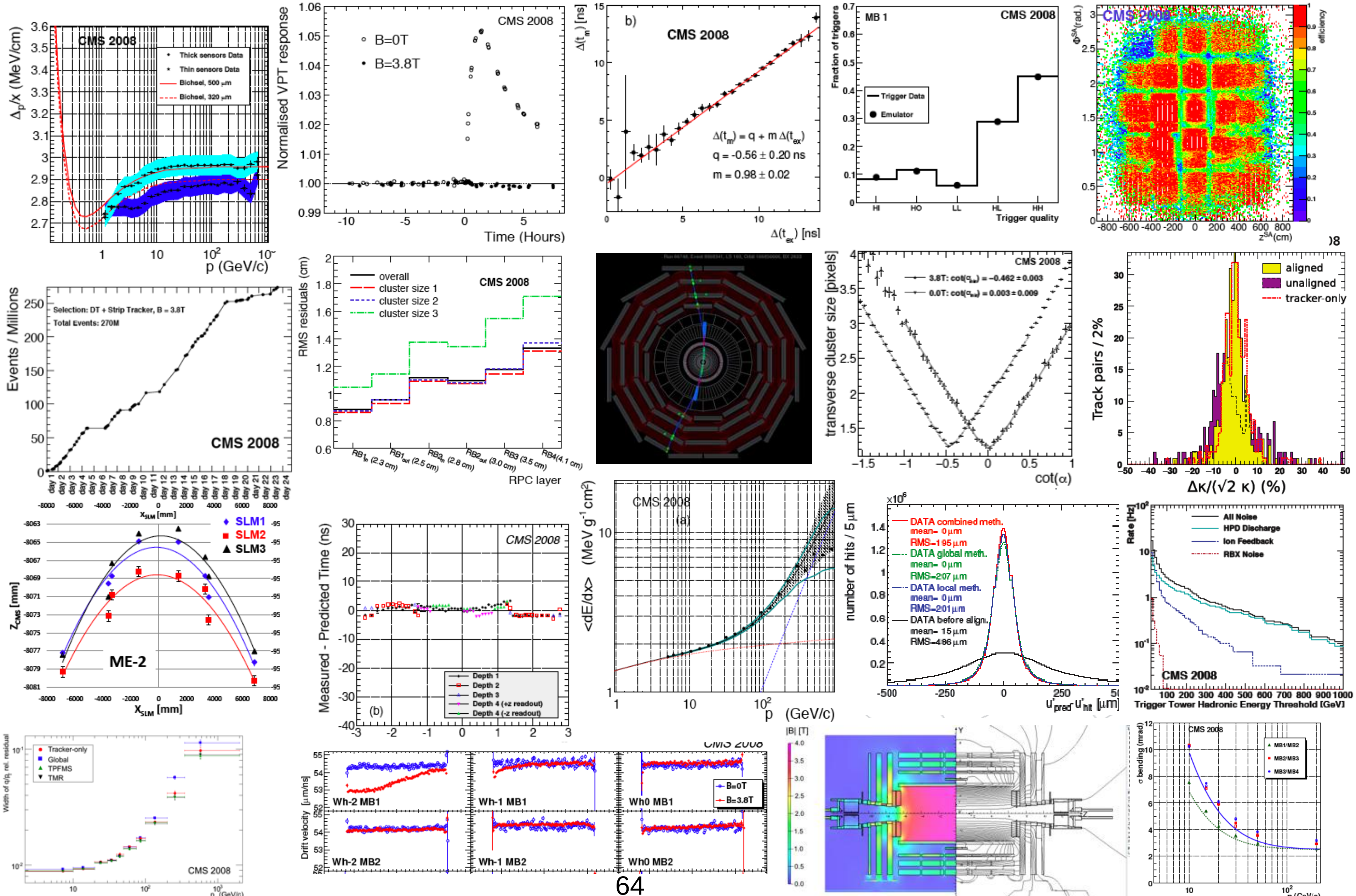

Collisions at 7 and 8 TeV!

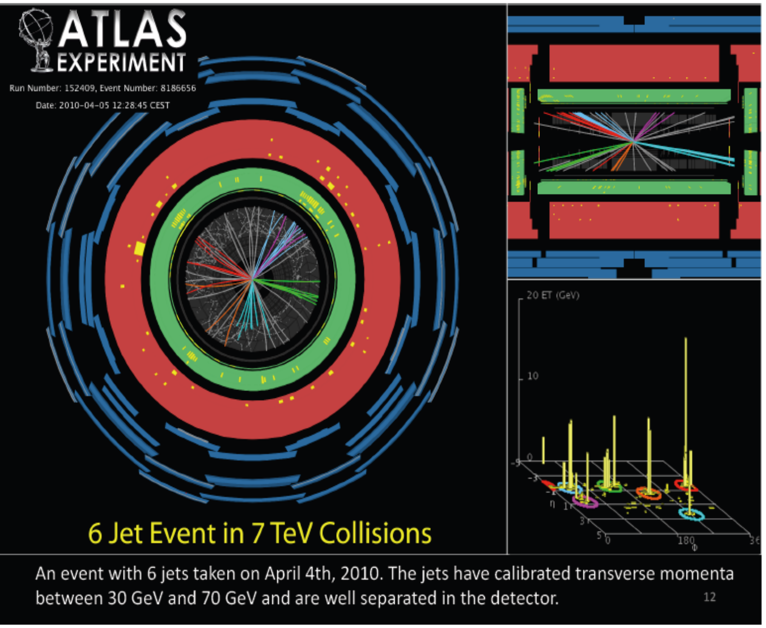

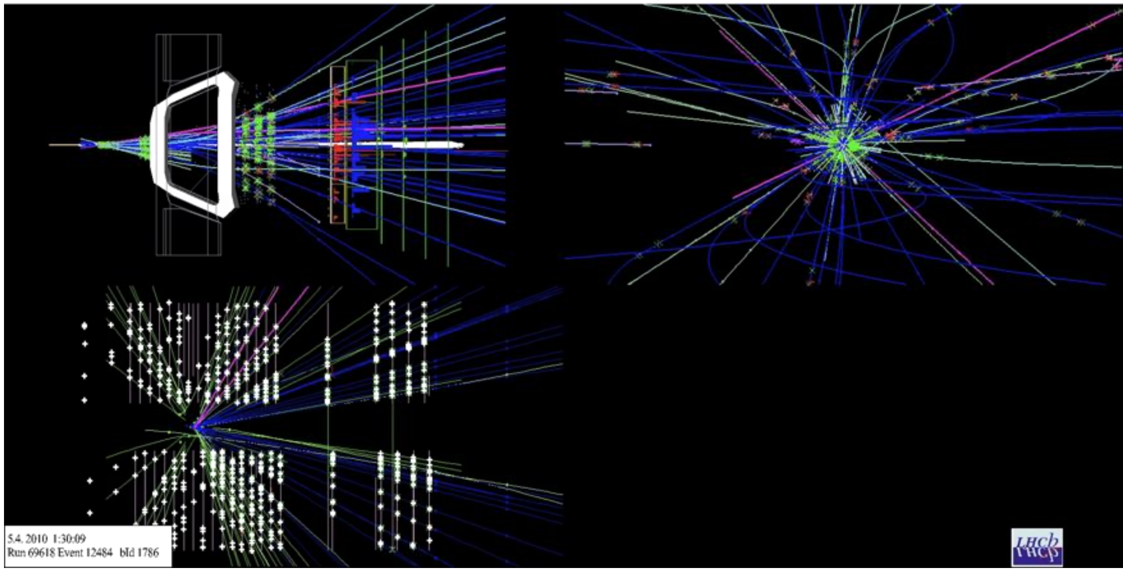

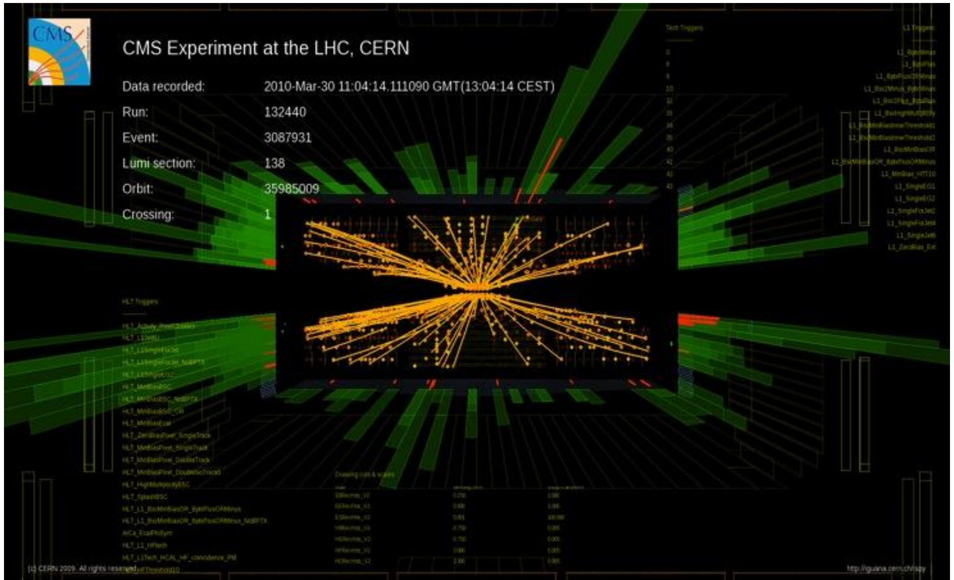

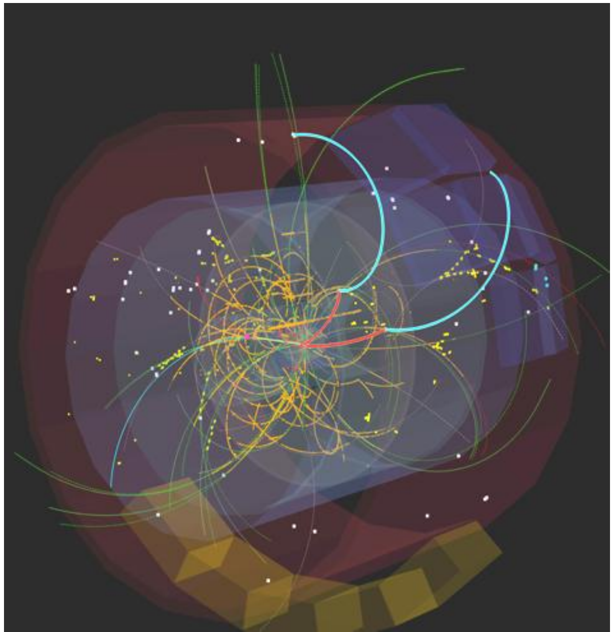

LHC Detectors are well-described in simulation e.g. Tracking - Material

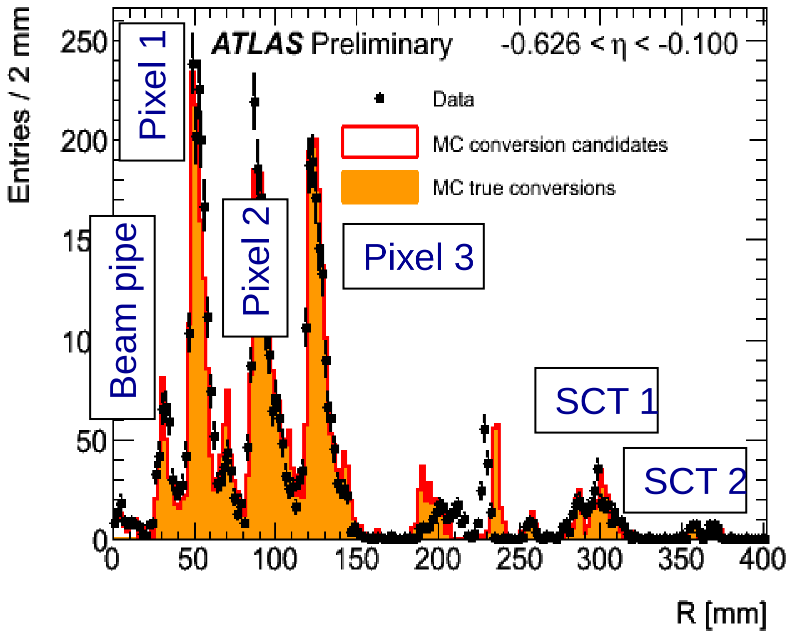

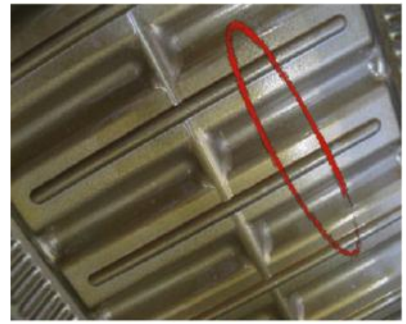

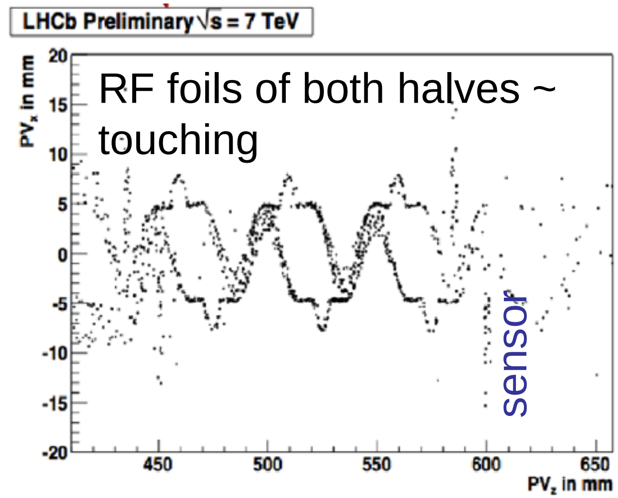

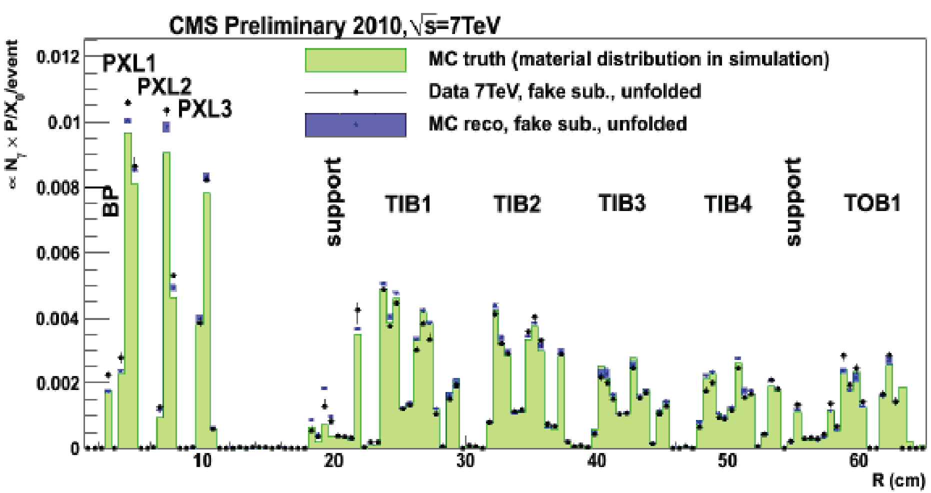

Amount of material gamma conversions data-MC

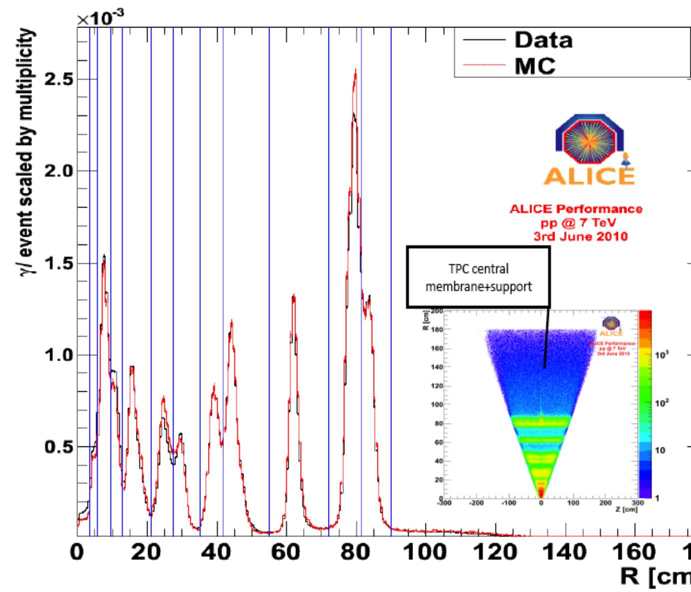

Commissioning with Beam : Tracking- Resonances

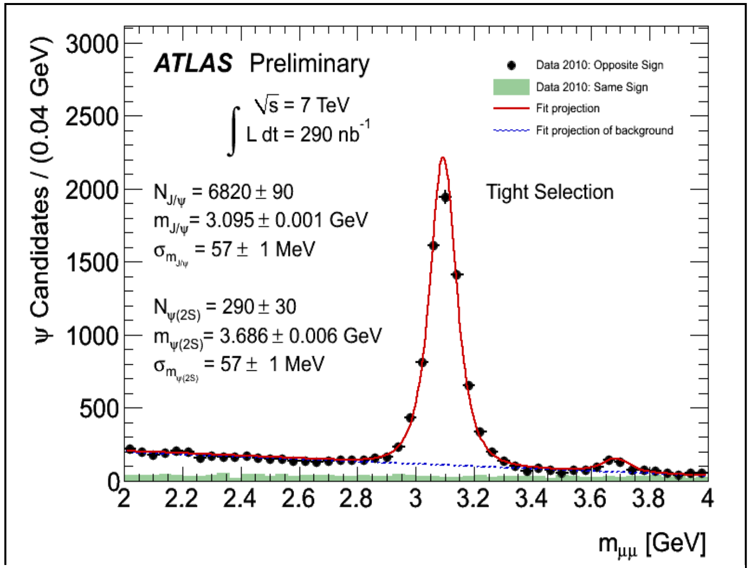

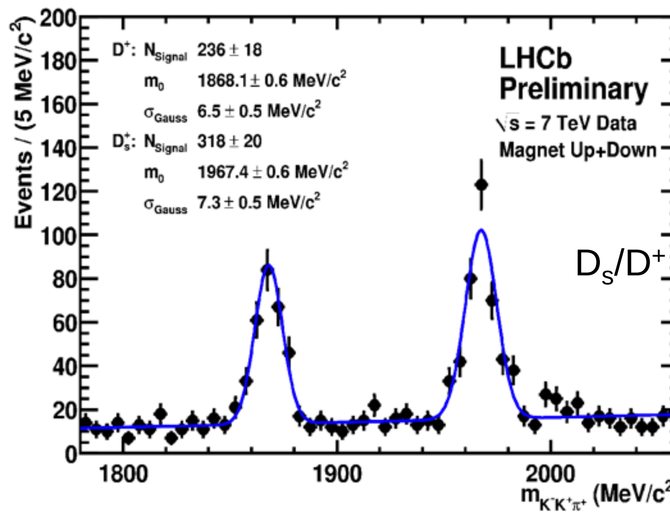

D_s/D^+ to $K\pi\ \pi$

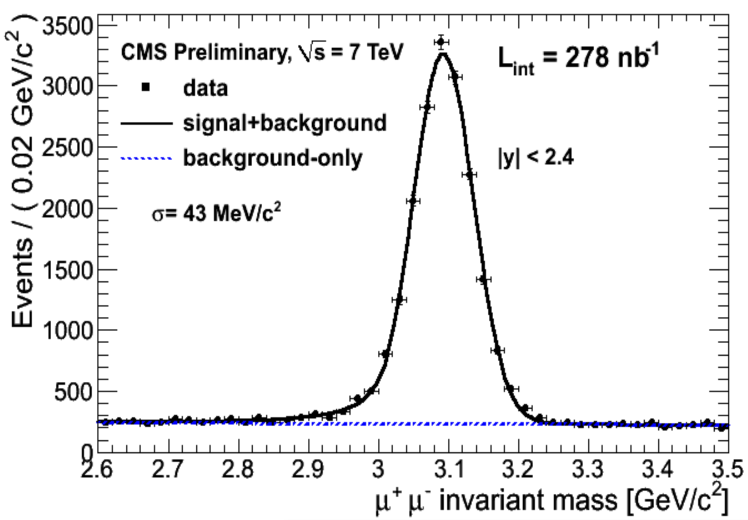

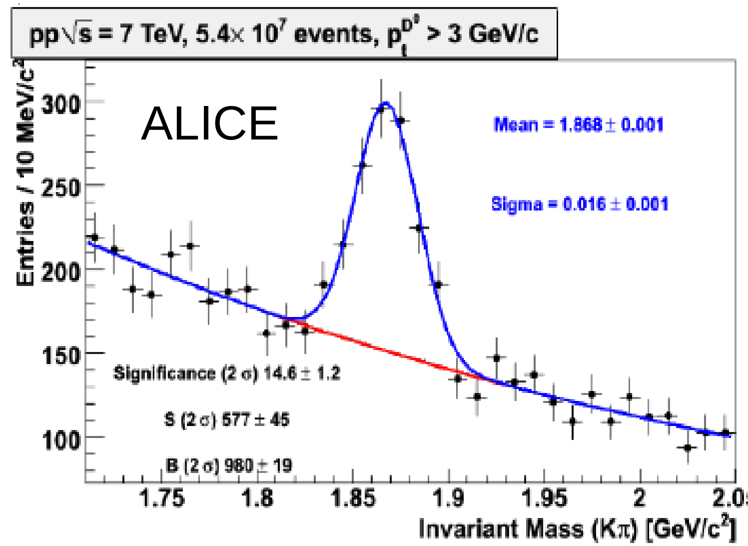

Magnetic field, momentum scale, track reconstruction efficiency; all remarkably well understood

Commissioning with Beam : Tracking-ECALs

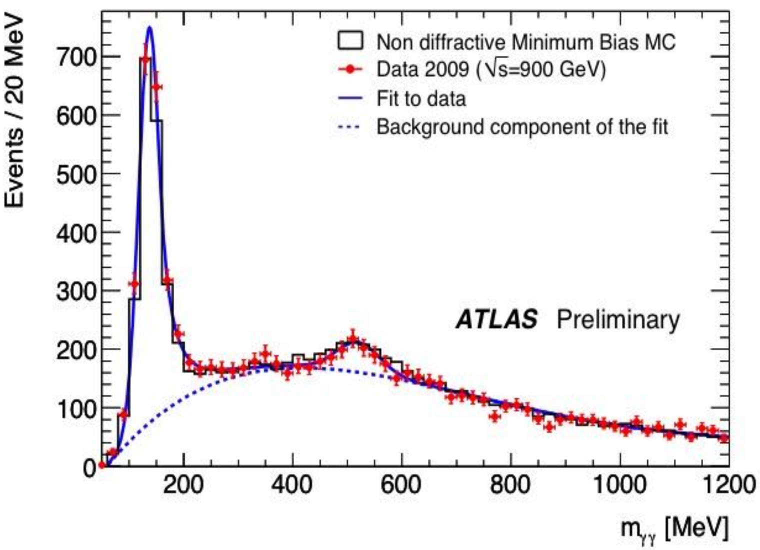

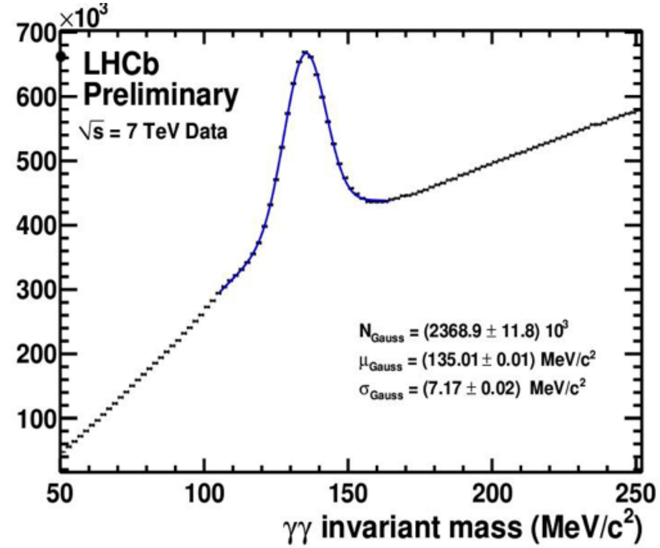

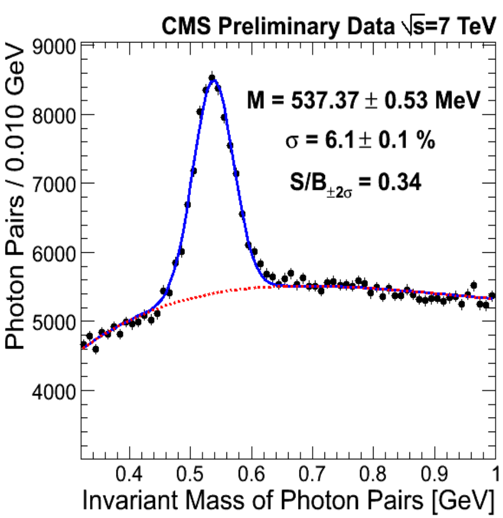

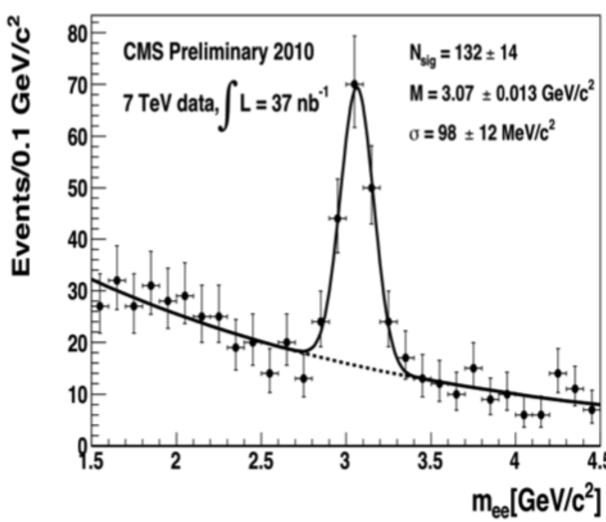

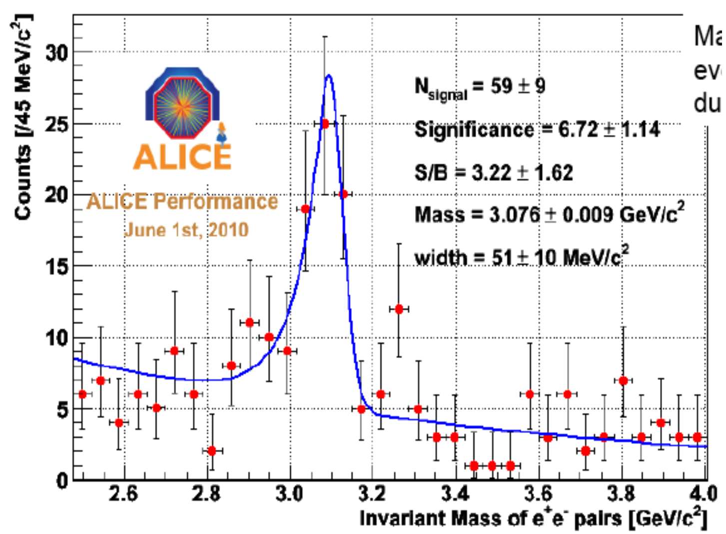

Electromagnetic calorimeters "out of the box" calibration at >≈ 1%

Commissioning with Beam: Understanding Muons, b-tagging, Triggers

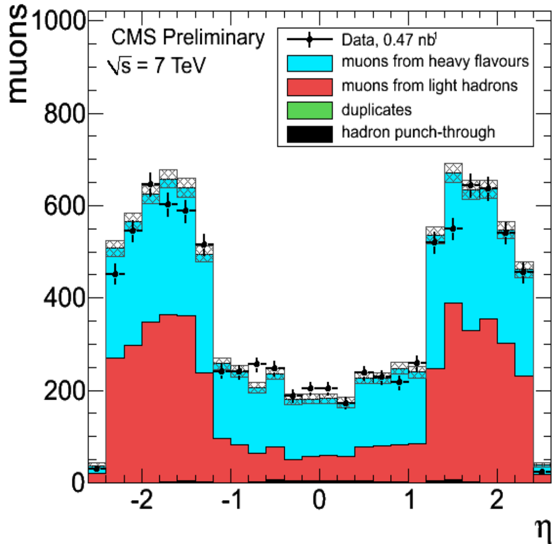

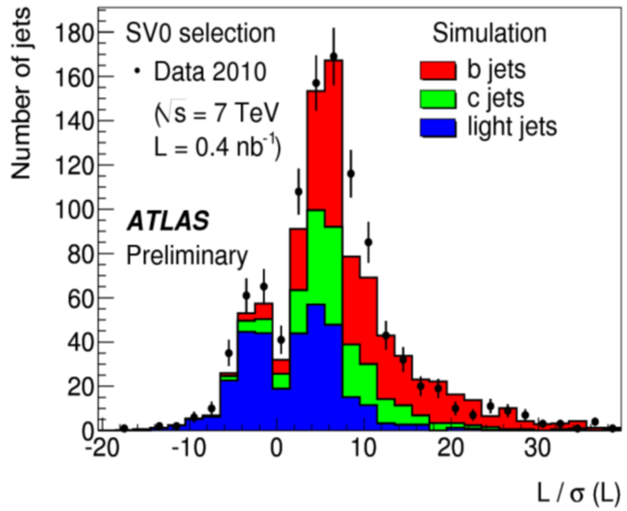

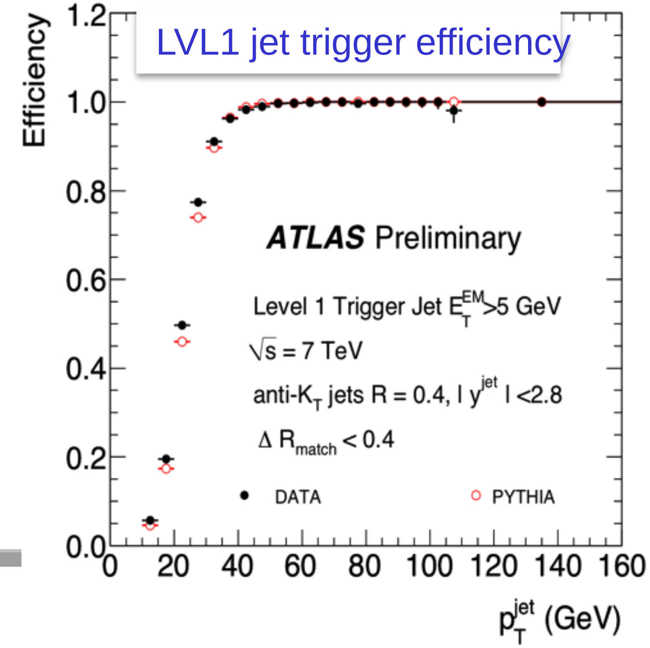

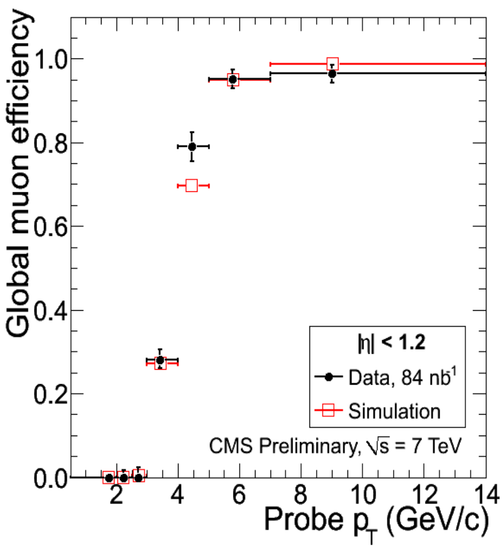

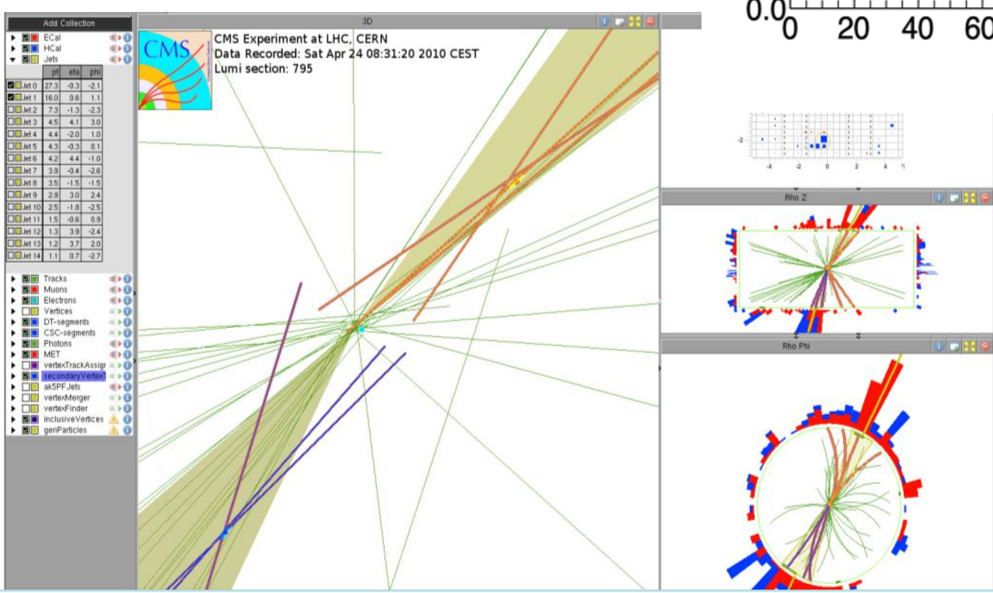

Muons remarkably well understood, b-tagging progressing well, newer triggers being rapidly understood as luminosity increases

Combining All Information: Particle Flow

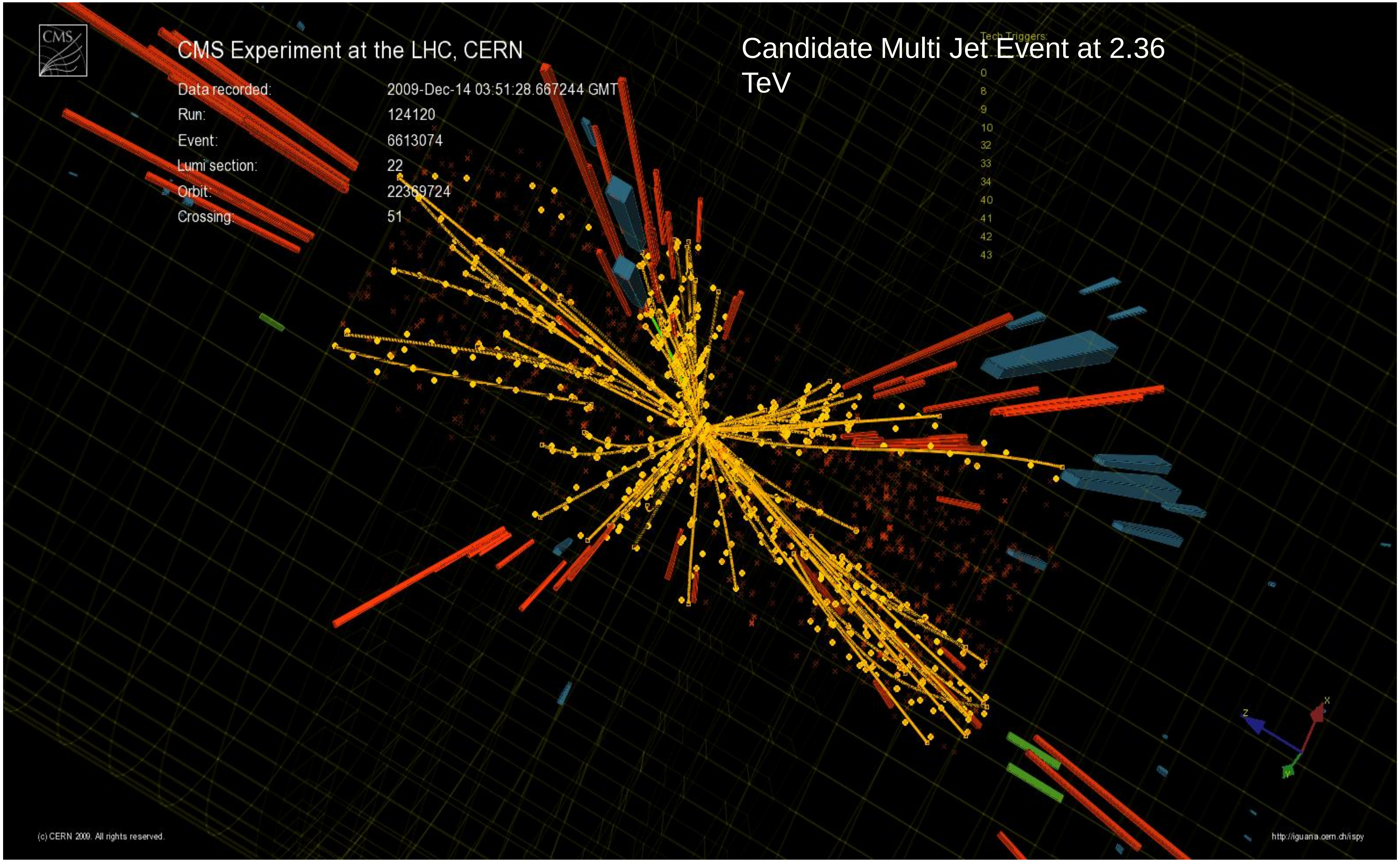

Combining Calorimetry and Tracking

Particle Flow -reconstruct all stable particles in the event

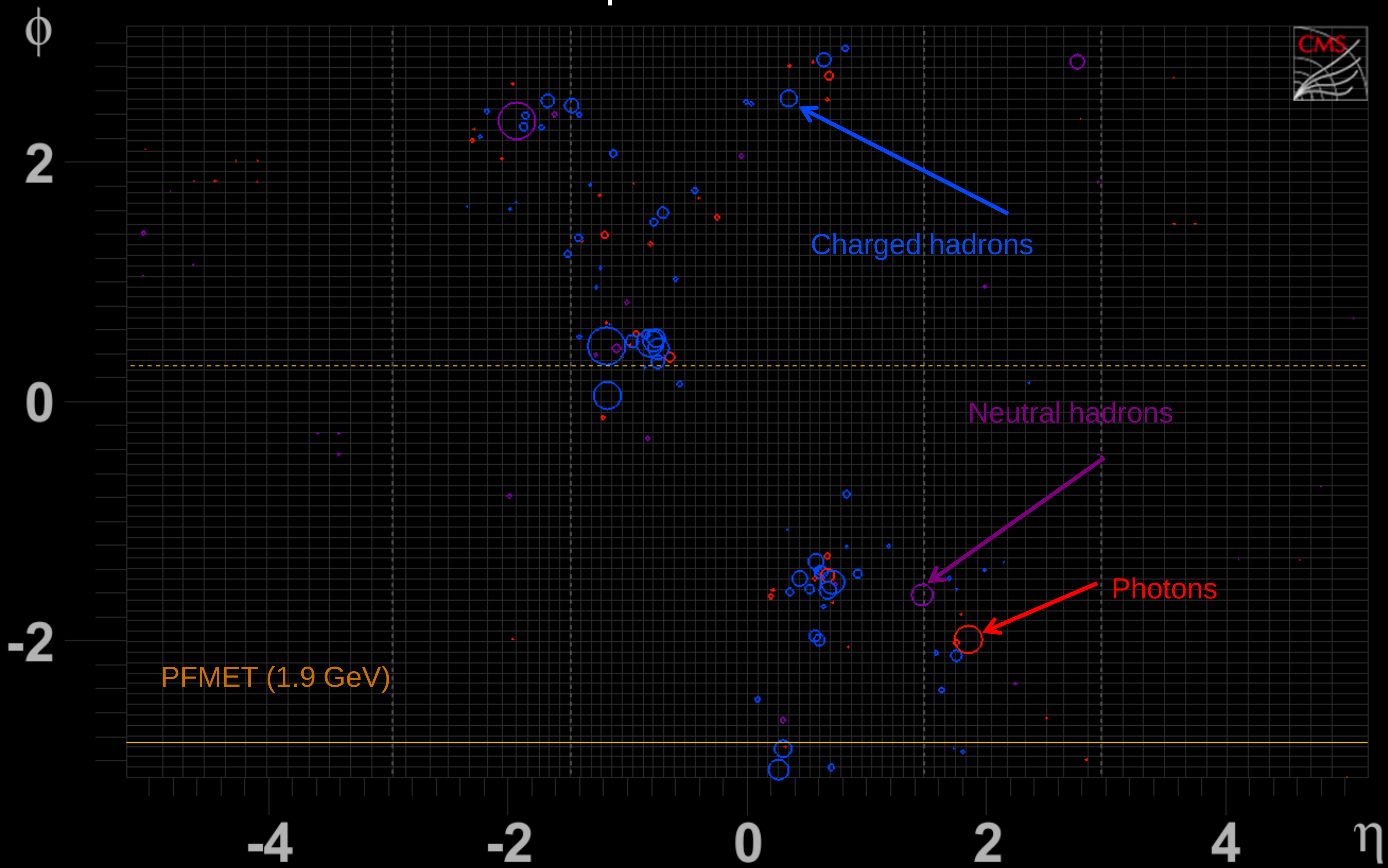

Analysing Complex Events

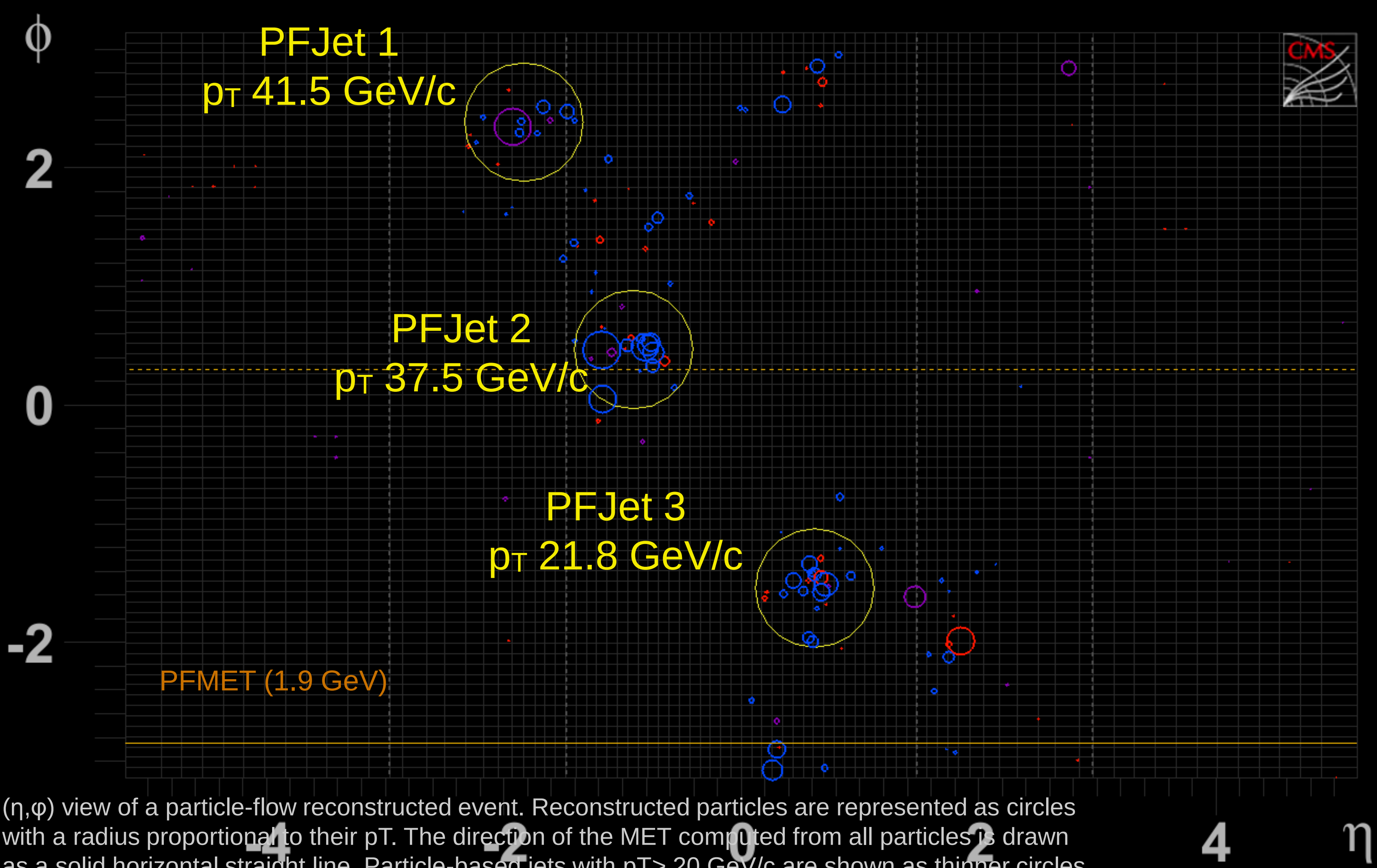

(η,φ) view of a particle-flow reconstructed event. Reconstructed particles are represented as circles with a radius proportional to their pT. The direction of the MET computed from all particles is drawn as a solid horizontal straight line. Particle-based jets with pT> 20 GeV/c are shown as thinner circles representing the extension of the jet in the (η,φ) coordinates.

Beam Commissioning: Calorimetry

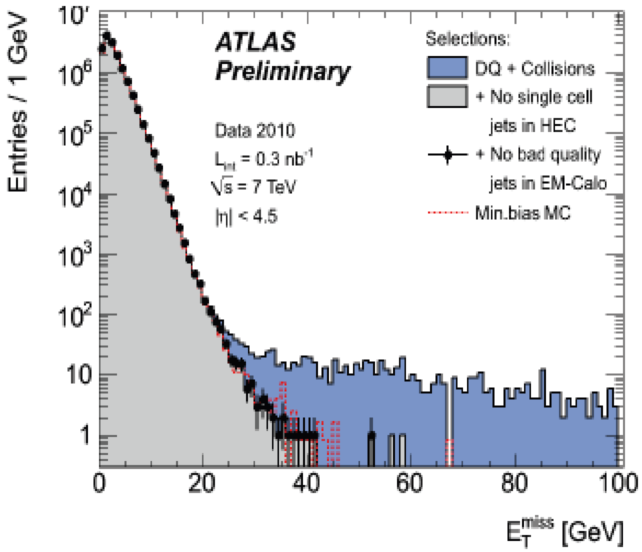

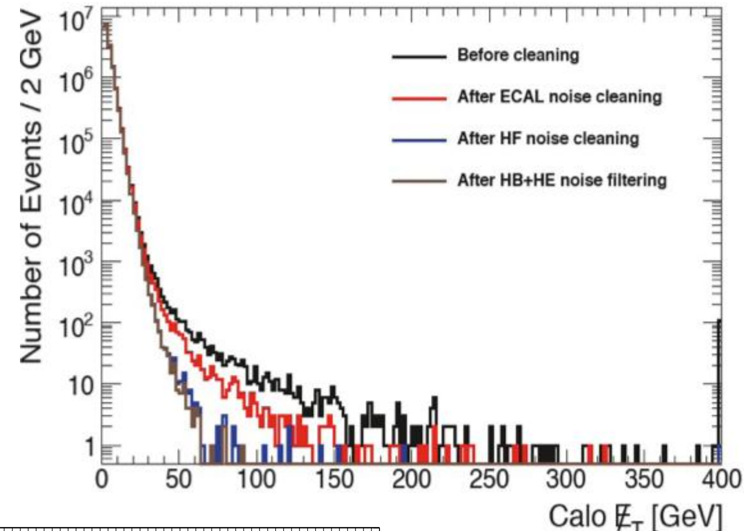

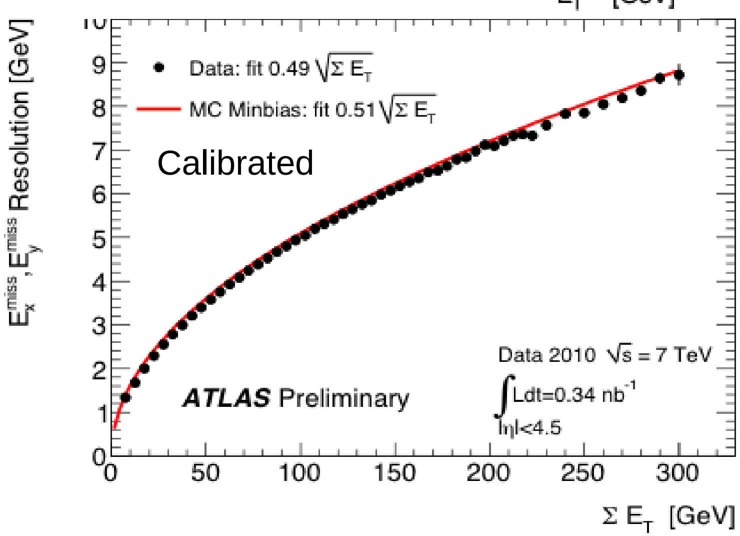

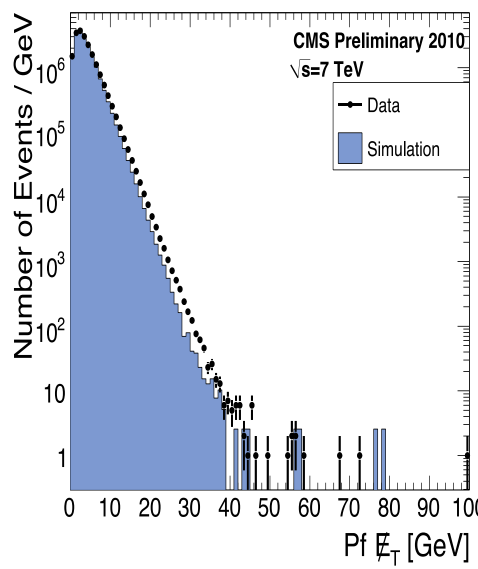

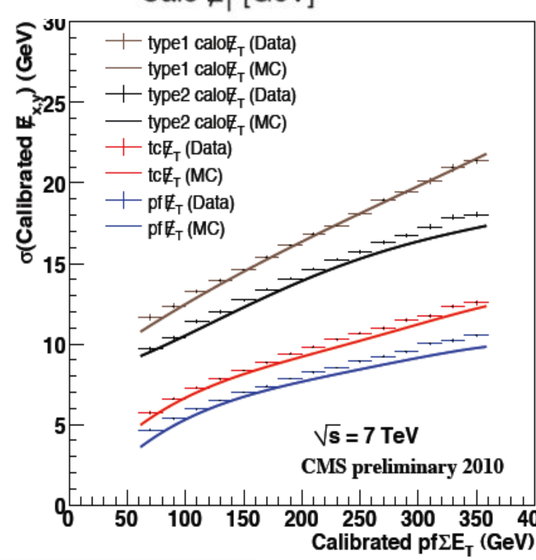

MET distributions exponential over >5 orders of magnitude; augurs well for searches

50 Years of Particle Physics; e.g. CMS

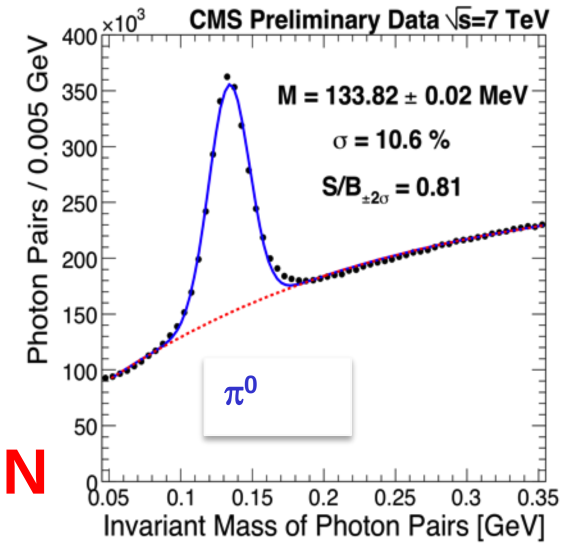

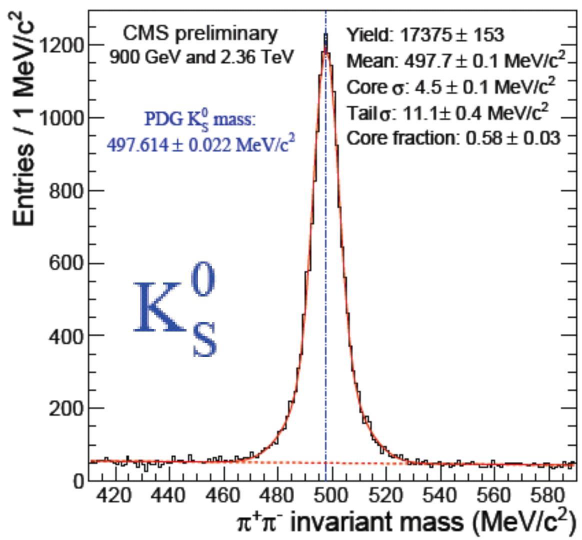

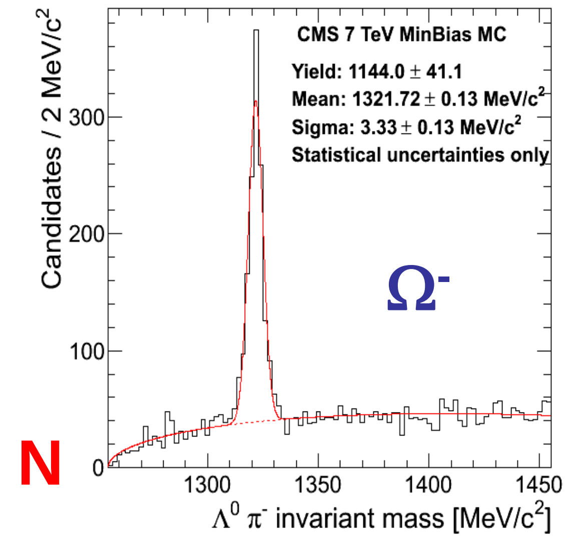

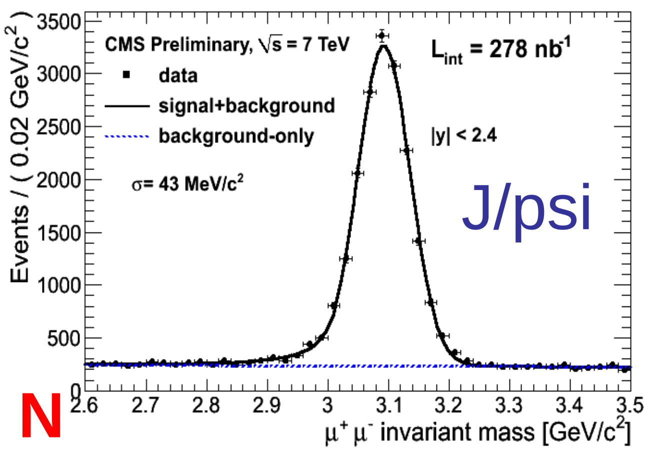

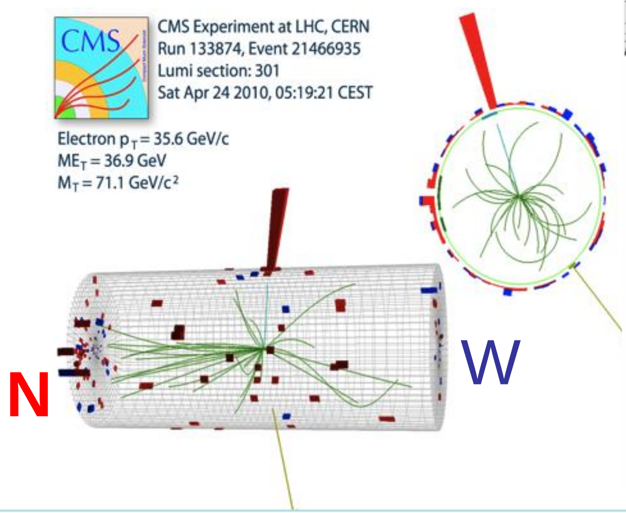

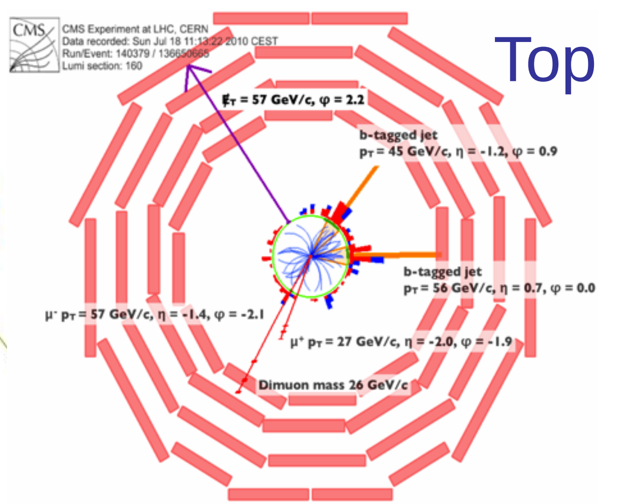

Sophisticated software and computing systems in place and functioning

Rediscovering the SM and Beyond

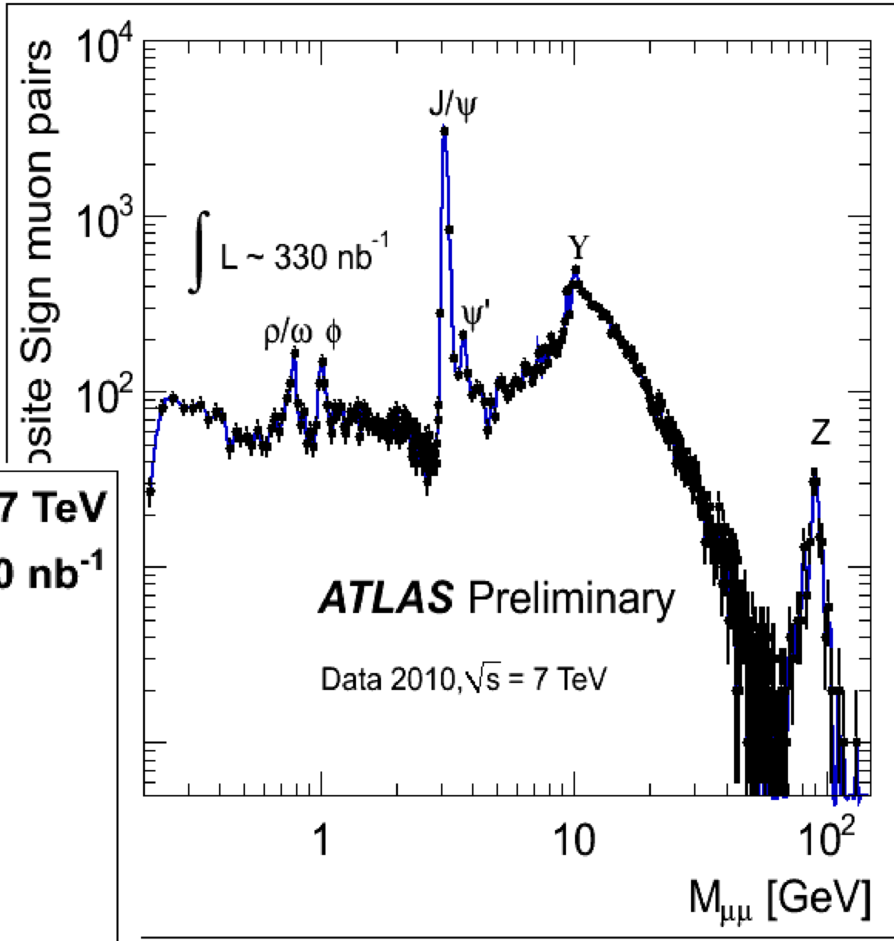

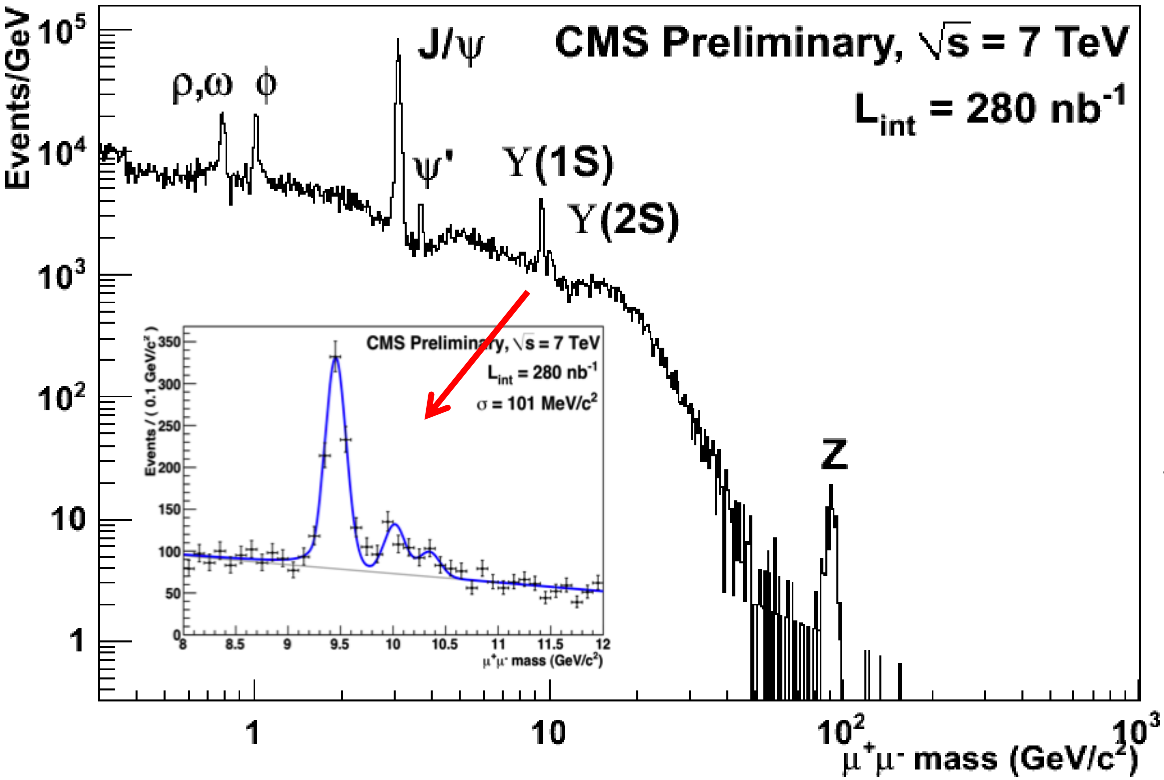

Study of track-based missing pT

- Provide an alternative measurement to Calo-based MET
  - Different detector, has different un-correlated systematic effect
  - Can associate tracks to primary vertex, can calculate pTmiss and SumPt based on primary vertex of the event, thus more correlated to the true MET of the main physics process
  - Should deteriorate less than calorimeter based variables as instantaneous luminosity increases (as long as our vertex resolution is good)
  - Has less effect due to cosmic muons and beam background

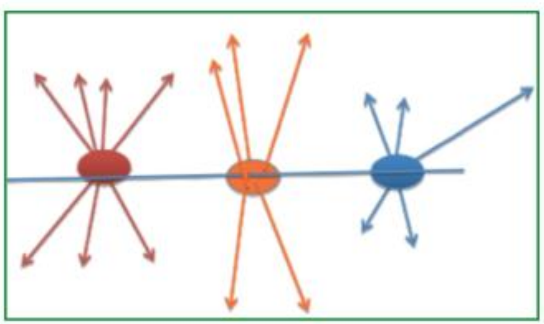

vertex-based missing pT

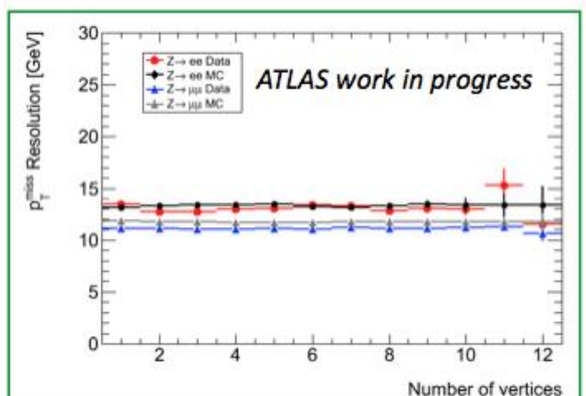

missing pT resolution VS # of vertices

- Several presentations in the ATLAS jet-Etmiss group and group meetings
- Work in collaboration with Academia Sinica

Putting it all together…

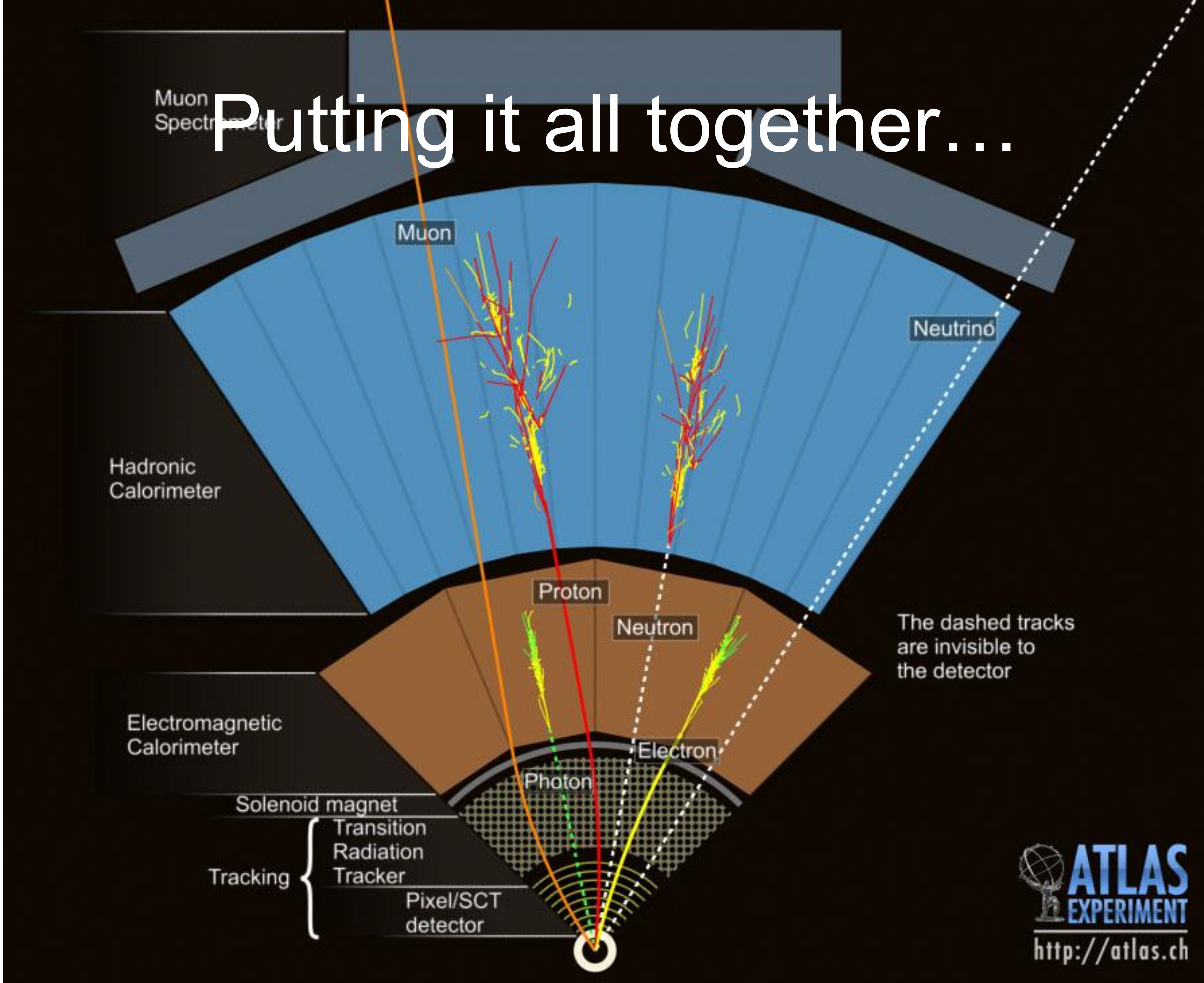

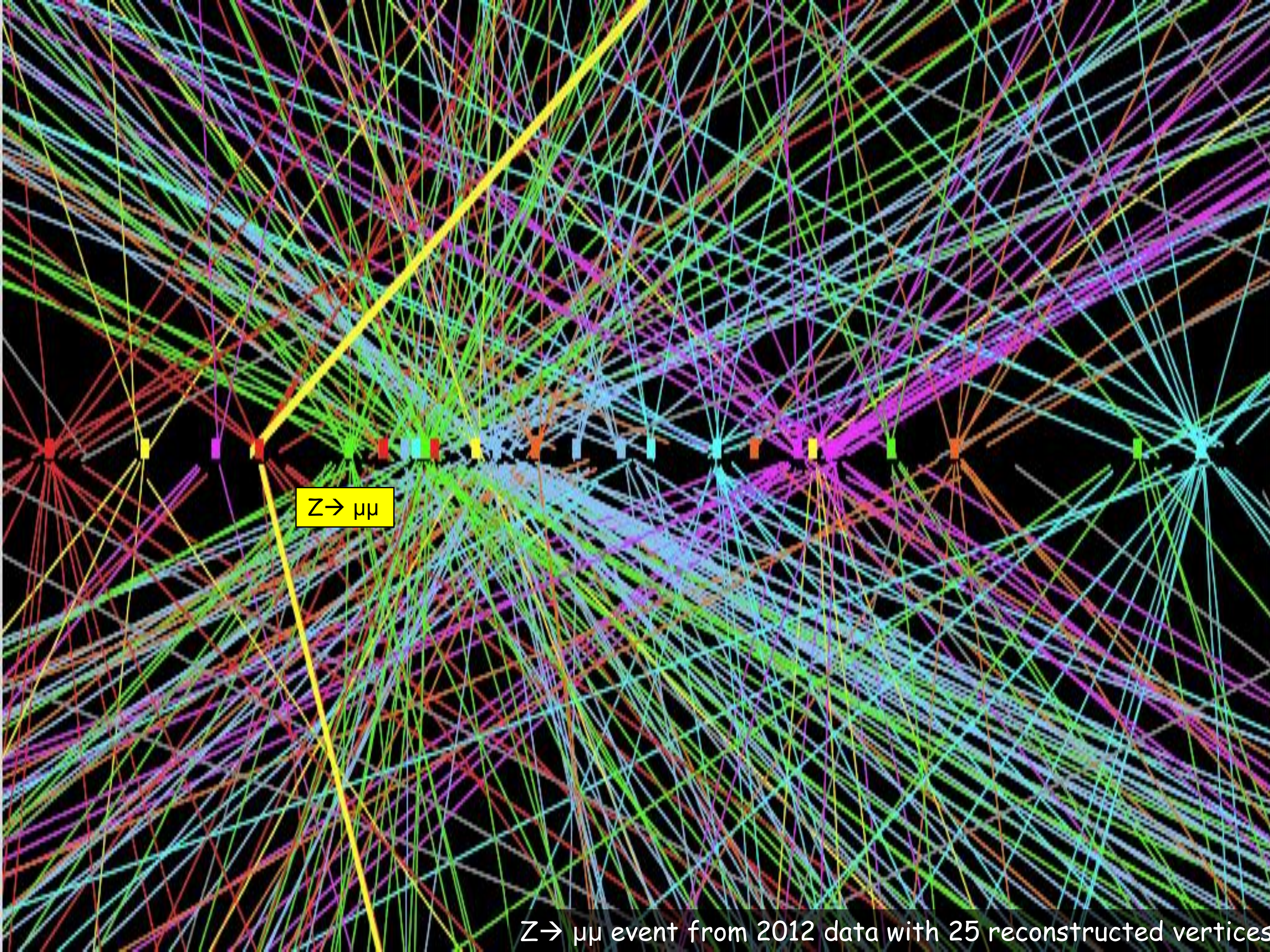

Z→ μμ event from 2012 data with 25 reconstructed vertices

SM Higgs production and decay modes

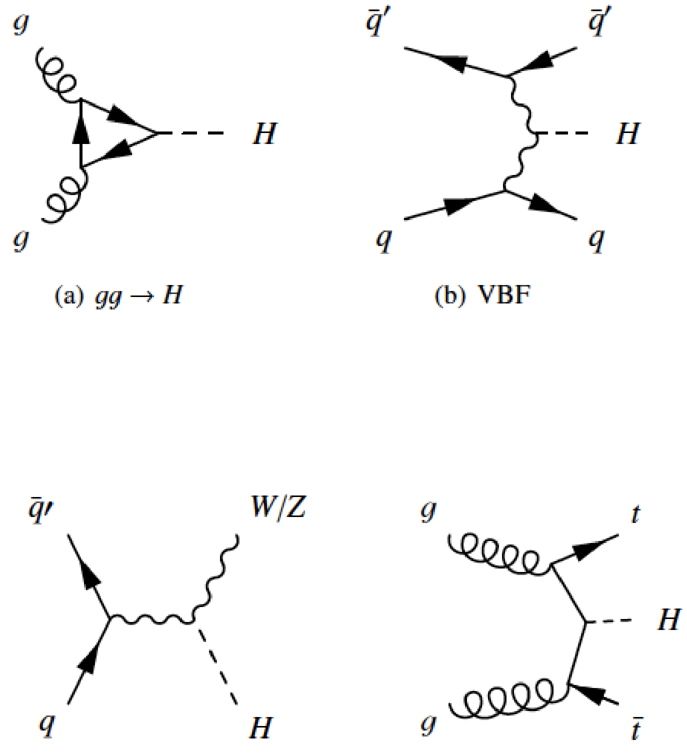

(a) gg → H
(b) VBF
(c) VH
(d) tt̄H

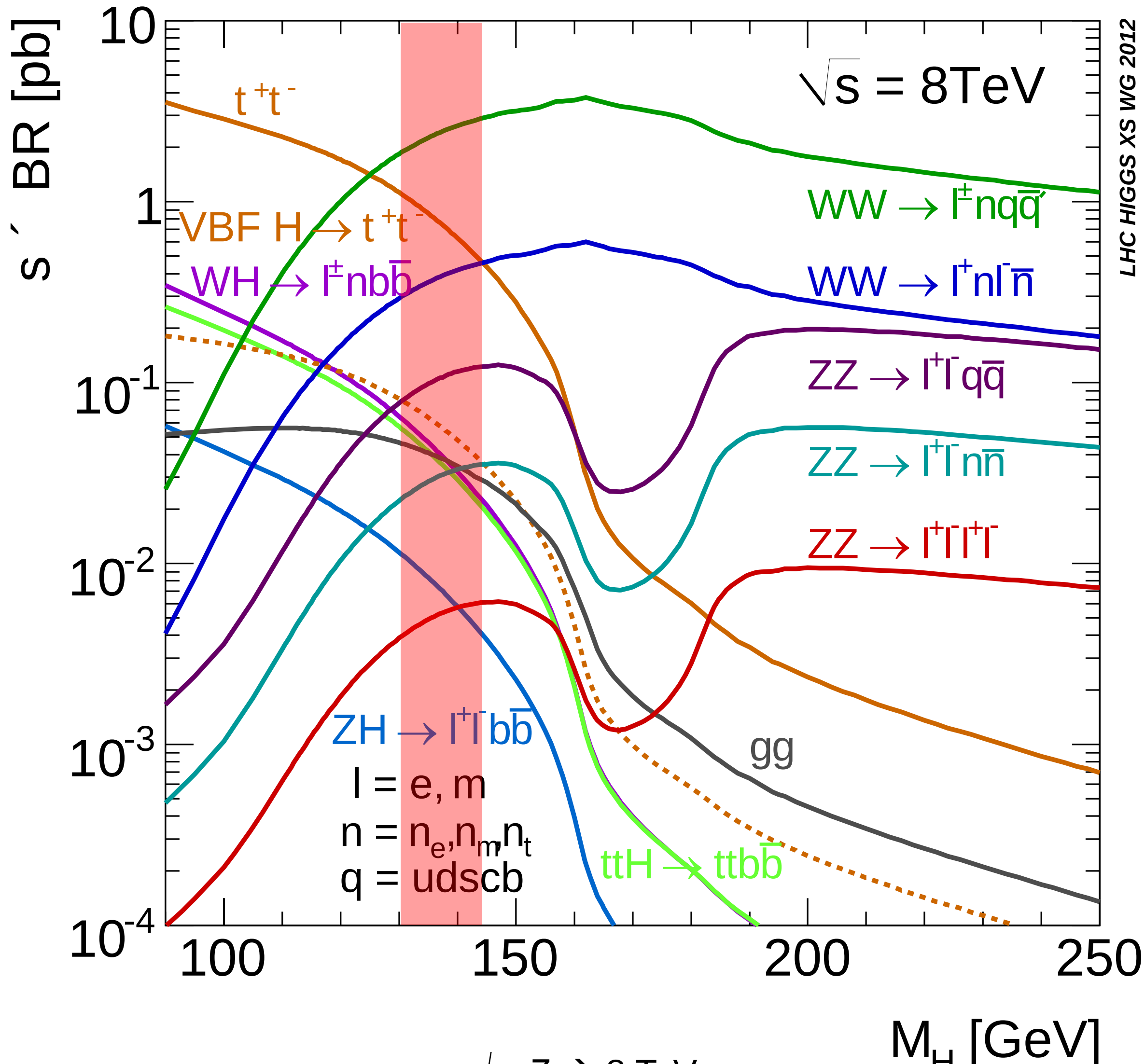

√s=7 → 8 TeV:

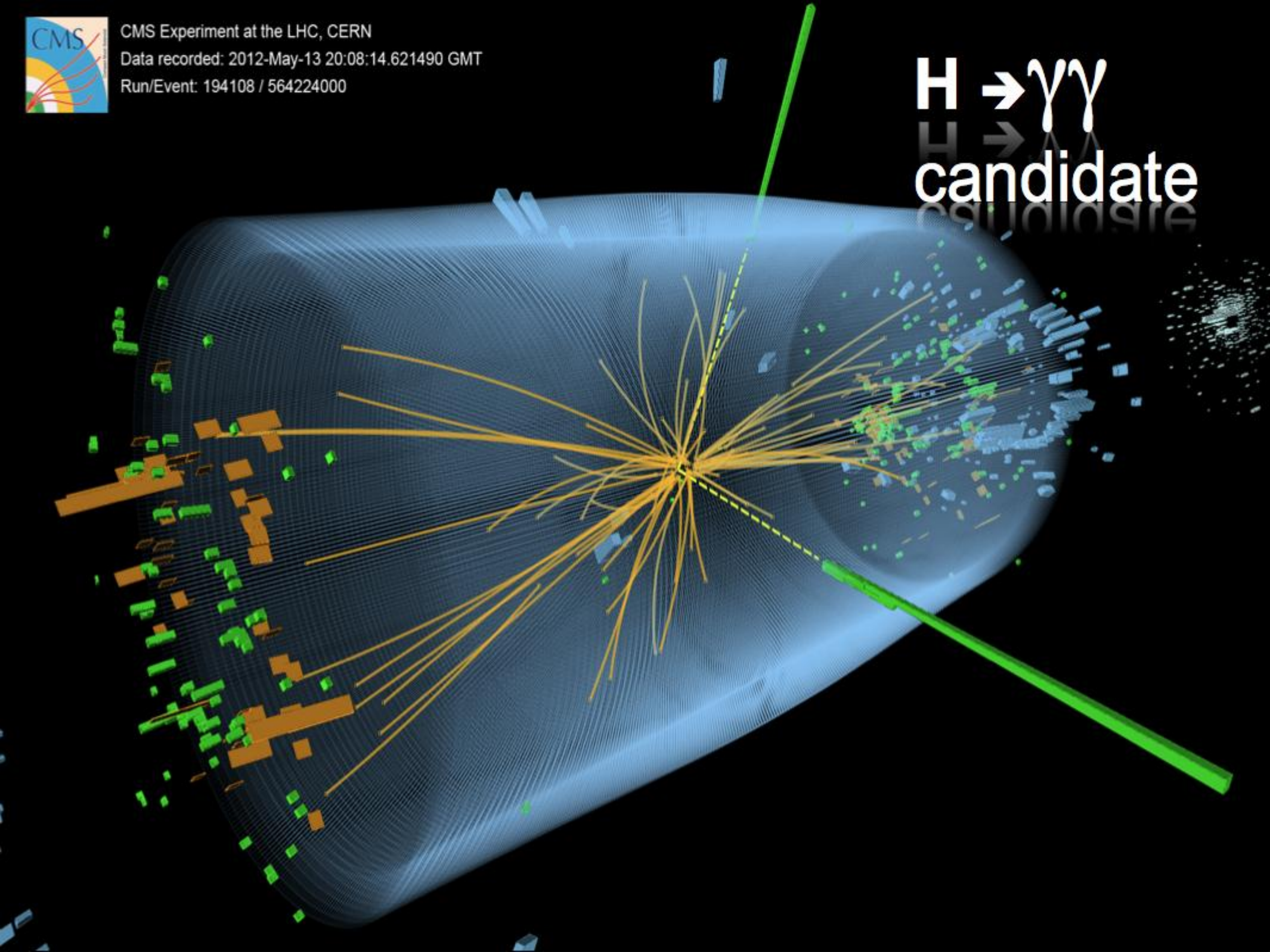
CMS Experiment at the LHC, CERN
Data recorded: 2012-May-13 20:08:14.621490 GMT
Run/Event: 194108 / 564224000
H →γγ
candidate

H → $\gamma\gamma$

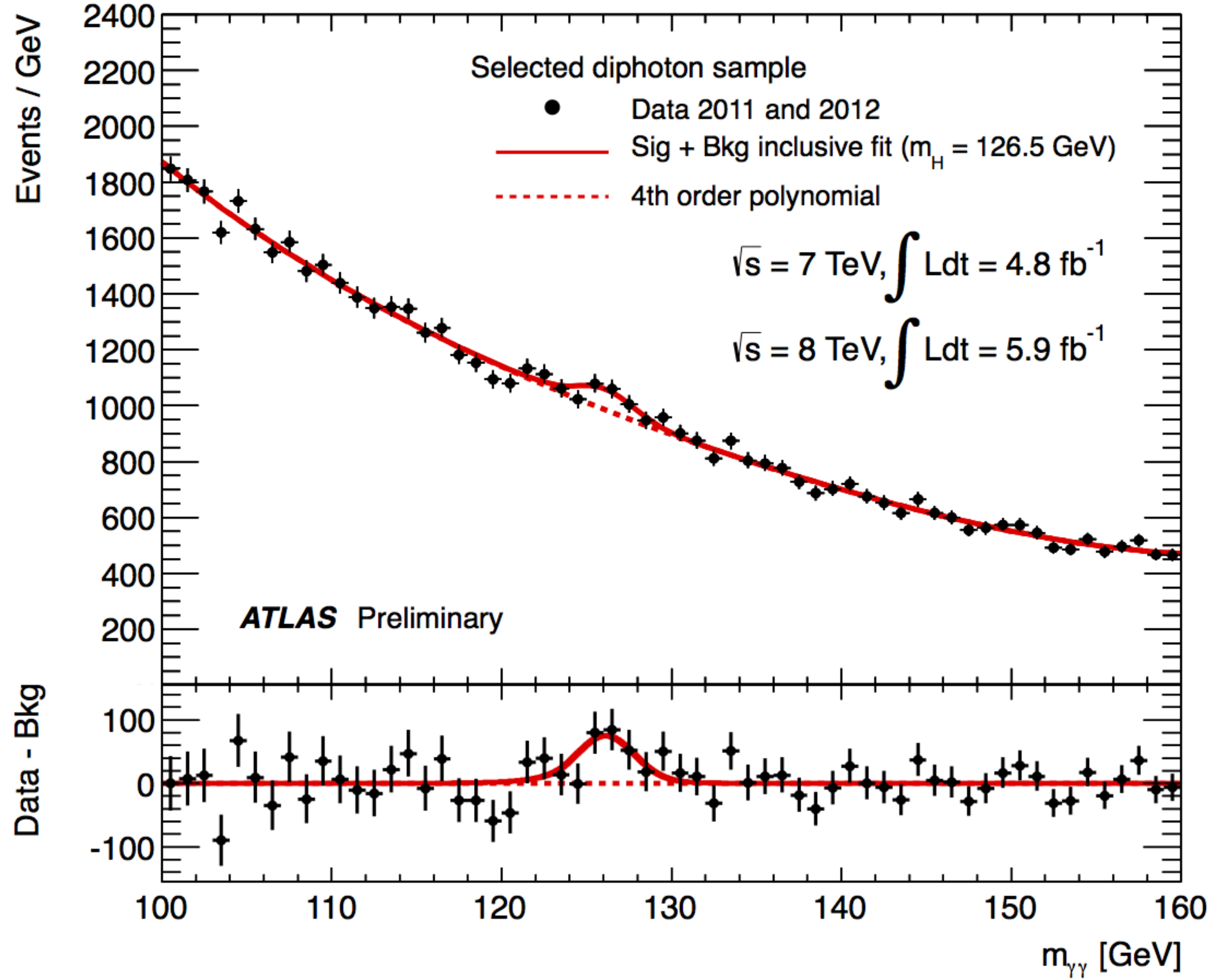

4μ candidate with $m_{4\mu}$= 125.1 GeV

p_T (muons)= 36.1, 47.5, 26.4, 71 .7GeV m_{12}= 86.3 GeV, m_{34}= 31.6 GeV
15 reconstructed vertices

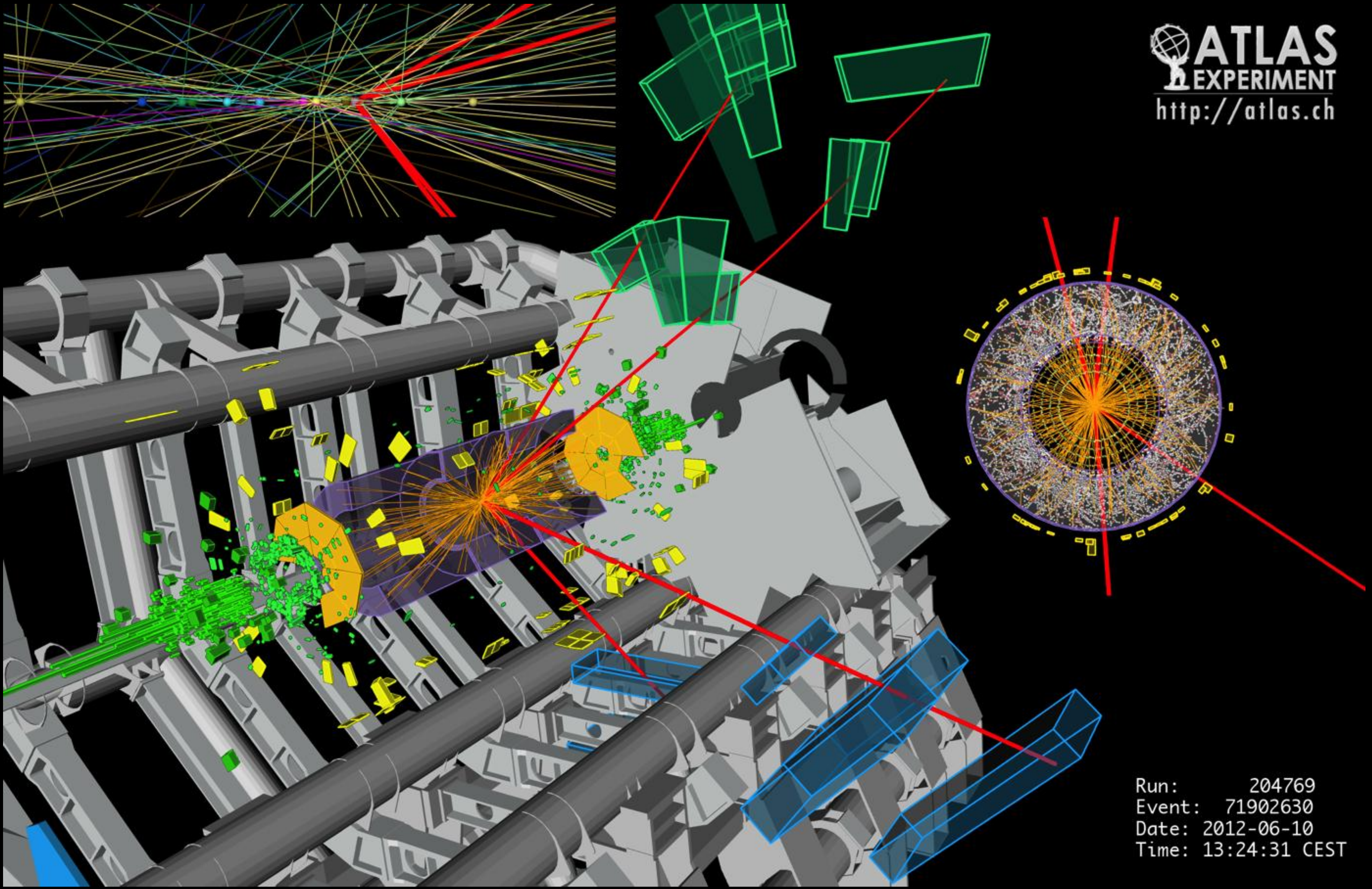

4e candidate with m_{4e}= 124.6 GeV

p_T (electrons)= 24.9, 53.9, 61.9, 17.8 GeV m_{12}= 70.6 GeV, m_{34}= 44.7 GeV
12 reconstructed vertices

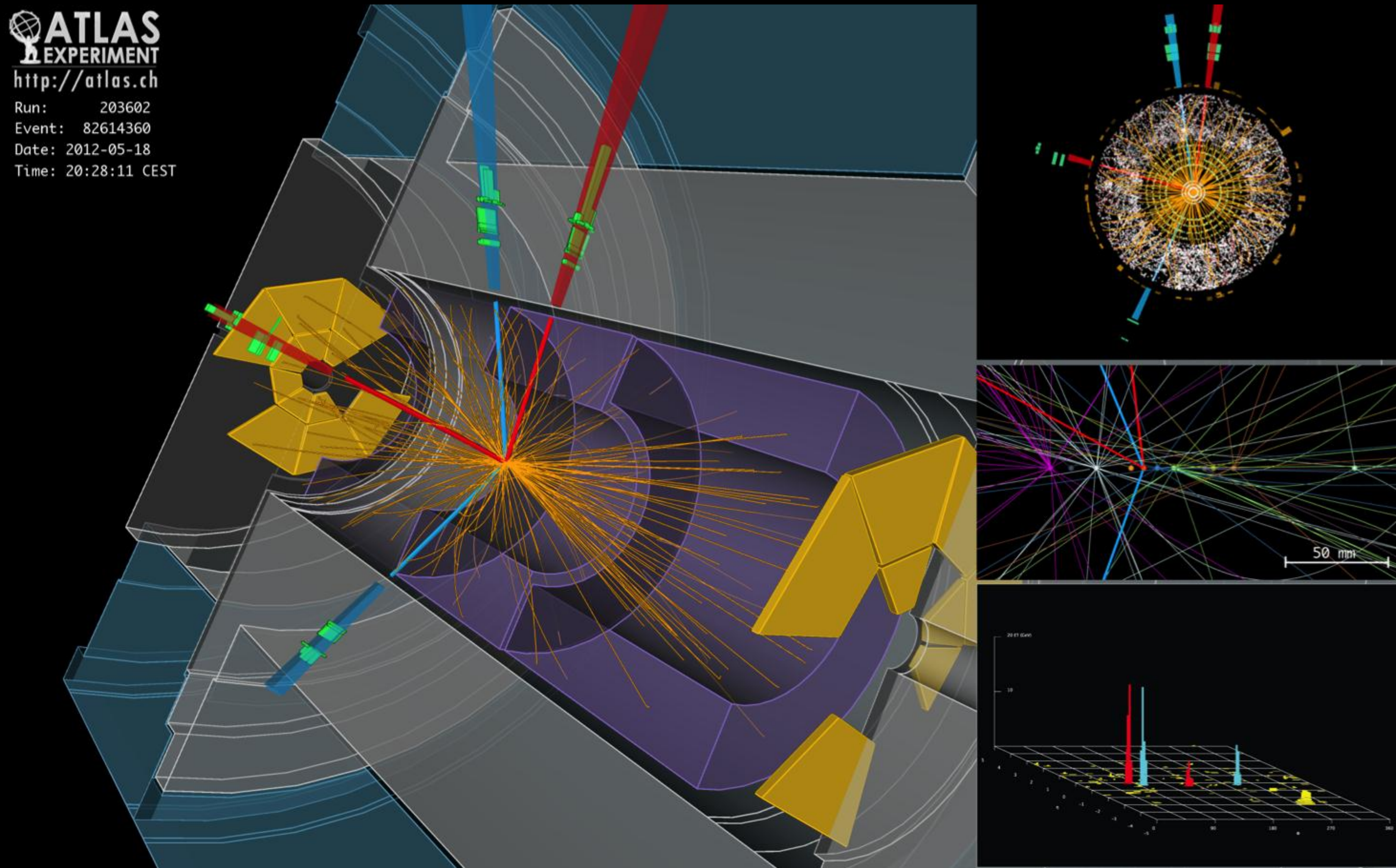

2e2μ candidate with $m_{2e2\mu}$ = 123.9 GeV

p_T (e,e,μ,μ)= 18.7, 76, 19.6, 7.9 GeV, m (e^+e^-)= 87.9 GeV, m($\mu^+\mu^-$) =19.6 GeV
12 reconstructed vertices

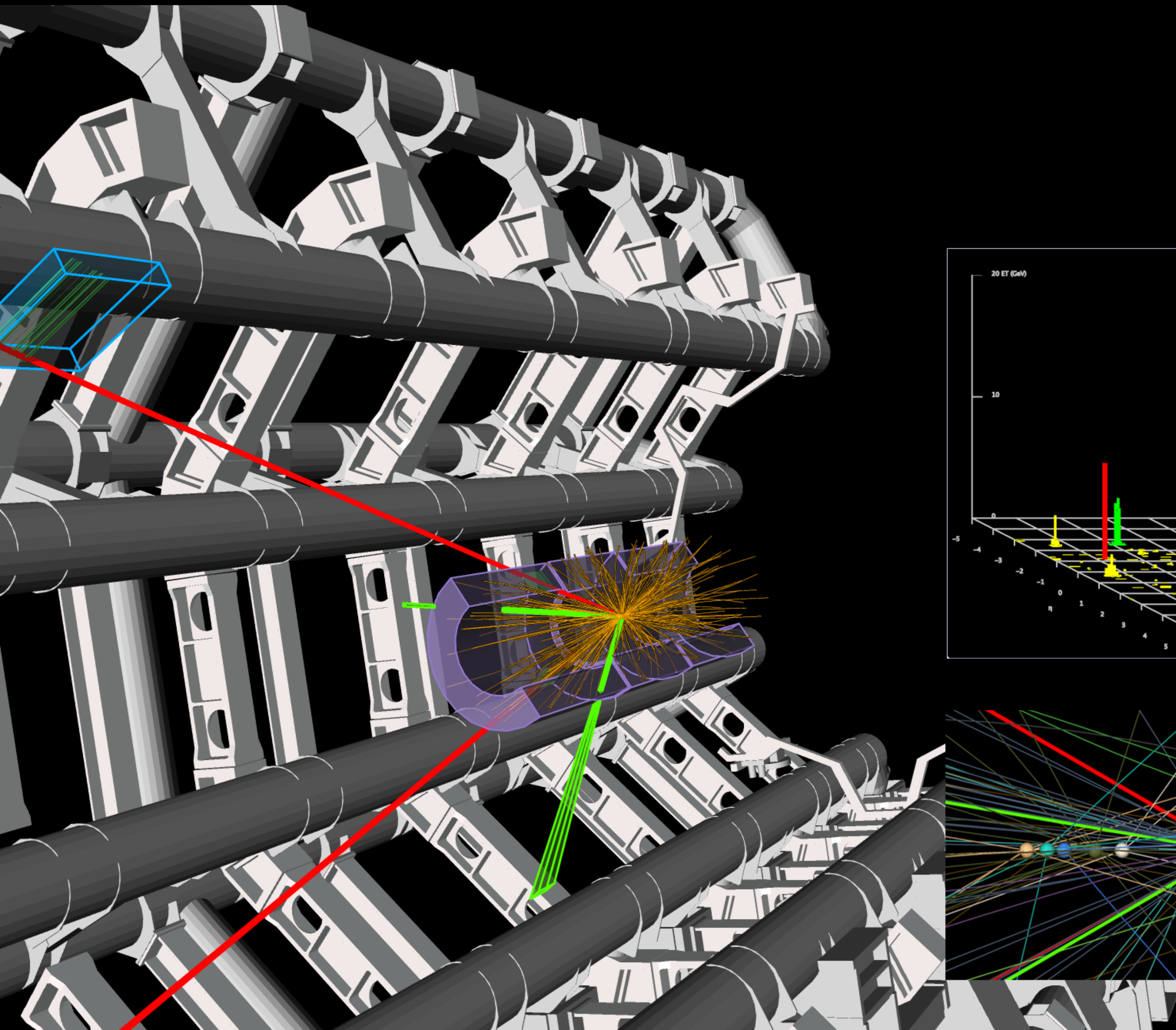

ATLAS EXPERIMENT
http://atlas.ch
Run: 205113
Event: 12611816
Date: 2012-06-18
Time: 11:07:47 CEST

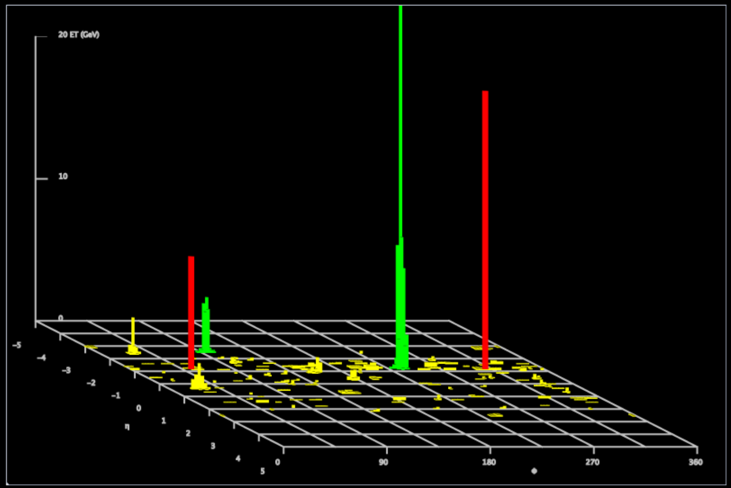

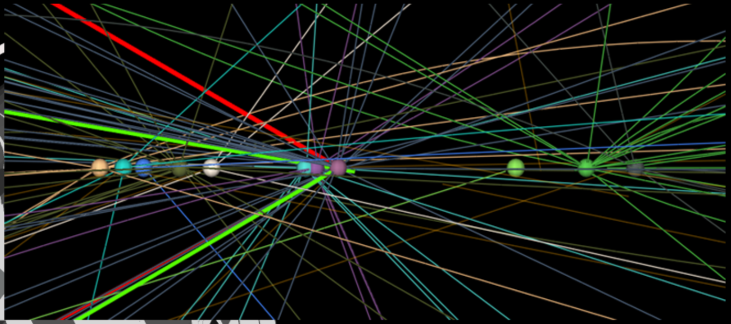

H → 4 leptons combined results

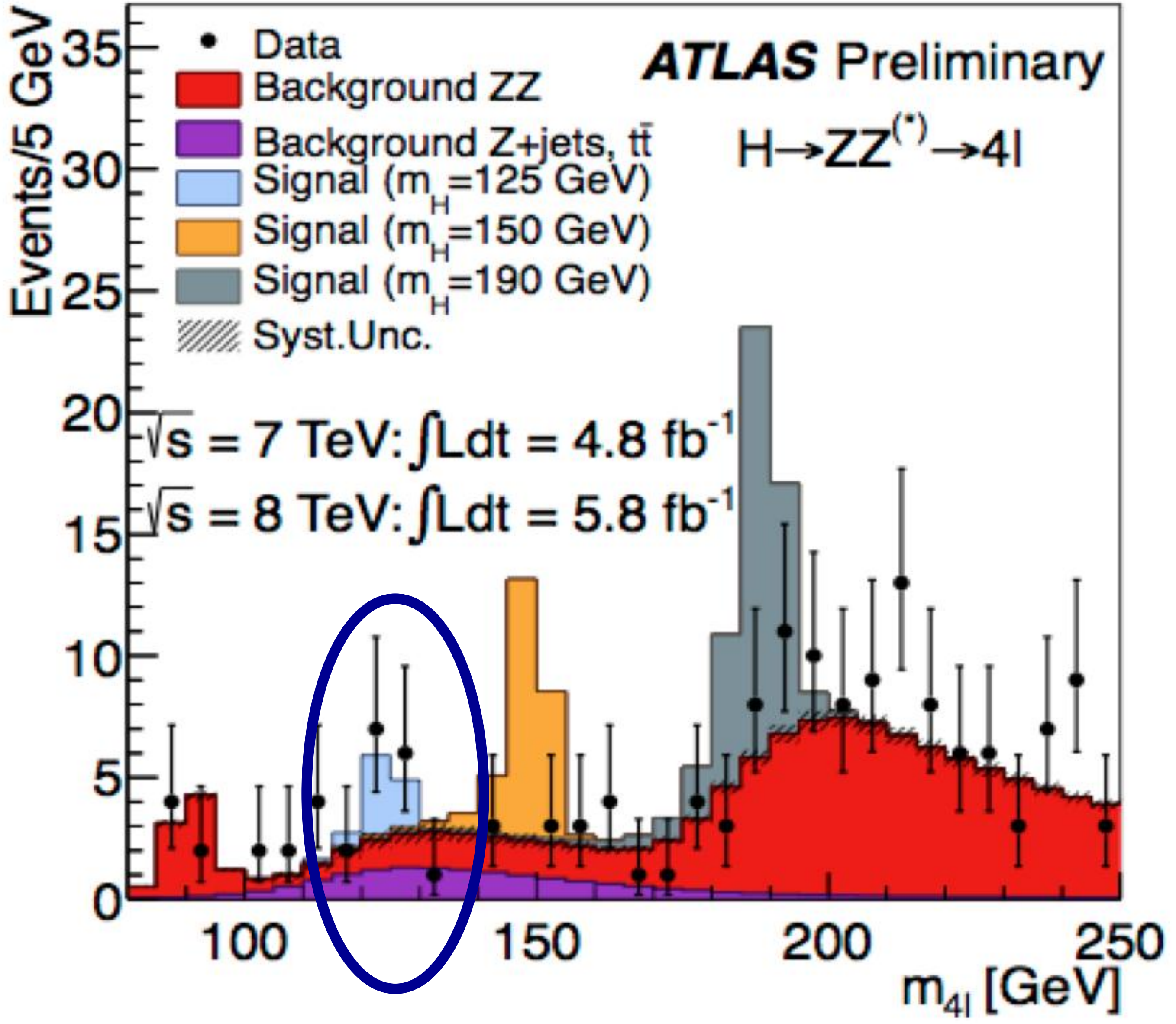

ATLAS "Excess"

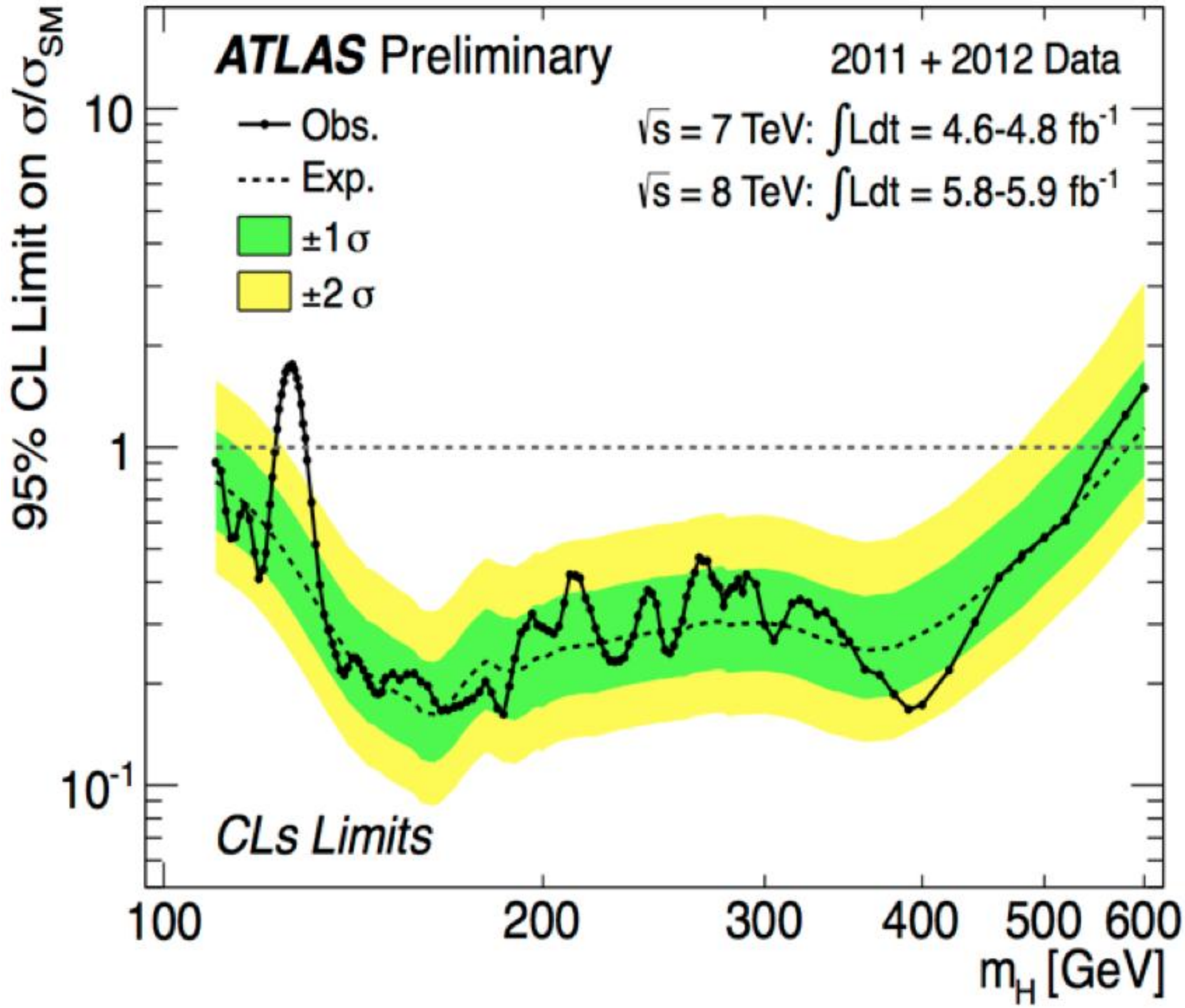

5σ Confidence limit --- DISCOVERY !

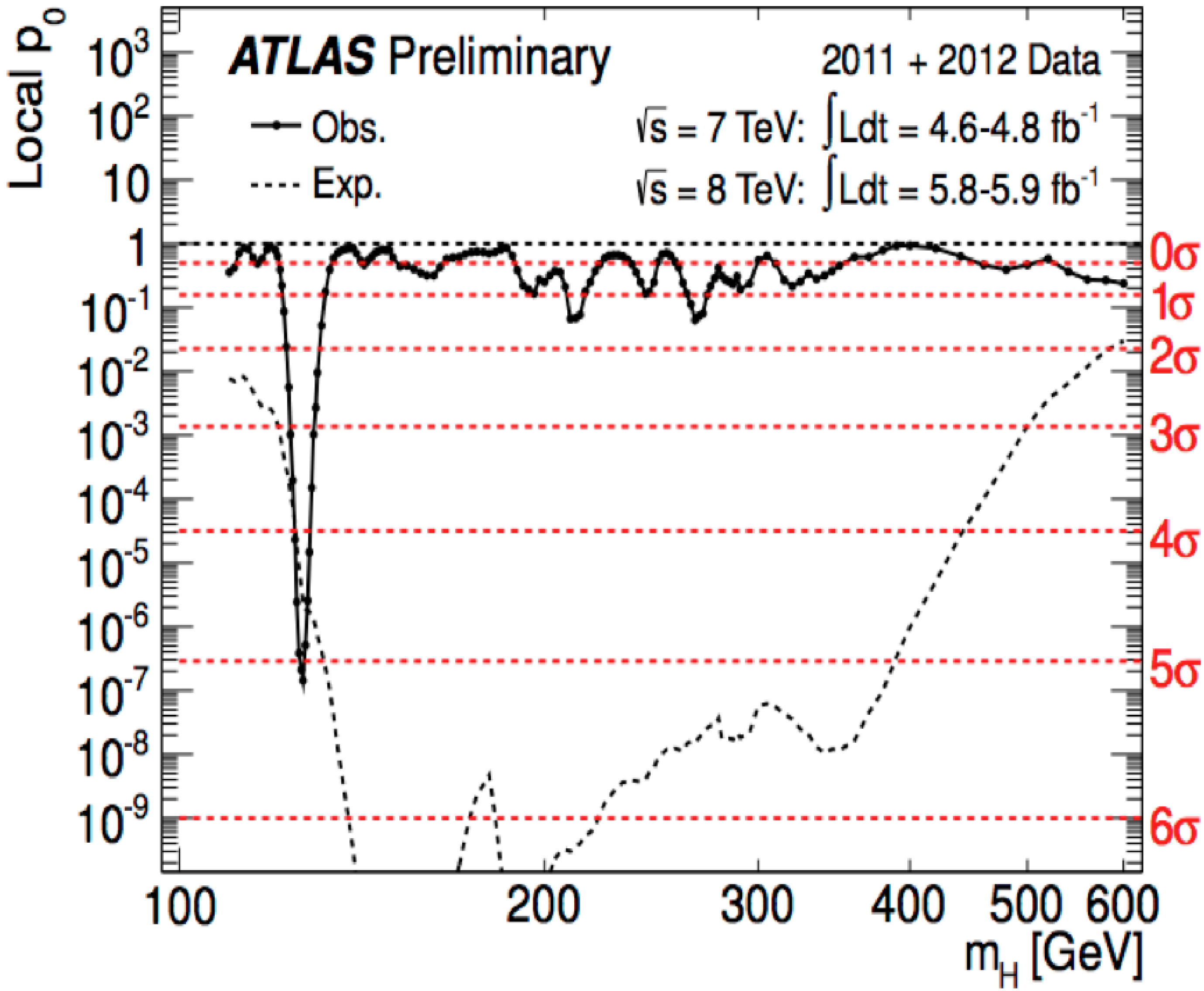

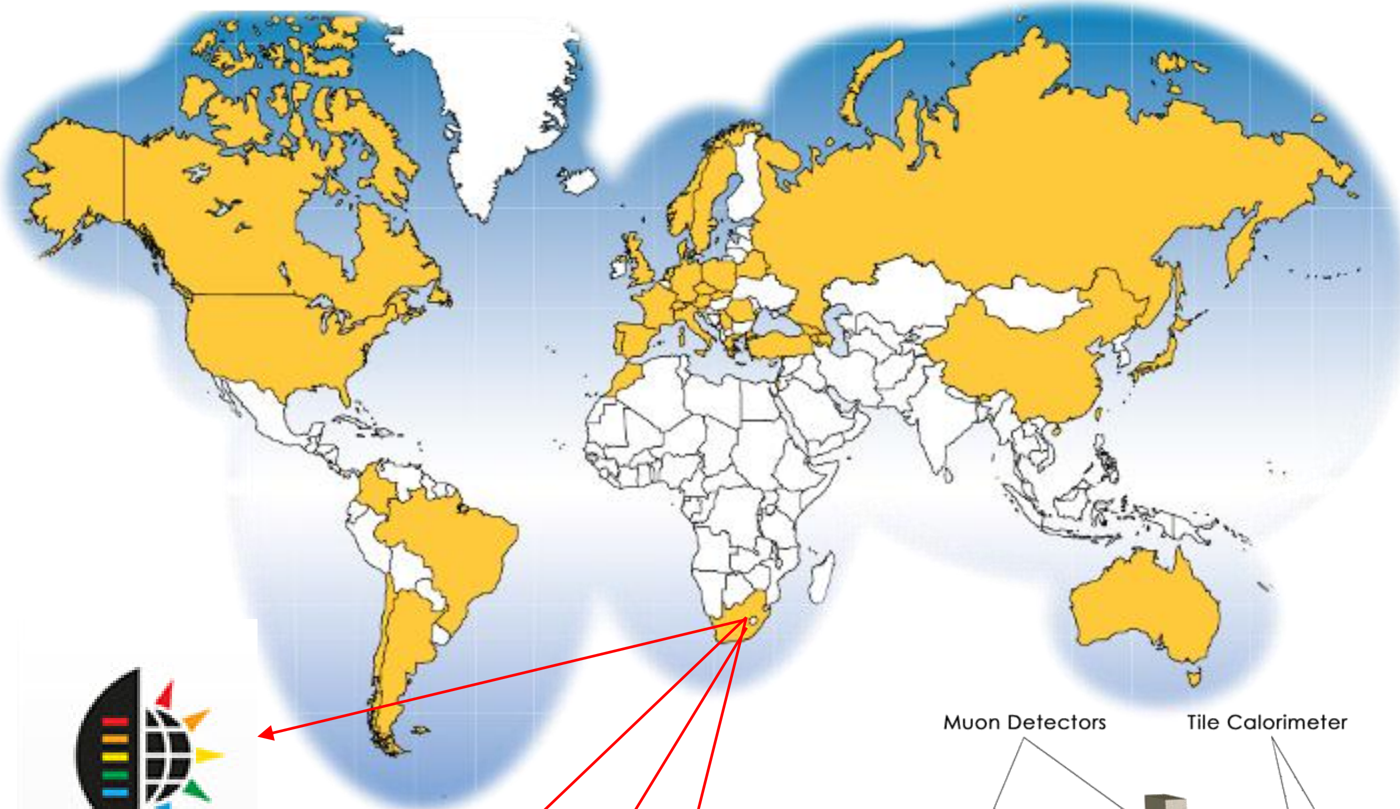

ATLAS

UNIVERSITY OF JOHANNESBURG

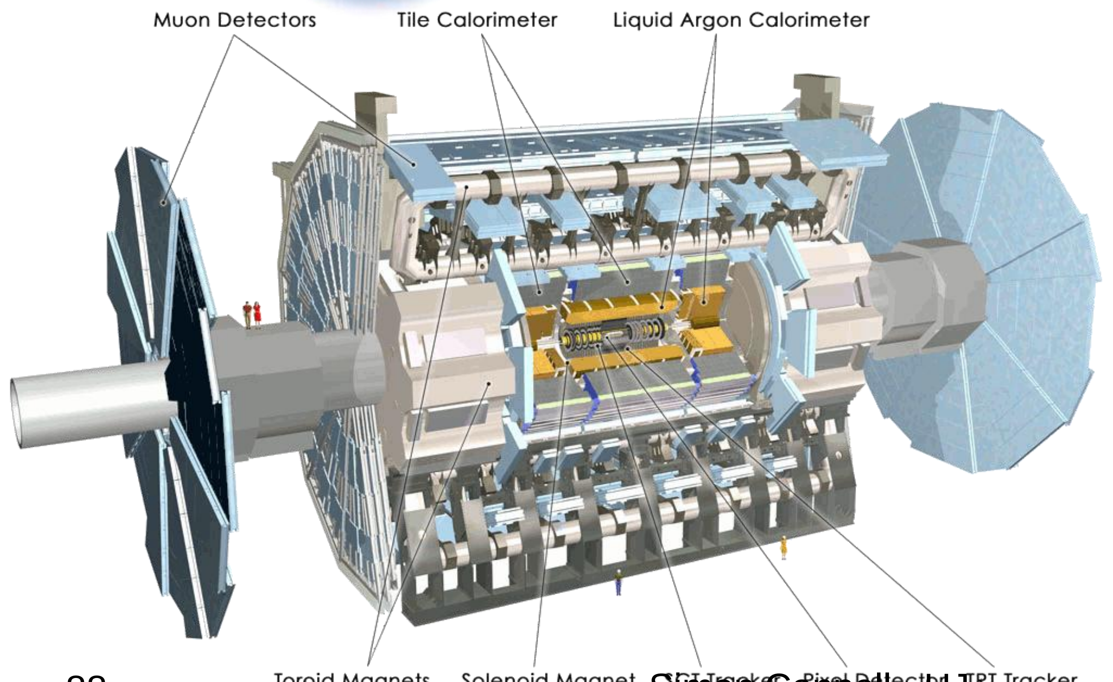

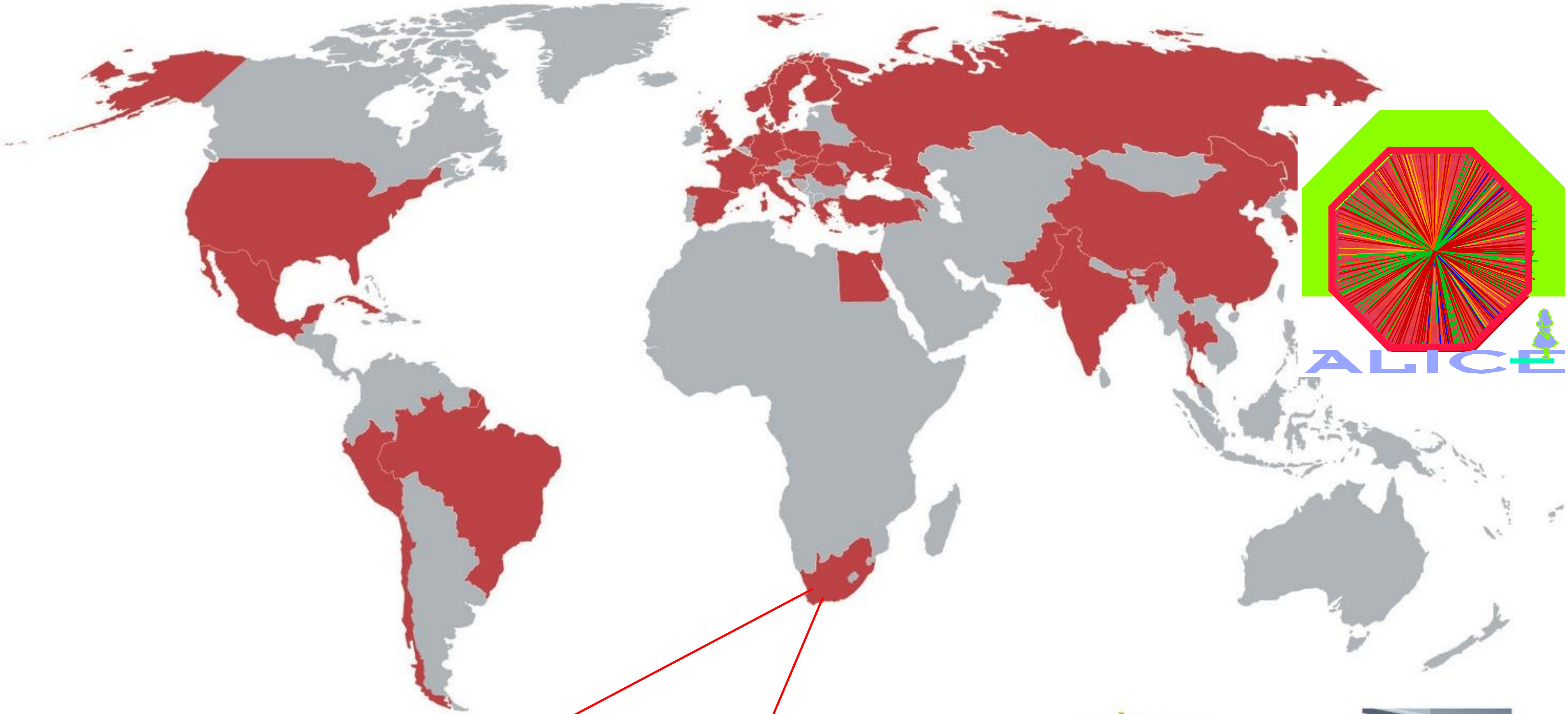

ALICE

NRF
National Research Foundation

iThemba LABS
Laboratory for Accelerator Based Sciences

SPES BONA

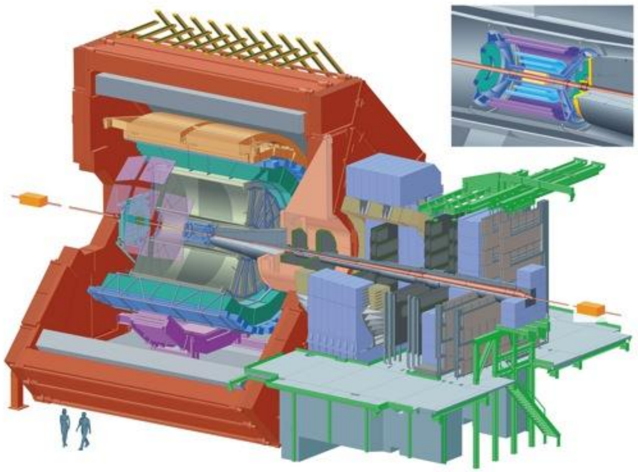

SA-CERN Programme

SA-CERN would like to receive applications for students.
There are a limited number of positions available within SA-CERN for applications originating from Africa.
Please send

1. Letter of Motivation
2. CV
3. Degree Transcripts
4. Two Referee Reports in support of the application.

SA-CERN has groups involved in

1. **Theory** (Particle Physics, Nuclear Physics) contact Steven Karataglides <stevenka@uj.ac.za>
2. **ISOLDE** (Materials Science), ISOLDE (Nuclear Physics) contact Krish Bharuth-Ram <kbr@tlabs.ac.za>
3. **ALICE** contact Jean Cleymans <Jean.Cleymans@uct.ac.za>
4. **ATLAS** contact Simon Connell <shconnell@uj.ac.za>